ISTANBUL TECHNICAL UNIVERSITY ★ GRADUATE SCHOOL OF SCIENCE ENGINEERING AND TECHNOLOGY

PROBABILITY BASED VOLUMETRIC "HEAT IN-PLACE" METHODS FOR PREDICTING POWER (ELECTRICITY) GENERATION POTENTIAL OF LIQUID-DOMINATED GEOTHERMAL SYSTEMS

M.Sc. THESIS

Melek ALTIN

Department of Petroleum and Natural Gas Engineering

Petroleum and Natural Gas Engineering Programme

JUNE, 2017

ISTANBUL TECHNICAL UNIVERSITY ★ GRADUATE SCHOOL OF SCIENCE ENGINEERING AND TECHNOLOGY

PROBABILITY BASED VOLUMETRIC "HEAT IN-PLACE" METHODS FOR PREDICTING POWER (ELECTRICITY) GENERATION POTENTIAL OF LIQUID-DOMINATED GEOTHERMAL SYSTEMS

M.Sc. THESIS

Melek ALTIN
(505141514)

Department of Petroleum and Natural Gas Engineering

Petroleum and Natural Gas Engineering Programme

Thesis Advisor: Prof. Dr. Mustafa ONUR

JUNE, 2017

ISTANBUL TEKNİK ÜNİVERSİTESİ ★ FEN BİLİMLERİ ENSTİTÜSÜ

SIVI-EGEMEN JEOTERMAL SİSTEMLERİN GÜÇ (ELEKTRİK) ÜRETİM POTANSİYELİNİN OLASILIĞA DAYALI HACİMSEL "YERİNDE DEPOLANMIŞ ISI POTANSİYELİ" YÖNTEMİ İLE ÖNGÖRÜLMESİ

YÜKSEK LİSANS TEZİ

Melek ALTIN
(505141514)

Petrol ve Doğal Gaz Mühendisliği Anabilim Dalı

Petrol ve Doğal Gaz Mühendisliği Programı

Tez Danışmanı: Prof. Dr. Mustafa ONUR

HAZİRAN, 2017

Melek ALTIN, a M.Sc. student of İTU Graduate School of Science Engineering and Technology student ID 505141514, successfully defended the thesis entitled "PROBABILITY BASED VOLUMETRIC "HEAT IN-PLACE" METHODS FOR PREDICTING POWER (ELECTRICITY) GENERATION POTENTIAL OF LIQUID-DOMINATED GEOTHERMAL SYSTEMS", which she prepared after fulfilling the requirements specified in the associated legislations, before the jury whose signatures are below.

Thesis Advisor :	**Prof. Dr. Mustafa ONUR** Tulsa University	.....
Jury Members :	**Prof. Dr. İbrahim KOCABAŞ** İzmir Katip Çelebi University	.....
	Assistant Prof. Dr. İhsan M. Gök İstanbul Technical University	.....

Date of Submission : 03 May 2017
Date of Defense : 19 June 2017

To my family,

FOREWORD

First I would like to express my eternal gratitude and thanks to my advisor Prof. Dr. Mustafa Onur for his valuable guidance to my thesis and for encouragement to my professional and academic improvement. I also would like to thank to my thesis committee members; Prof. Dr. İbrahim Kocabaş of İzmir Katip Çelebi University and Assist. Prof. Dr. İhsan Murat Gök of İstanbul Technical University for their valuable comments and suggestions to my thesis.

I would like to thank also to my family, for their patience, understanding and infinite support during my Masters of Science studies.

I would also like to thank all my instructors in the Department of Petroleum and Natural Gas Engineering in Istanbul Technical University for teaching professional knowledge that has been valuable for my advancement in my academic studies.

May 2017

Melek ALTIN
(Geological Engineer)

TABLE OF CONTENTS

Page

ABBREVIATIONS

AUP : Analytical Uncertainty Propagation
AUPM : Analytical Uncertainty Propagation Method
CDF : Cumulative Distribution Function
CLT : Central Limit Theorem
Dist. : Distribution
EGS : Enhanced or Engineered Geothermal Systems
GW : Gigawatt
GWh/yr : Gigawatt hour/year
IAPWS : International Association for the properties of Water and Steam
kW_e : Kilo Watt Electricity
Max : Maximum
MC : Monte Carlo
MCM : Monte Carlo Method
Min : Minimum
MIT : Massachusetts Institute of Technology
MREI : Mineral Research and Exploration Institute
Mod : Moderate
MWe : Mega Watt Electricity
MWt : Mega Watt Thermal
NAFZ : North Anatolian Fault Zone
NIST : The National Institute of Standards and Technology
P10 : Proved Reserve
P50 : Probable Reserve
P90 : Possible Reserve
PDF : Probability Density Function
TDS : Total Dissolved Solids
TJ/yr : Terajoule/year
TSE : Taylor Series Expansion
USGS : United States Geological Survey

SYMBOLS

A	: Area (m^2)
cp_l	: Liquid specific heat capacity (kJ/kg-^{0}C)
cp_s	: Solid specific heat capacity (kJ/kg-^{0}C)
E_r	: Recoverable energy at the wellhead (kW)
$E[X]$	: Expectation of the variable *X*
g	: Gas phase
H	: Thickness (m)
$h_{gl}(T_{sep})$	: Heat of vaporization at separator temperature (kJ)
h_R	: Enthalpy of the liquid water at the resource temperature (kJ/kg)
h^r	: Enthalpy of the liquid water at T^r (rejection) (kj/kg)
$h_{sfl}(T_c)$	: Enthalpy of the secondary fluid in liquid phase at T_c (kJ/kg)
$h_{sfg}(T_b)$	: Enthalpy of the secondary fluid in gas phase at T_b (kJ/kg)
$h_{sfgl}(T_b)$	: Heat of vaporization for the secondary fluid at T_b
$h_{stm}(T_{sep})$	: Enthalpy of the steam at T_{sep} (kJ/kg)
$h_w(T_c)$	: Enthalpy of liquid phase at condenser temperature (kJ/kg)
l	: Liquid phase
L_f	: Load factor (fraction)
m_w	: Mass could be produced at the wellhead (kg)
m	: Mass flow rate (kg/s)
p_{in}	: Turbine inlet pressure (bar)
$p_{sfb}(T_c)$	: Bubble point pressure of the secondary fluid at T_c (bar)
PW	: Electricity production potential (MWe)
PW_{USGS}	: Electricity production potential according to USGS method (MWe)
q_w	: Heat produced at the wellhead (kJ)
q_R	: Heat stored in the reservoir (kJ)
R_g	: Recovery factor (fraction)
$s_{sfg}(T_b)$	: Entropy value of the secondary fluid in gas phase at T_b (kJ/kg-^{0}C)
$s_{sfl}(T_c)$	: Entropy of the secondary fluid in liquid phase at T_c (kJ/kg-^{0}C)
s_R	: Entropy of the liquid water at the resource temperature (kJ/kg-^{0}C)
s^r	: Entropy of the liquid water at Tr (rejection) temperature (kJ/kg-^{0}C)
$s_{stm}(T_{sep})$	: Entropy of the steam at T_{sep} (kJ/kg-^{o}C)
$s_w(T_c)$	: Entropy of liquid phase at condenser temperature (kJ/kg-^{o}C)
T_b	: Bubble-point temperature (^{0}C)
T_c	: Condenser Temperature (^{0}C)
T_{cK}	: Absolute condenser temperature (K)
T_p	: Pinch-point temperature (^{0}C)
t_p	: Project life (s)
T_R	: Resource Temperature (^{0}C)
T^r	: Reference (Rejection, Dead State, Abandonment) Temperature (^{o}C)

var : Variance
$V_{sf}(T_c, p_{sfb})$: Specific volume of the secondary fluid (m^3/kg)
W_A : Maximum available work (kJ)
$(W_A)_n$: Normalized maximum available work (kJ)

Greek Symbols
φ : Porosity (fraction)
$(\rho c_p)_R$: Volumetric, isobaric, specific heat capacity of the rock (kJ/m^3-^{0}C)
ρ_l : Liquid density (kg/m^3)
ρ_s : Solid density (kg/m^3)
η_c : Conversion (utilization) efficiency (fraction)
η_{th} : Thermal conversion efficiency (fraction)
μ : Mean
σ^2 : Variance
μ_{X_i} : Mean of input variables
$\mu_{\ln X_i}$: Mean values of the natural logarithm of input variables
$\sigma^2_{\ln X_i}$: Variance of the natural logarithm of input variables
$\sigma^2_{X_i}$: Variance of input variables
θ : Sensitivity
$g'(\mu)$: First derivative of g around the mean values of the input variable
$g''(\mu\mu)$: Second derivative of g around the mean values of the input variable

LIST OF TABLES

Page

LIST OF FIGURES

Page

PROBABILITY BASED VOLUMETRIC "HEAT IN-PLACE" METHODS FOR PREDICTING POWER (ELECTRICITY) GENERATION POTENTIAL OF LIQUID-DOMINATED GEOTHERMAL SYSTEMS

SUMMARY

Reserve estimation is the vital part of reservoir engineering to be able to get an idea about the accumulation and the producibility of the reserve. One should make realistic guesses about the areal extension, thickness, resource temperature, porosity, density, isobaric, volumetric specific heat capacity of reservoir rock to be able to make reserve estimations of the geothermal resource. Also recovery factor is an important input parameter having the most uncertainty in estimation of the recoverable portion of the reserve in geothermal field.

It is very usual to use a volumetric probabilistic approach for the purpose of getting recoverable reserve estimations because deterministic approaches do not consider uncertainty propagation in estimation. USGS (United States Geologic Survey) and MIT (Massachusetts Institute of Technology) methods are widely used for volumetric probabilistic approaches to reserves with estimated input data distributions of the reservoir parameters (Garg and Combs, 2015), (Başel, 2010). When these methods are associated with probabilistic methods like MC (Monte Carlo) or its simple alternative Analytic Uncertainty Propagation (Onur et al. 2010), they give probabilistic results to assess the uncertainty in the estimation by using commonly used statistical markers of P10 (proved), P50 (probable) and P90 (possible).

Clearly it is impossible to have an exact idea for the geothermal in-situ reserves due to the included uncertainties related to reservoir characteristics such as tectonic settlement, fracture networking, porosity, thickness, areal extension, heat flow mechanism or so. That is why researchers often use stochastic approaches instead of deterministic ones. Monte Carlo simulation or analytical based uncertainty propagation methods give results by using statistical markers P10 (proved), P50 (probable) and P90 (possible) to propagate the uncertainty. These markers represent the confidence of the estimated results belong to real geothermal reserve. "P" stands for the percentile of confidence. As an example;

If one says;

- The estimated P10 value is 200 MWe then that means there is at least a 90% probability (chance of occurance) that the exact, unknown reserves recovered will be equal or exceed the estimated value of 200 MWe. This is equivalent to starting that there is a 10% chance of occurance that the estimated value of 200 MWe will be equal or less than the unknown reserves recorded.
- The estimated P50 value is 300 MWe then that means there is at least a 50% probability (chance of occurance) that the exact, unknown reserves recovered will be equal or exceed the estimated value of 300 MWe. This is equivalent to

starting that there is a 50% chance of occurance that the estimated value of 300 MWe will be equal or less than the unknown reserves recorded.

- The estimated P90 value is 400 MWe then that means there is at least a 10% probability (chance of occurance) that the exact, unknown reserves recovered will be equal or exceed the estimated value of 400 MWe. This is equivalent to starting that there is a 90% chance of occurance that the estimated value of 400 MWe will be equal or less than the unknown reserves recorded.

These examples show that the P10 provides a conservative estimate of reserves, while the P90 provides an overoptimistic estimate of reserves. If the distribution of reserves is symmetrical, which is rarely the case, it could be said that P50 value has a more confidence to occur because it is closer or equal to the mean value of the real potential of reserve. However, the distribution of the reserves is usually log-normal and hence, it is usually preferable to consider the tails of the distribution (Capen 1996, 2001).

For example, P10 is the value used to solicit financing from banks and these statistical markers are also required by private and government institutions or agencies to classify the potential of the oil, gas or geothermal reservoirs as well as providing finance to the projects proposed by the investors or decision makers (Capen 2001).

USGS and MIT methods use arbitrarily chosen reference temperature and thermal power conversion efficiency values for their estimations without taking the second law of thermodynamic and the installed power conversion system into consideration. So this leads to overestimated results of reserve estimations, as shown by Garg and Combs (2015).

Garg and Combs (2015) proposed a new method that a geothermal field must be treated with an approximation that relies on the resource temperature of the reservoir. If the reservoir temperature value is higher than 180 ^{o}C than this reservoir is proper for single or double flash power conversion system and if the reservoir temperature is between 57-180 ^{o}C then a binary power plant should be installed to be able to produce electricity from the resource efficiently. Also the input parameters used for the volumetric probabilistic reserve estimation should be chosen related and accordant to the power conversion system.

Monte Carlo simulation method is the widely used method for reserve approximations in a probabilistic way and also analytical uncertainty propagation method presents an alternative analytical way to probabilistic reserve estimations giving very close resultant values in comparison to Monte Carlo simulations.

In this thesis, all volumetric estimations of power generation potential based on USGS, MIT and Garg and Combs (2015) have been evaluated by MC simulation and AUP methods. The working equations of AUPM for each of the three methods have been derived in this thesis. Then, the applications of AUP method have been presented and compared with the MC simulation results applied to USGS, MIT and Garg and Combs (2015) methods. The results predicted by the new AUPM equations derived in this work showed an excellent agreement, not requiring extensive MC simulations and a commercial software use.

Suggestions were made about the usage of USGS and MIT methods that give overestimated results by the usage of arbirtarily chosen reservoir input parameters.

At the last section of this thesis, Garg and Combs (2015) method was applied to 25 geothermal fields of Turkey, which are amenable to power generation, by MCM and AUPM approximations. The same 25 fields were originally considered and studied by Başel in 2010 in her PhD thesis by using the MIT method. In Başel's dissertation, these geothermal fields were all treated by a reference temperature of 100 ^{0}C when estimating Turkey's power generation potential. However, today it is well known that binary power conversion plants are designed to generate electricity from resources having reservoir temperature values ranging from 57 to 180 ^{0}C. It is shown here that Garg and Combs (2015) method without any usage of arbitrary values and considering the installed power conversion system and thermodynamic properties of the produced water or the secondary fluid of the power conversion system is the best method to eliminate the subjectivity in selecting the reference (or abandonment) temperature and conversion efficiency and hence to estimate or predict the power generation of a geothermal field or country more realistically. In this thesis, it also shown that the AUPM and MC based Garg and Combs (2015) method predict the power generation of of the 25 geothermal fields of Turkey considered in Başel's PhD dissertation as P10 = 661 MWe, P50 = 1165 MWe, and P90 = 1909 MWe, based on arithmetic summation. On the other hand, for the same geothermal fields, Başel (2010) predicted the power generation potential as: P10 = 840 MWe, P50 = 1428 MWe, and P90 = 2371 MWe. As the same data for all 25 geothermal fields provided by Başel, it is clearly the MIT method used by Başel overestimates the power generation potential of Turkey based on these 25 geothermal fields.

SIVI-EGEMEN JEOTERMAL SİSTEMLERİN GÜÇ (ELEKTRİK) ÜRETİM POTANSİYELİNİN OLASILIĞA DAYALI HACİMSEL "YERİNDE DEPOLANMIŞ ISI POTANSİYELİ" YÖNTEMİ İLE ÖNGÖRÜLMESİ

ÖZET

Keşfedilen bir jeotermal rezervuarda ne kadar ısı depolandığı ve bu ısının ne kadarının elektrik veya güç üretimine çevrilebileceği konusunda gerçekçi yaklaşımlarda bulunabilmesi jeotermal rezervuar mühendisliğinin en önemli gereklerinden biridir. Jeotermal kaynakların ne kadar rezerv içerdiği konusunda yapılacak yaklaşımlarda alansal uzanım, kalınlık, kaynak sıcaklığı, gözeneklilik, yoğunluk, sabit basınçta hacimsel belirlenimsel ısı kapasitesi gibi parametreler için gerçekçi tahminler yapmak gerekir. Ayrıca üretilebilirlik faktörü de jeotermal rezervin ne kadarının üretilebilir olduğu konusunda yapılacak yaklaşımlarda kullanılacak en büyük belirsizliği içeren önemli bir parametredir.

Deterministik yaklaşımlar belirsizliği sayısallaştırmadığı için üretilebilir rezerv tahminlerinde hacimsel olasılıklı yaklaşımlar sıkça kullanılmaktadır. USGS (Birleşik Devletler Jeolojik Araştırma) ve MIT (Massachusetts Teknoloji Enstitüsü) yöntemleri bu amaçla sıkça kullanılan hacimsel olasılıklı yöntemler olarak rezervuar girdi veri parametrelerini dağılımsal yaklaşımlarla incelerler. Bu yöntemler Monte Karlo (MK) simulasyon yöntemi ya da ona basit bir alternatif olan Analitik Belirsizlik Yayılma (ABY) (Onur et.al. 2010) yöntemiyle ilişkilendirildiklerinde üretilebilir rezerve ilişkin yaygınca kullanılan olasılıklı P10 (kanıtlanmış), P50 (olası) ve P90 (olasılıklı) istatistiksel sonuçları ortaya koyarlar.

Tektonik yapı, çatlak dağılımı, gözeneklilik, kalınlık, alansal yayılım, ısı akışı mekanizmaları gibi rezervuar karakteristiklerindeki belirsizlikler nedeniyle jeotermal sahaların yerinde rezerv hesaplamalarında bu parametrelere ait kesin bilgi ve görüşlere sahip olabilmenin olanaksızlığı açıktır. Bu nedenle araştırmacılar açısından belirlenimsel yöntemlerden ziyade olasılıksal modellere yönelmek daha gerçeğe yakın sonuçlara ulaşabilmek açısından önem taşımaktadır. Monte Karlo modelleme ve analitik belirsizlik yayılım yöntemleri sonuçlarını belirsizliği sayısallaştırarak P10 (kanıtlanmış), P50 (olanaklı) ve P90 (olası) değerleri şeklinde ortaya koymaktadırlar.

Örneğin;

- Eğer bu hesaplamalar sonucunda tahmin edilen P10 değeri 200 MWe ise bunun anlamı sahanın gerçek üretilebilir rezerv değerinin 200 MWe'den %90 olasılıkla daha fazla olduğudur. Yani tahmin edilen 200 MWe'lık potansiyel rezervin bilinmeyen gerçek değerden daha az ya da bu değere eşit olma olasılığı %10'dur.
- Eğer tahmin edilen P50 değeri 300 MWe ise bunun anlamı sahanın erçek üretilebilir potansiyeldeğerinin 300 MWe'den %50 olasılıkla daha fazla

olduğudur. Yani tahmin edilen 300 MWe'lık potansiyel rezervin bilinmeyen gerçek değerden daha az ya da bu değere eşit olma olasılığı %50'dir.

- Benzer şekilde, eğer tahmin edilen P90 değeri 400 MWe ise bu sahanın gerçek üretilebilir elektrik potansiyeli değerinin %10 olasılıkla 400 MWe'den daha fazla olduğu anlamına gelir. Yani tahmin edilen 400 MWe'lık potansiyel rezervin bilinmeyen gerçek değerden daha az ya da bu değere eşit olma olasılığı %90'dır.

Bu örneklemeler P10 değerinin biraz daha karamsar ve P90 değerinin ise aşırı iyimser tahminler ortaya koyduğunu göstermektedir. Eğer tahmin edilen rezerv simetrik bir dağılım gösteriyorsa, ki bu nadiren rastlanan bir durumdur, P50 değerinin ortalama potansiyel değerine daha yakın ya da eşit olması bu değerin gerçekleşmesi olasılığının güvenilirliğini arttırmaktadır. Ancak rezerv dağılımları genellikle log-normal bir dağılım gösterdiklerinden P10 değerinin kullanımı daha tercih edilir olarak görülmektedir (Capen 1996, 2001).

Örneğin P10 değeri özel ve kamu yatırımlarımcılarının ya da kuruluşlarının petrol, doğal gaz ya dajeotermal reservuar potansiyelini sınıflandırmak ve projelere maddi destek sağlamak konusunda yatırımcıların ve karar verici mekanizmaların değerlendirdiği ölçütlerdir (Capen, 2001).

USGS ve MIT yöntemleri kurulu bulunan ya da kurulacak olan güç çevrim sisteminin türünü ve termodinamiğin ikinci yasasını göz önünde bulundurmaksızın keyfi seçilmiş referans sıcaklıkları ve çevrim verimliliği parametreleriyle çalışırlar. Bu durum Garg ve Combs (2015) tarafından gösterildiği gibi güç üretim potansiyeli tahminlerinde üzere aşırı iyimser sonuçların elde edilmesine neden olur.

Garg ve Combs (2015) jeotermal sahalardan üretilebilir güç potansiyelinin hesaplanmasında kaynak sıcaklığına bağlı olarak çalışan yeni bir yaklaşım önerdiler. Bu yaklaşıma göre eğer kaynak sıcaklığı 180 ^{0}C'nin üzerinde ise bu jeotermal saha tekli ya da ikili flash güç çevrim sistemleri için uygundur. Eğer kaynak sıcaklığı 57 ^{o}C ile 180 ^{o}C arasındaysa bu jeotermal sahadan en yüksek verimde güç üretebilmek için kurulması gerekli güç çevrim santrali türü çiftli akışkan (binary) olmalıdır. Ayrıca bu yeni yaklaşım hacimsel olasılıklı rezerv tahminlerinde girdi parametrelerinin de bu güç çevrim sisteminin termodinamik özellikleriyle uyumlu olmasını gerekli kılmaktadır.

Olasılıklı rezerv yaklaşımlarında Monte Karlo simulasyon yöntemi oldukça sık kullanılan bir yöntem olmakla birlikte Analitik Belirsizlik Yöntemi de Monte Karlo Yöntemi'ne çok yakın sonuçlar veren (1%-5% farkla) bir alternatif yöntemdir.
Bu tez çalışmasında incelenen USGS, MIT ve Garg & Combs (2015) yöntemlerinin tümü hem MK simülasyon yöntemiyle hem de AB yöntemiyle incelenmiş ve sonuçlar MK yöntemi ile karşılaştırmalı olarak verilmiştir. Her üç yaklaşım için ABY denklemleri türetilmiştir.

Daha sonra ABY yönteminin USGS, MIT ve Garg & Combs (2015) yaklaşımlarına uygulamaları gösterilmiş ve bulunan sonuçlar MK simulasyon yönteminden bulunan sonuçlarla kıyaslanmıştır. ABY yönteminden elde edilen sonuçlar MK yönteminden elde edilen sonuçlarla mükemmel bir uyum göstermiş ve böylece hacimsel

yaklaşımlarda geniş kapsamlı MK simulasyonlarının ve bu amaçla ticari yazılımların kullanımının gereksizliğini ortaya konmuştur.

Kullanılan keyfi ve rastgele değerler sonucunda aşırı iyimser değerler ortaya koyan USGS ve MIT yöntemlerinin uygun kullanımları ile ilgili önerilerde bulunulmuştur. Bu tezin son bölümünde, Garg ve Combs (2015) yöntemi, Başel'in 2010 doktora tezinde üzerinde çalışmış olduğu 25 jeotermal sahaya aynı girdi parametreleri kullanılarak uygulanmış ve Başel'in MIT yöntemi ile değerlendirdiği güç potansiyeli tahminleri, Garg & Combs (2015) Monte Karlo ve Analitik Belirsizlik yöntemlerinin kullanımıyla elde edilen sonuçlarla kıyaslanmıştır. Böylelikle MIT yönteminin ne kadar iyimser sonuçlar ortaya koyduğu değerlendirilmiştir. Bu 25 jeotermal saha, kaynak sıcaklıkları 100 ^{0}C'nin üzerinde olduğu için elektrik üretimine uygun sahalar olarak değerlendirilmiştir. Ancak günümüzde kaynak sıcaklığı 57-180 ^{0}C arasında olan jeotermal sahalardan en verimli biçimde güç üretebilen çift akışkanlı (binary) güç çevrim sistemleri geliştirilmiştir. Garg ve Combs (2015) yöntemi Monte Karlo ve Analitik Belirsizlik yöntemi yaklaşımlarıyla, hiçbir rastgele ya da keyfi değerin kullanımına meydan vermeksizin, kurulu güç çevrim sisteminin ve sistemde kullanılan jeotermal ya da ikincil akışkanın termodinamik özelliklerine bağlı olarak, aşırı iyimserlikten uzak, daha gerçekçi rezerv tahmin tahminleri yapabilmeyi mümkün kılmaktadır. Bu yöntem, referans sıcaklık (ya da terk sıcaklığı) ve güç çevrim verimliliği parametrelerinin kullanımındaki öznelliği ortadan kaldıran en iyi yöntemdir. Bu tez çalışmasında, Garg ve Combs yöntemi kullanılarak MK ve AB yaklaşımları ile, sözü edilen 25 saha için elde edilen üretilebilir güç potansiyel değerleri aritmetik toplamı P10=661 MWe, P50=1165 MWe ve P90=1909 MWe olarak bulunmuştur. Öte yandan aynı sahalar için Başel (2010) P10=840 MWe, P50=1428 MWe ve P90=2371 MWe değerlerini öngörmüştür. Bu 25 jeotermal saha için aynı rezervuar girdi parametreleri kullanılmış olması dolayısıyla MIT yönteminin bu 25 saha için Türkiye'nin güç üretim potansiyelini aşırı iyimser tahmin ettiği gayet açıktır.

1. INTRODUCTION

Today geothermal reserves are being used for electricity generation widely in the Aegean region of Turkey where tectonically very active horst-graben systems have been found. At the stage of exploration or development, it is important to get a probabilistic approach to producible reserves in the geothermal field. USGS (US Geological Survey, 1970) and MIT (Massachusetts Institute of Technology, 2006) methods have been used with Monte Carlo simulations up until today (Garg and Combs, 2015). But lately with the development of geothermal sector, a new approach was proposed by Garg and Combs (2015) showing the deficiencies of USGS and MIT methods for their arbitrary usage of reference temperatures and power conversion efficiency values and the overestimated results as a consequence.

Garg and Combs (2015) proposed a new method that could be applied by AUP (Analytical Uncertainty Propagation) and MC (Monte Carlo) methods far away from arbitrary input parameters and bring a new aspect to reserve estimations by taking the second law of thermodynamics and proper values accordingly determined by the power conversion system into consideration.

1.1 Background and Literature Review

According to the inventory prepared by MREI (Mineral Research and Exploration Insttitute) in 2005, which still has not been upgraded today, Turkey has 12 geothermal field amenable to electricity potential (Table 1.1).

Başel (2010) in her PhD dissertation listed 25 geothermal fields which she determined as the geothermal fields which are amenable to electricity production with resource temperatures higher than 100 ^{o}C. Table 1.2 presents this list with the resource temperature values in a probabilistic manner.

Başel (2010) assumed that geothermal fields having resource temperature values higher than 100 ^{o}C is amenable to electricity production in her PhD, worked on 25 geothermal fields and made Monte Carlo simulation based electricity production potential estimations.

Table 1.1 : Electricity potential fields with resource temperatures based on 2005 inventory of MREI.

Field Name	Resource Temperature T_R ºC
Denizli-Kızıldere	242
Aydın-Germencik-Ömerbeyli	232
Manisa-Alaşehir-Kurudere	184
Manisa-Salihli-Göbekli	182
Çanakkale-Tuzla	174
Aydın-Salavatlı	171
Kütahya-Simav	162
İzmir-Seferihisar	153
Manisa-Salihli-Caferbey	150
Aydın-Yılmazköy	142
İzmir-Balçova	136
İzmir-Dikili	130

Table 1.2 : 25 Electricity production potential fields taken from Başel, 2010, PhD.

Field Name	Distribution	TR ºC		
		min	mode	max
Alaşehir, Sarıkız-Manisa	Triangular	125	165	200
Atça-Aydın	Uniform	125	-	150
Balçova-İzmir	Triangular	110	135	145
Dikili-İzmir	Triangular	110	130	220
Germencik-Aydın	Triangular	205	220	235
Gümüşköy-Aydın	Uniform	105	-	150
Kızıldere 1-Denizli	Triangular	195	205	215
Kızıldere 2-Denizli	Triangular	230	240	245
Nazilli-Aydın	Triangular	140	180	200
Pamukören 1-Aydın	Uniform	180	-	200
Pamukören 2-Aydın	Uniform	200	-	220
Caferbeyli 1 -Manisa	Uniform	130	-	150
Caferbeyli 2-Manisa	Uniform	180	-	200
Umurlu-Aydın	Uniform	150	-	170
Salavatlı-Aydın	Triangular	145	170	230
Seferihisar 1-İzmir	Uniform	130	-	155
Seferihisar 2-İzmir	Uniform	110	-	130
Simav-Kütahya	Triangular	160	200	230
Tekkehamam 1-Denizli	Triangular	120	140	160
Tekkehamam 2-Denizli	Triangular	140	180	200
Tekkehamam 3-Denizli	Triangular	140	170	200
Tuzla-Çanakkale	Triangular	170	200	230
Salihli Doğu-Manisa	Uniform	150	-	170
Hıdırbeyli Kuzey-Aydın	Triangular	120	140	170
Hıdırbeyli Güney-Aydın	Triangular	140	170	200
İmamköy, Yılmazköy-Aydın	Triangular	145	180	220
Kavaklıdere-Manisa	Triangular	180	215	240
Ortakçı-Aydın	Uniform	135	-	165
Salihli Kuzeydoğu-Manisa	Constant	-	-	170
Umurlu Güney-Aydın	Uniform	150	-	170
Erciş, Zilan-Van	Triangular	120	140	168

She made the summation of production potential values in two different ways by using arithmetic summation and probabilistic summation. At the end she calculated the arithmetic average of the two values obtained from arithmetic and probabilistic methods to get a conclusive result for Turkey's electricity production potential.

As a result of this study Başel (2010) estimated the electricity production potential of 25 fields having resource temperatures higher than 100 ^{o}C as 1269 MWe (P10), 1500 MWe (P50) and 1839 MWe (P90) based on probabilistic summation of the field potentials and 840 MWe (P10), 1428 MWe (P50) and 2371 MWe (P90) based on the arithmetic summation of the fields with electricity production potentials. Then she recommended getting the arithmetic average of the probabilistically and arithmetically calculated summation results.

Then in 2013 Başel et al. revised this study by using 38 fields which are amenable to electricity production and gave the results as 1673 (P10), 2263 (P50) and 3140 (P90) MWe but they didn't give any reservoir characteristics information about the fields such as thickness, porosity, recovery factor, area and even the names of the fields they studied. Hence, their results cannot be reproduced and compared with other methods.

Based on a personal communication which was made with Akkuş (retired from MREI) in 2016, today Turkey has 39 geothermal fields amenable to electricity production but only mostly represented reservoir temperature values are available data for the fields. Unfortunately, other data necessary to have a realistic estimation of Turkey's power generation potential are not available.

1.2 Problem Statement

Widely used USGS and MIT methods use arbitrarily chosen reference temperature values and thermal conversion efficiencies. For example while using USGS method for volumetric probabilistic calculation of reserves, one choses the reference temperature as 15-25-35 or 40 ^{o}C and for conversion efficiency one can choose 0.4, 0.3, 0.16 etc. arbitrarily and these values are not depend on something. They are only subjective guesses. The same problem is also valid for MIT method. For example Başel (2010) in her PhD thesis used 100 ^{o}C reference temperature value for all fields she examined. Also in literature, there is variety of usages of these values arbitrarily (Garg and Combs, 2011).

The MIT method does not consider about enthalpy and entropy changes of the geothermal system in neither reservoir conditions nor the surface wellhead conditions.

On the other hand, in both methods generally a recovery factor value higher than "0" is used even if there is no idea about a geothermal field in the very early exploration phase.

Those reasons result in obtaining too optimistic estimates of power generation potential of geothermal systems from the USGS and MIT methods as discussed Garg and Combs (2010, 2011, 2015) and Grant (2015).

1.3 Objectives of Research

Garg and Combs (2015) proposed and showed a new formulation of volumetric probabilistic calculation of geothermal reserves by considering the second law of thermodynamics and the power conversion system dependency of the input parameters. They showed that input parameters such as reference temperature and conversion efficiency must be chosen according to the basic power conversion system that is appropriate for a geothermal system under consideration, such as single flash or binary. Also the secondary fluid thermodynamic properties must be used while working on binary power plants.

Garg and Combs (2015) also proposed that the recovery factor must be taken into consideration as "0" for the geothermal fields in very early stage of exploration. So in this thesis the new formulations of Garg and Combs (2015) for binary and flash power plants have been presented and evaluated in different cases where recovery factor is "0" or higher than zero in comparison to USGS and MIT results.

To do so, all volumetric estimations of power generation potential based on USGS, MIT and Garg and Combs (2015) have been evaluated by MC simulation and AUP methods. The derivation of AUP method equations for each of the three methods is one of the main of objectives of this thesis. Another objective is to show the use of the AUP method with each of the USGS, MIT and Garg and Combs (2015) methods and compare the results obtained from the AUP with those the MC simulation results.

One more objective of this research is to show the usage of Garg and Combs (2015) method in different cases, to correlate the results with the USGS and MIT methods and to show which values of reference temperature and conversion efficiencies

should be used in the USGS and MIT methods to get closer results to the ones to be obtained from the Garg and Combs (2015) method.

The other objective is to show and evaluate the applications of AUP mathematical method as a simple alternative to the MC simulation method while making approximations to geothermal reserves and producible amount of power from these resources without requiring extensive MC simulations and use of a commercial software.

Also one of the objective of this research is to compare the power generation potential of 25 geothermal fields (as presented in Başel (2010) dissertation) predicted in this thesis by using the Garg and Combs (2015) method with that predicted by Başel (2010) who considered a reference (or abondenment) temperature of 100 ^{o}C for all 25 geothermal fields.

1.4 Significance of the Study

This study shows how to apply AUP technique for probabilistic reserve input parameters in triangular and random data distributions as an alternative to MC simulation method and also shows the applications of Garg and Combs (2015) method related to the type of the power conversion system and correlates the results with the 25 geothermal fields studied by Başel in 2010 in her PhD dissertation.

1.5 Scopes of the Study

The scope of this study is to show the reasons of overestimations of USGS and MIT volumetric probabilistic methods while approaching to geothermal reserves and to show the new Garg and Combs (2015) flash and binary methods which give much more realistic reserve estimates that stated by Garg and Combs (2015) and Grant (2015) in the literature.

The secondary scope is to evaluate and show the application of AUP method as a mathematical alternative to MC simulation method and to give correlations of AUP and MC methods in different cases.

1.6 Thesis Structure

In Chapter I, an introduction is given for the subject of this study. After background and literature review sections, the problem, the objectives and the scopes of this study are stated and thesis structure was explained.

In Chapter II, first, the relation of geothermal energy and tectonism is explained with geothermal system and reserves as P10 (proved), P50 (probable) and P90 (possible) descriptions. Then classifications of enthalpy and physical state (Bodvarsson, 1964; Axelsson and Gunnlaugsson 2000) of geothermal waters were given with the geothermal resource temperature map, well distibution, installed capacity by January, 2016 data of MREI with Başel, 2013 electricity production potential estimation results. Then the most current 39 geothermal field names have been listed with their resource temperature values. Geothermal energy installed capacities of Turkey and other countries in the world were also given in correlation.

In Chapter III, the working mechanism of single flash, binary and sophisticated/hybrid power plants are described and power conversion efficiency concept is introduced.

In Chapter IV, volumetric heat in place method is explained with USGS, MIT, Garg & Combs single flash and binary applications and evaluated by case studies.

In Chapter V, sources of uncertainty in power generation potential by volumetric methods were evaluated with classification of data with large uncertainty and data with less or no uncertainty. Different cases were designed to be able to see the effect of different probability distribution types on results.

In Chapter VI, the AUPM (Analytical Uncertainty Propagation Method) for prediction of power generation potential is evaluated with the derivation of AUPM, computation of statistical markers as P10, P50, P90, analytical formulas for mean and variance of the input parameter X_i with the mean and variance of the input parameter $\ln X_i$ for uniform and triangular distribution types. Then Taylor series expansion methods were applied to be able to evaluate the mean and variance of a

random non-linear function *g(X)* with first order derivatives but the analytical result and random sampling has showed 66% difference in variance of $\ln X_i$ where the lower limit of X_i is equal to zero. So second order derivatives were applied to get more closer results to the one obtained from Monte Carlo simulation. By application of second order expansion of Taylor series the difference were reduced to 61% in uniform distribution.

For triangular distribution the same application method is followed since the first expansion results of Taylor series for triangular distributions where the minimum limit of X_i is equal to zero, the difference between the analytical result and Monte Carlo simulation was 42% where it was recorded as 36% after the second order expansion of Taylor series. Then the formulas for normal and log-normal distributions are given.

In Chapter VII, the application of Garg and Combs, USGS and MIT methods by using MC and AUP approximations were evaluated with different cases to get an idea about the most proper way of usage of USGS and MIT methods with reference temperature and conversion efficiency values much more far away from being arbitrarily chosen. The application of Kızıldere, Germencik and Salavatlı fields were evaluated for flash and binary power conversion systems with MC simulation and AUPM as a good alternative to MCM (Monte Carlo Method).

Also in this chapter a special case has been designed where the lower limit of recovery factor is equal to zero to be able to see the resultant difference between the producible power potential in both the analytically calculated variance of natural logarithm of recovery factor is used and randomly generated simulation based variance of natural logarithm of recovery factor is used (there was 34.2% difference between them).

In Chapter VIII, simple arthmetic sum and probabilistic sum is explained.

In Chapter IX, the power generation potential of 25 geothermal fields with all the same reservoir information as given in Başel's PhD thesis (2010) is predicted by

using Garg and Combs method in AUP and MC applications and the results are compared with the results reached by Başel (2010).

In Chapter X, conclusions and recommendations for future work are summarized.

In Appendix A, pentane liquid and vapor phase thermodynamic properties on the saturation curve (NIST, 2010) is listed as ordered with 5 ^{o}C temperature increment; in Appendix B, pentane liquid and vapor phase thermodynamic properties on the saturation curve (NIST, 2010) is listed as ordered with 0.5 bar pressure increment and in Appebdix C, reservoir characteristics information used in volumetric probabilistic reserve estimations of 25 fields examined for electricity production potential is given.

2. GENERAL VIEW OF GEOTHERMAL ENERGY IN THE WORLD AND IN TURKEY

In this chapter, information provided on geothermal energy basics as well as past and current status of geothermal enery use in the world and in Turkey.

2.1 Geothermal Energy Basics

Heat in earth is caused by the inner stratum magma which temperature values range from 700 ^{o}C to 1300 ^{o}C (Url-1). Magma especially could be seen at the surface of the earth such as lava flows from volcanoes including melted rock mixtures settled in very deep depths of the earth.

Crust of the earth is divided into plates which are mobile sliding on the asthenosphere and excluding quick movements caused by earthquakes, continents move 1-1.5 cm in average each year and we call this as active plate tectonism of our planet. Active tectonism of the plates causes divergence of the plates in extensional areas where crust gets thinner, weaker and normal faulted structure gives magma the chance to rise up to the surface easily with intense network of faults and fractures such as the formation of horst-graben systems occurrence as a result product of this motion forming the Gediz, Bakırçay, Büyük Menderes and Küçük Menderes grabens in the West of Turkey (Figure 2.1) or it can be occurred in depressional areas causing convergence by subduction of plates where thrust faults and overlaps are formed with again a dense subsurface fracture network such as the subduction of Arabian plate under the Anatolian Plate forming thrust fault and overlap successions at the Southeastern part of Turkey (Figure 2.2). Also transform fault zones such as North Anatolian Fault zone (NAFZ) are the places where transform motions of crustal plates occur laterally with respect to each other (Figure 2.3).

Today it is also known that the active plate tectonic boundries are the places where most geothermal activities occurred on Earth due to the mentioned crustal activities (Url-5). Turkey, as being located in this very active tectonism area (Figure 2.4), is in

an important situation for geothermal energy exploration, exploitation and production (Figure 2.5).

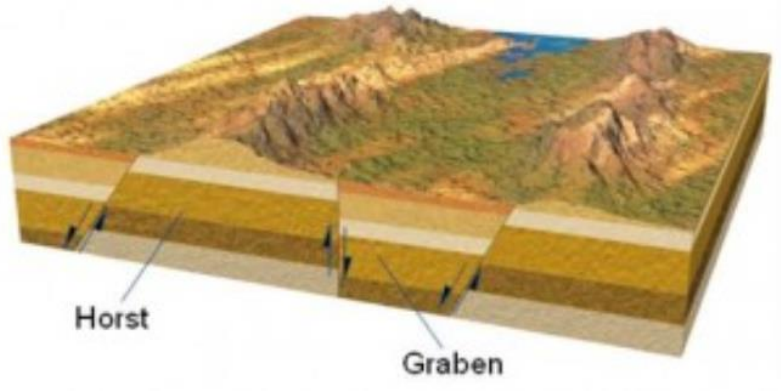

Figure 2.1: Horst-graben systems (Url-2).

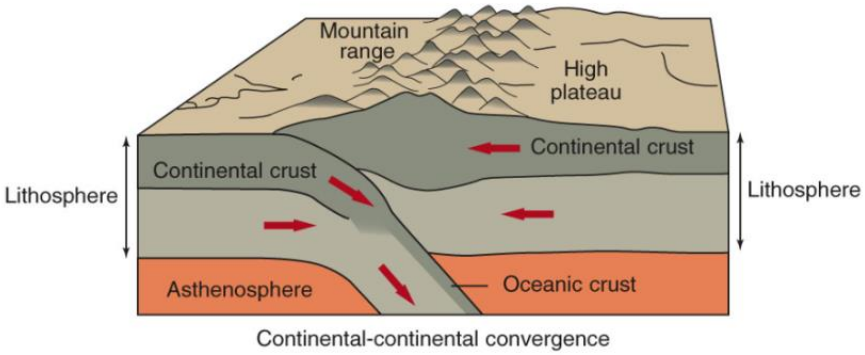

Figure 2.2 : Depressional regime subduction system (Url-3).

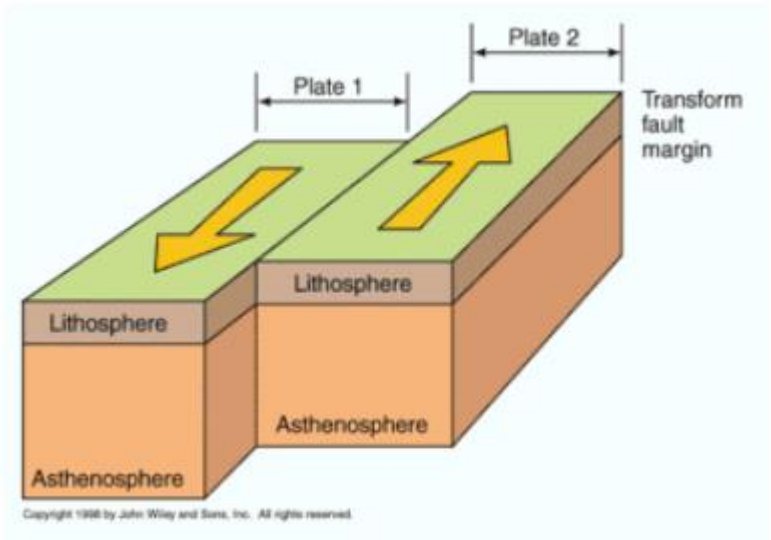

Figure 2.3 : Transform motion of crustal plates (Url-4).

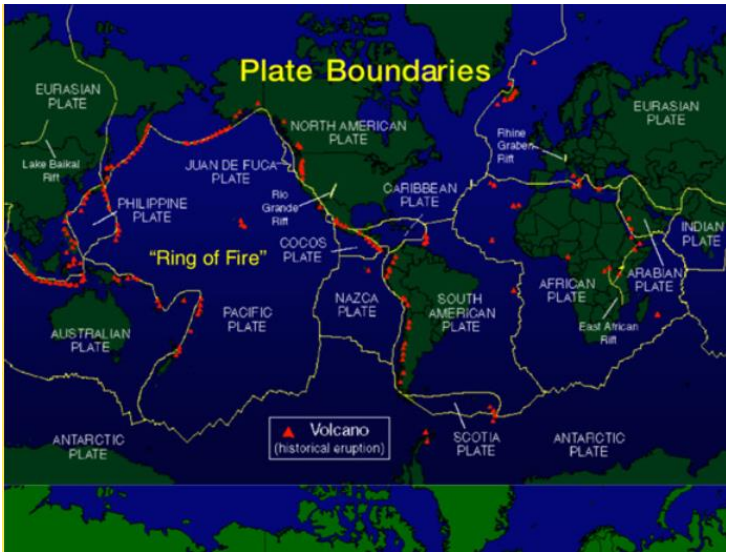

Figure 2.4 : Active plate tectonic boundries in the world (Url-5).

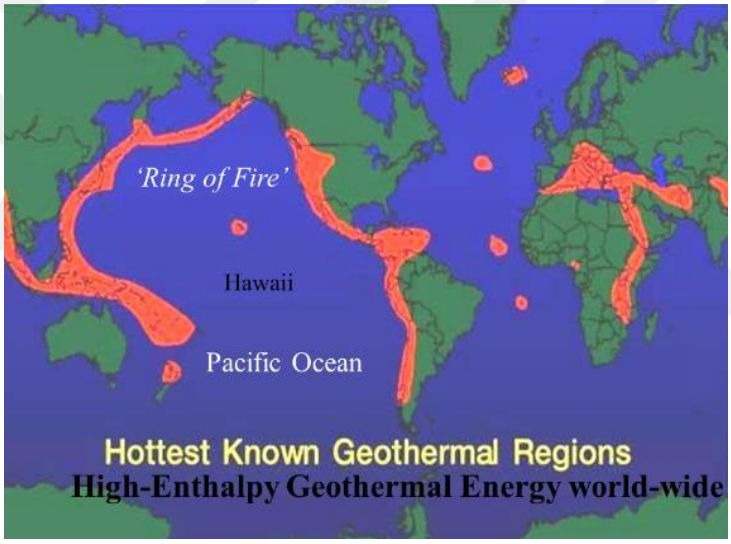

Figure 2.5 : Geothermal regions with high enthalpy in the world (Url-6).

2.2 Geothermal System

Geothermal power is generated by using geothermal heat energy via various types of conversion mechanisms. To be able to discuss a geothermal system, we need to have a heat source such as magma intrusions into the lithosphere, a meteoric originated aquifer connected to the surface with fractures, fissures or faults, a porous reservoir rock to store the liquid, and there must be an impermeable cap rock avoiding the liquid to escape upwards and also a recharge mechanism belonging to the surface

environmental and structural condition is a vital part of a geothermal system (Figure 2.6).

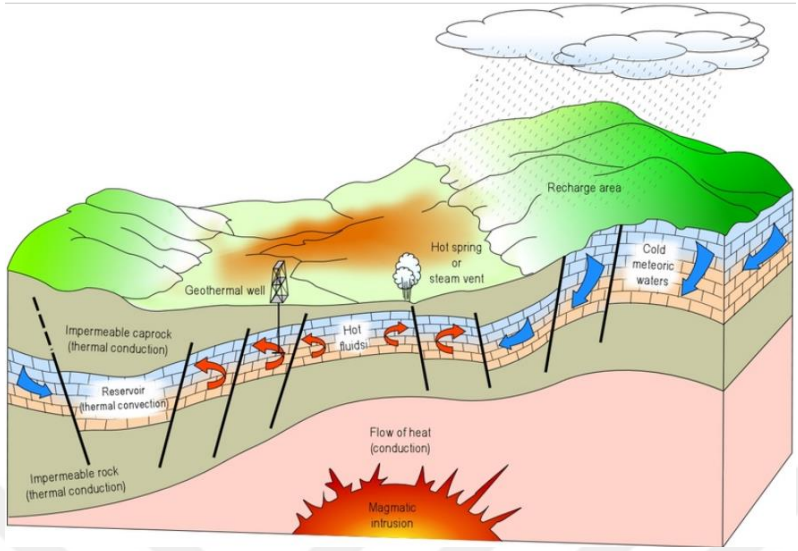

Figure 2.6 : Schematic representation of an ideal geothermal system (Url-7).

In geothermal systems, the meteoric water filters into the deeper parts of the Earth, is heated by the heat source magma and circulate to the surface via faults and fractures supplying a network between inside and outside of the lithosphere.

The classification and sub-division of geothermal sources is given by Muffler and Cataldi (1977). These subdivisions are illustrated through a modified McKelvey diagram (Figure 2.7), in which the degree of geologic assurance regarding resources is set along the horizontal axis and the economic/technological feasibility (often equivalent to depth) is set along the vertical axis (Muffler and Cataldi, 1977).

The economical feasibility of geothermal sources decreases as the depth increases based on Figure 2.7. Resource term covering also reserves indicates economic, sub-economic which is the usable part and a portion of the residual amount of the geothermal source as being discovered plus undiscovered.

Heat transfer in earth occurs in two different ways; conductively by rocks is called hot dry rock, as being the main issue of EGS (Enhanced or Engineered Geothermal Systems) which has no application in our country by now, and convectively by the liquid itself. It also should be stated that EGS could be applied both to conductive and convective systems. In this thesis only liquid dominated systems are studied for their potential of electricity production.

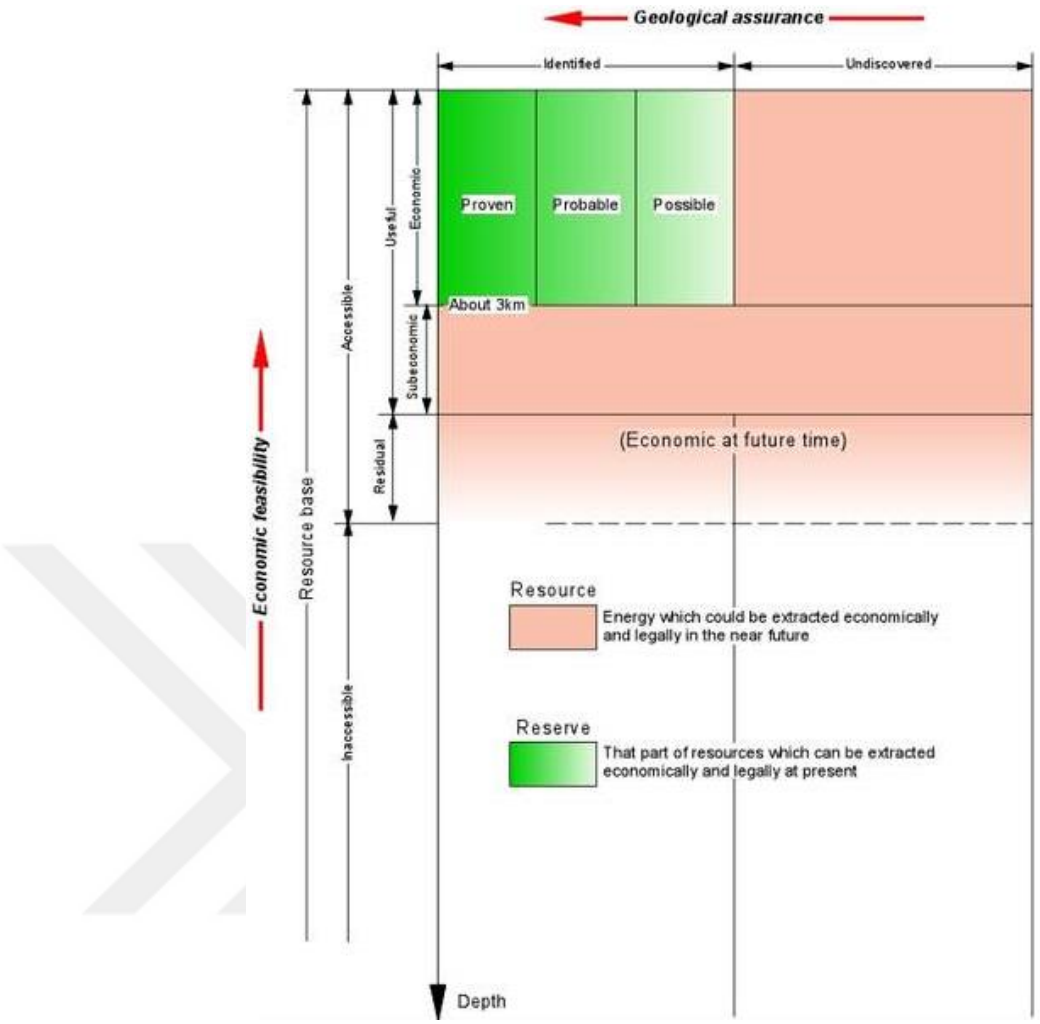

Figure 2.7 : McKelvey Diagram showing the sub-divisions and sub-categories of geothermal systems (modified from Muffler and Cataldi, 1977).

Geothermal energy is a kind of clean and renewable energy with the advantages of thermal purposes such as heating of buildings, big shopping centers, hotels, maintaining supply to greenhouses but the most important advantage of geothermal energy is electricity generation according to the source temperature of geothermal water.

Geothermal systems may be divided into three temperature classes such as low-temperature (<90^{o}C), moderate-temperature (90 - 150^{o}C), and high-temperature (>150^{o}C) (White and Williams, 1975; Muffler, 1979; Williams et al., 2008b). A somewhat similar classification is also given by Bodvarsson (1964) and Axelsson

and Gunnlauggsson (2000) as shown in Table 2.1, which is taken from Saemundsson (2009).

Table 2.1 : Classifications of geothermal systems on the basis of temperature, enthalpy and physical state (Bodvarsson, 1964; Axelsson and Gunnlaugsson 2000).

Low-temperature (LT) systems with reservoir temperature at 1 km depth below 150 ^{o}C. Often characterized by hot or boiling springs. ***Medium-temperature*** (MT) systems with reservoir temperature at 1 km depth between 150-200 ^{o}C.	***Low-enthalpy*** geothermal systems with reservoir fluid enthalpies less than 800 kJ/kg, corresponding to temperatures less than about 190 ^{o}C.	***Liquid-dominated*** geothermal reservoirs with the water temperature at, or below, the boiling point at the prevailing pressure and the water phase controls the pressure in the reservoir. Some steam may be present.
High-temperature (HT) systems with reservoir temperature at 1 km depth above 200 ^{o}C. Characterized by fumaroles, steam vents, mud pools and highly altered ground.	***High-enthalpy*** geothermal systems with reservoir fluid enthalpies greater than 800 kj/kg.	***Two-phase*** geothermal reservoirs where steam and water co-exist and the temperature and pressure follow the boiling point curve. ***Vapour-dominated*** geothermal systems where temperature is at, or above, the boiling point at the prevailing pressure and the steam phase controls the pressure in the reservoir. Some liquid water may be present.

It is worth nothing that all geothermal reservoirs discovered in Turkey until now are liquid-dominated geothermal systems. So, based on Table 2.1, a liquid-dominated geothermal reservoir is defined as the one with the water temperature at, or below, the boiling point at the prevailing pressure and the water (or geothermal brine) phase controls the pressure in the reservoir. Some non-flowing discontinuous steam phase may be present.

High-temperature systems include both liquid- and vapor-dominated resources. Moderate-temperature systems are almost exclusively liquid-dominated, and all low-temperature systems are liquid-dominated.

All three temperature classes are suitable for direct use applications, but in general moderate- and high-temperature systems are viable for electric power generation. Systems at the upper end of the low-temperature range can be exploited for electric power generation if sufficiently low temperatures are available for cooling the working fluid in a binary power plant (Williams et al., 2011).

Other thermal classification systems have been proposed, with most focusing on dividing geothermal resources into a similar set of three or, more simply, two classes that define a progression from low to high temperature (or enthalpy) geothermal resources (Figure 2.8).

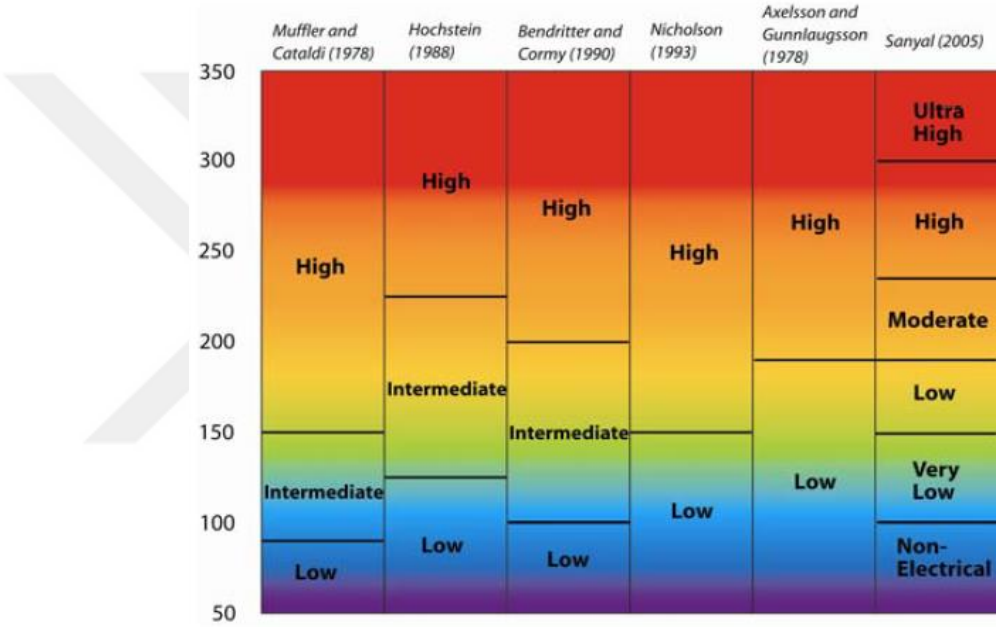

Figure 2.8 : Example classifications of geothermal resources by temperature (Celsius) (Williams et al., 2011).

In each case the temperature/enthalpy boundaries are set at temperatures thought to be significant in either a thermodynamic or an economic utilization context. This approach has been refined to the greatest degree by Sanyal (2005), who proposed a series of divisions focused on thermal boundaries of significance to the geothermal developer. For example, the boundary at 100 °C is tied to the boiling point of water, whereas that at 190 °C is related to the ability of geothermal wells to self-flow (as opposed to requiring pumping of reservoir fluids) (Williams et al., 2011).

Today it is possible to generate electricity commercially by using binary power plant systems with resource temperature values between 200 ^{o}C down to 57 ^{o}C (Url-8) where a second fluid such as iso-butane, iso-pentane, having lower saturation

temperature values and some other advantages works together with the essential geothermal liquid. Besides, for resource temperature values higher than 180 ^{o}C flash power conversion systems are preferred to be constructed to achieve most efficient power conversion from the geothermal liquid.

2.3 Geothermal Energy in Turkey

Turkey can be considered as rich in geothermal energy due to the very active tectonic regimes at the north, south and western regions (see Fig. 2.4). Geothermal exploration activities were started by MREI in 1962 in Turkey. At first, the work was focused on high enthalpy fields for potential power production; Kızıldere was discovered in 1968. The Balçova and Seferihisar, two medium-temperature geothermal fields, were found and studied in the 1960s and 1970s, respectively. A second high-enthalpy system, Germencik, and various other medium-enthalpy fields, such as Salavatlı-Sultanhisar and Simav, were discovered in the 1980s. Turkey's low and medium temperature resources have yet to be thoroughly explored and evaluated (Serpen et al., 2010). Today maximum recorded resource temperature is 287.5 ^{o}C in Manisa Alaşehir geothermal field as recorded by MREI (Akkuş, 2016).

Geothermal potential areas with highest source temperatures are clustered especially in the West Anatolia where Büyük Menderes, Küçük Menderes and Gediz grabens have been located with 78% rate (Figure 2.9) (Serpen et al., 2010), 9% is located in the central Anatolia, 7% is located in Thrace Basin, 5% is located in the Eastern Anatolia and the others cover 1% portion of the total potential in Turkey.

According to the resource temperature map prepared by MREI, the hottest areas are located in the Western and central parts of Turkey. Also some indications of hot waters could be seen in the eastern part of Turkey. Red filled areas show the geothermal resource temperatures higher than 100 ^{o}C. (Figure 2.10) (MREI). The information on Figure 2.10 is based on the data obtained from exploration and production geothermal wells drilled in Turkey.

However it should be noted that drilled well intensity is not the same for all the regions in Turkey; drilled wells are very much denser in the Western part where the Büyük Menderes, Küçük Menderes and Gediz grabens are located. 1559 geothermal wells have been drilled in Turkey up until now. Well distribution by regions is presented at Figure 2.11 (Akkuş and Alan, 2016). MREI has drilled 596 of these

wells; 319 geothermal fields are discovered and the total available heat capacity from all these wells is stated as 16098.8 MWt. Total direct use installed capacity is stated as 3272 MWt which shows that the utilization from the total available heat is around 20% (Akkuş and Alan 2016).

Table 2.2 shows the installed capacity in Turkey with the field and company names by the end of January 2016 (Akkuş and Alan, 2016).

Based on Akkuş and Alan (2016), MREI estimates the total geothermal potential of Turkey as 31500 MWt but this estimate is debatable as its basis of estimation or calculation cannot be found in the literature.

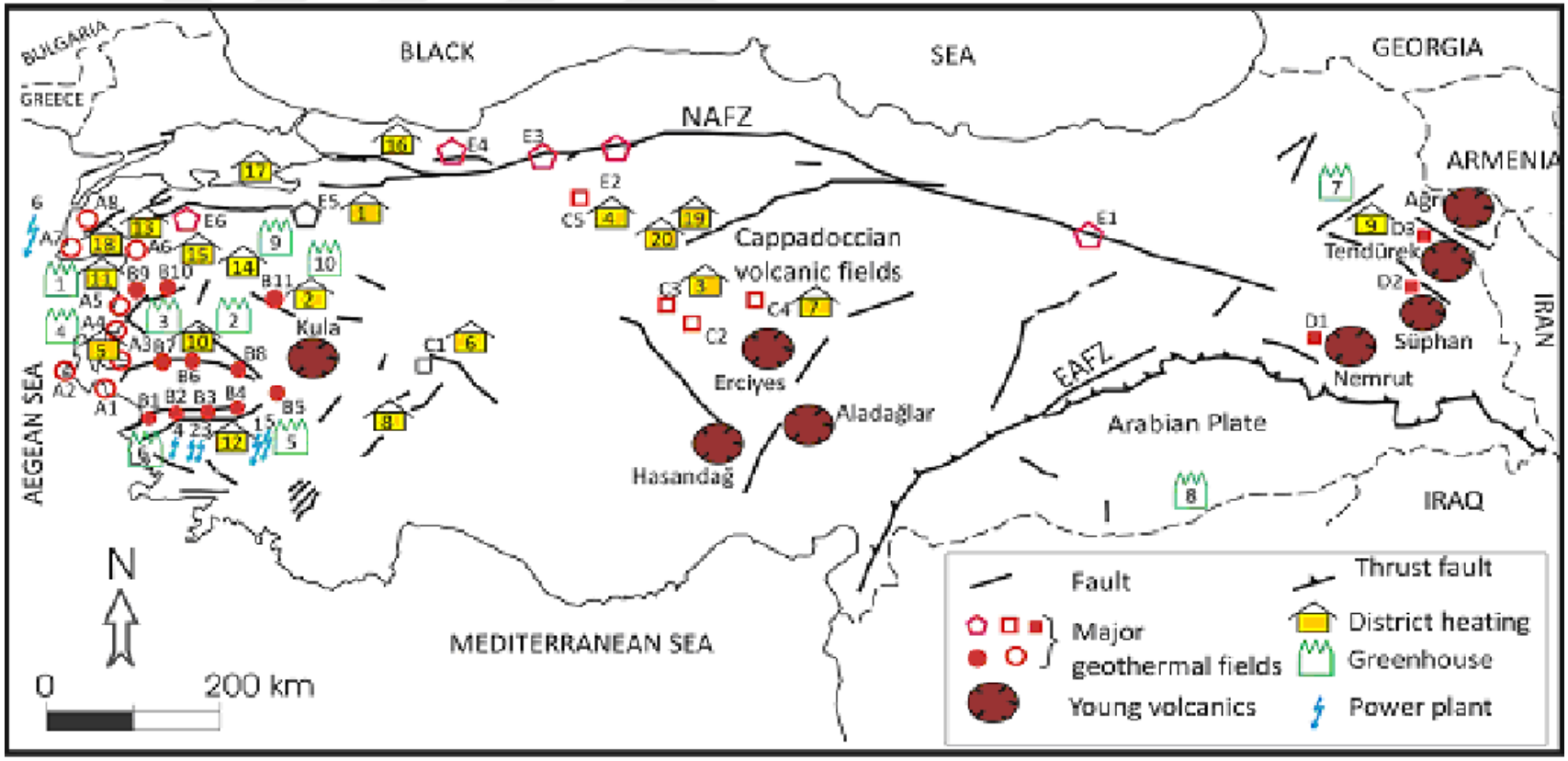

Figure 2.9 : Geothermal resources of Turkey (Serpen et al., 2010).

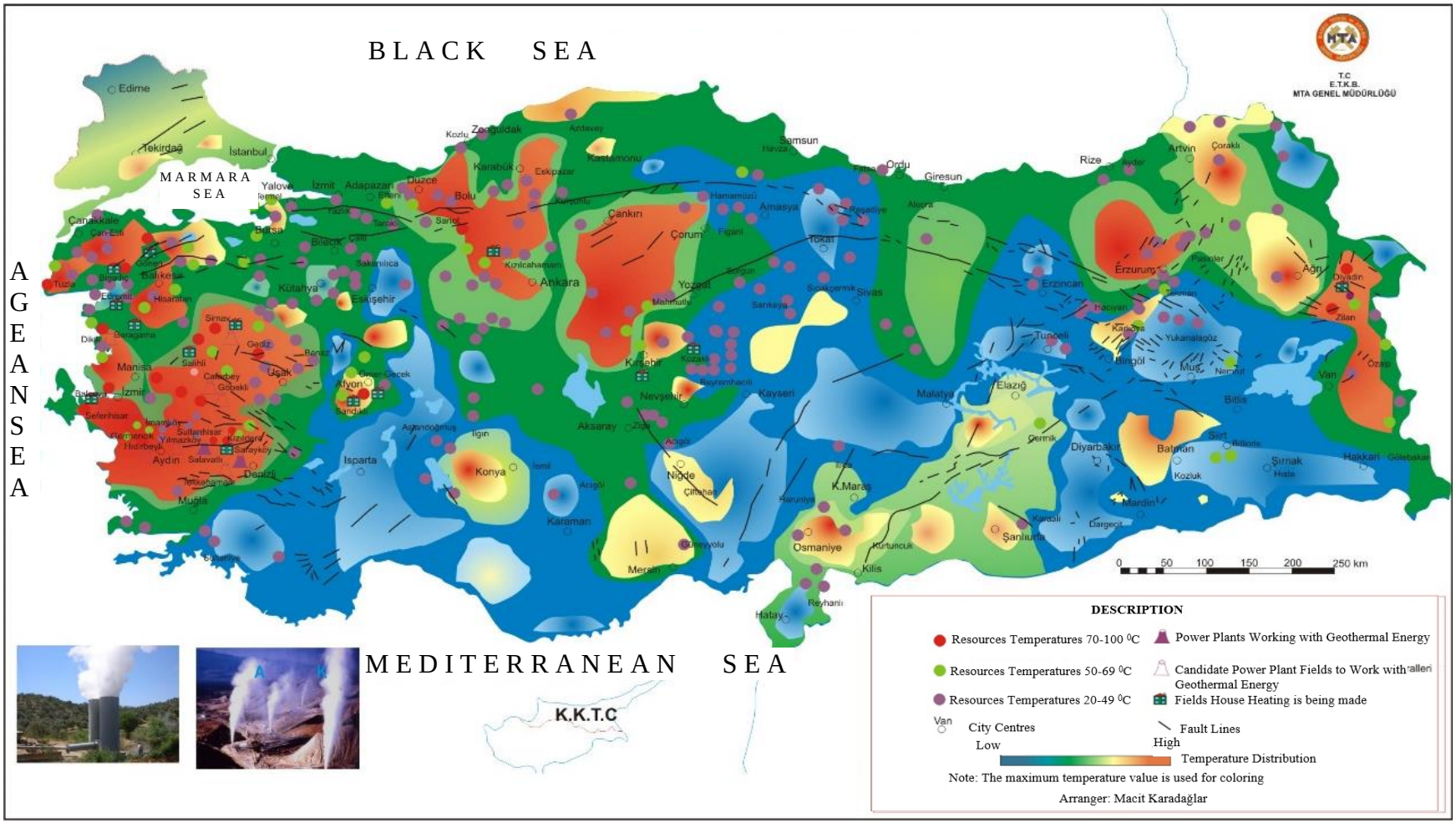

Figure 2.10 : Geothermal resource temperature map of Turkey (modified from MREI, Url-9).

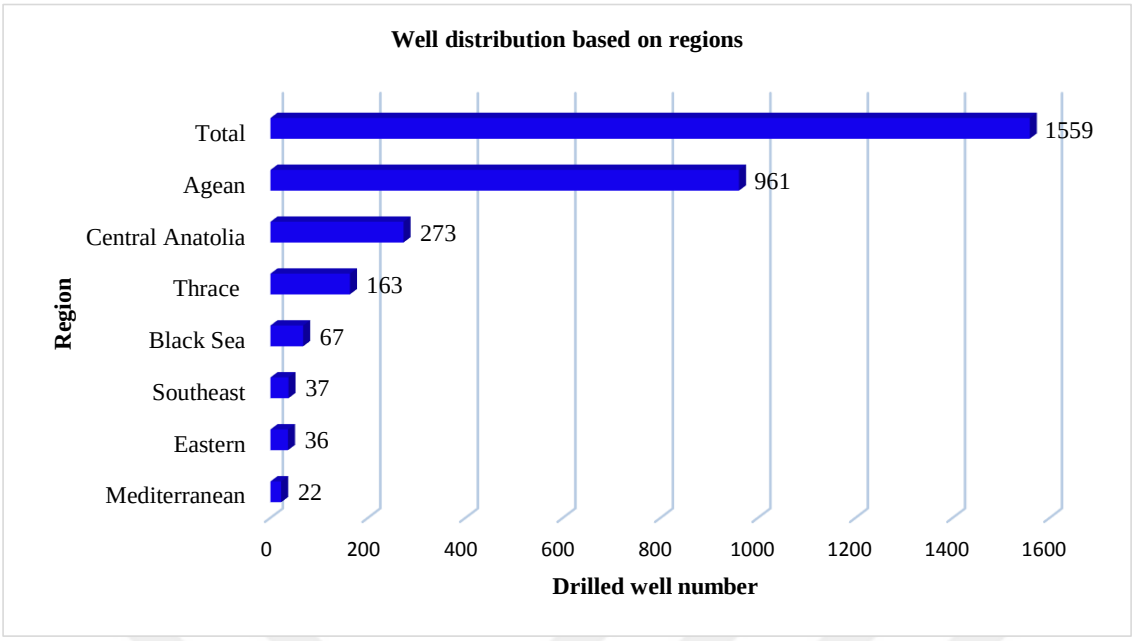

Figure 2.11 : Drilled geothermal well distribution by regions in Turkey (Akkuş and Alan, 2016).

Besides this estimate of MREI, in fact there are different estimates of the total geothermal potential of Turkey given by various sources; for example Başel et al., (2013) gives 50400 MWt (P50, Monte Carlo Simulation), Yılmazer gives 55000-60000 MWt and Turkey Geothermal Society gives 62000 MWt as mentioned in Akkuş and Alan's 2016 report.

A similar difference in estimations exists for the potential of electricity generation in Turkey. Based on Satman (2016), MREI estimates this value as 1200 MWe whereas Başel et al., (2013) predict it as 2263 MWe (P50, Monte Carlo Simulation Method). In her PhD thesis, Başel (2010) worked on 25 geothermal fields which are interpreted as amenable fields for electricity generation by using the MIT method. Başel (2010) predicted the power generation potential of these 25 geothermal fields as (based on an arithmetic sum): P10 = 840 MWe, P50 = 1428 MWe, and P90 = 2371 MWe. In 2013, Başel et al. presented an updated power generation potential of Turkey covering 38 geothermal fields, as presented in Table 2.3 below.

In their 2013 estimations, no information has been given for the field names and the other reservoir parameters used in simulations in 2013 work of Başel et al.

Table 2.2 : Installed capacity in Turkey by the end of January, 2016 (Akkuş and Alan, 2016).

City/District	Field Name	Company	Installed Capacity (MWe)	Resource Temperature (T_R, °C)	Type of power station****
Denizli/Sarayköy	Kızıldere	Zorlu Electricity Production	95	242	Single Flash+Triple Flash
Manisa/Alaşehir	Alaşehir		45	240.3	Double Flash
Denizli/Sarayköy	Kızıldere	Bereket Enegy Production	6.85	242	Binary
Aydın/Germencik	Ömerbeyli	Gürmat Electricity	162.3	239.51	Double Flash
Aydın/Germencik	Hıdırbeyli/Bozköy	Maren	92	141.78	Binary
Aydın/Kuyucak	Pamukören	Çelikler Geothermal	67.53+22.51	188.24	Binary
Aydın/Germencik	Gümüşköy	Gümüşköy Geothermal	13.2	165	Binary
Manisa/Alaşehir	Alaşehir	Türkerler Geothermal E	24	240.3	Binary
Aydın/Sultanhisar	Salavatlı	Menderes Geothermal	51.451	172.5	Binary
Çanakkale/Ayvacık	Tuzla	Tuzla Geothermal Energy	7.5	175	Binary
Çanakkale	Babadere	MTN Energy	8	225*	Binary
Aydın	Yılmazköy	Kipaş Enegy	24	190	Binary
Denizli/Sarayköy	Tosunlar	Akça Energy	3.807	242**	Binary
Aydın	Umurlu	Karkey	12	155***	Binary
		Total Installed Capacity (MWe):	**635**		

*Url-10

**Url-11

***Url-12

**** Type of power station information is taken from the "Geothermal Power Plants" Google Earth map from Haklıdır (2016), (Figure 3.1)

Table 2.3 : Prediction of geothermal electricity potential of Turkey (data taken from Başel et al., 2013).

Geothermal Potential (Electricity Generation)				
Number of Fields	T_R (°C)	MWe		
		P10	P50	P90
38	>100 C	1673	2263	3140

The results given in Table 2.3 were obtained by using the MIT volumetric method (to be discussed in Chapter 4 in this thesis) by taking a reference or abandonment temperature as 100 °C without consideration of any specific power generation system (single flash or binary) and the summation of the electric power generation of the geothermal fields was made arithmetically considering Turkey geothermal fields are fully independent from each other and probabilistically considering Turkey geothermal fields are related and dependent systems to each other both. The resultant electricity power generation estimations (P10, P50 and P90) are given in terms of arithmetic averages of arithmetic and probabilistic summations.

The first 16 fields given by Akkuş (2016) are the common studied fields by Başel PhD dissertation (2010) and is presented on MREI website with resource temperature values as could be seen at Figure 2.12.

Today Turkey has 39 geothermal fields amenable to electricity production as listed with their resource temperatures in Table 2.4 (Akkuş, 2016).

In this thesis, the electricity generation potential of Turkey based on the 25 fields where were considered in Başel PhD study is examined by using AUP method with the application of the Garg and Combs method (2015) considering installed power conversion system thermodynamic properties and using the second law of thermodynamics considering enthalpy and entropy changes of the reservoir fluid. Above 180 °C single or double flash power conversion systems are installed to generate electricity effectively. Garg and Combs (2015) approximation to electricity generation potential offers proper applications to power generation potential considering different power conversion systems and gives very realistic results of power generation potential of geothermal reservoirs.

In the last section of this thesis for the calculation of volumetric heat capacity and electricity production potential of the fields, all reservoir parameters will be taken from Başel's PhD dissertation (2010) as area, thickness, porosity, volumetric specific heat capacity of water etc.. to be able to make correlations between the results.

Figure 2.12 : Geothermal fields amenable to electricity production (MREI, Url-13).

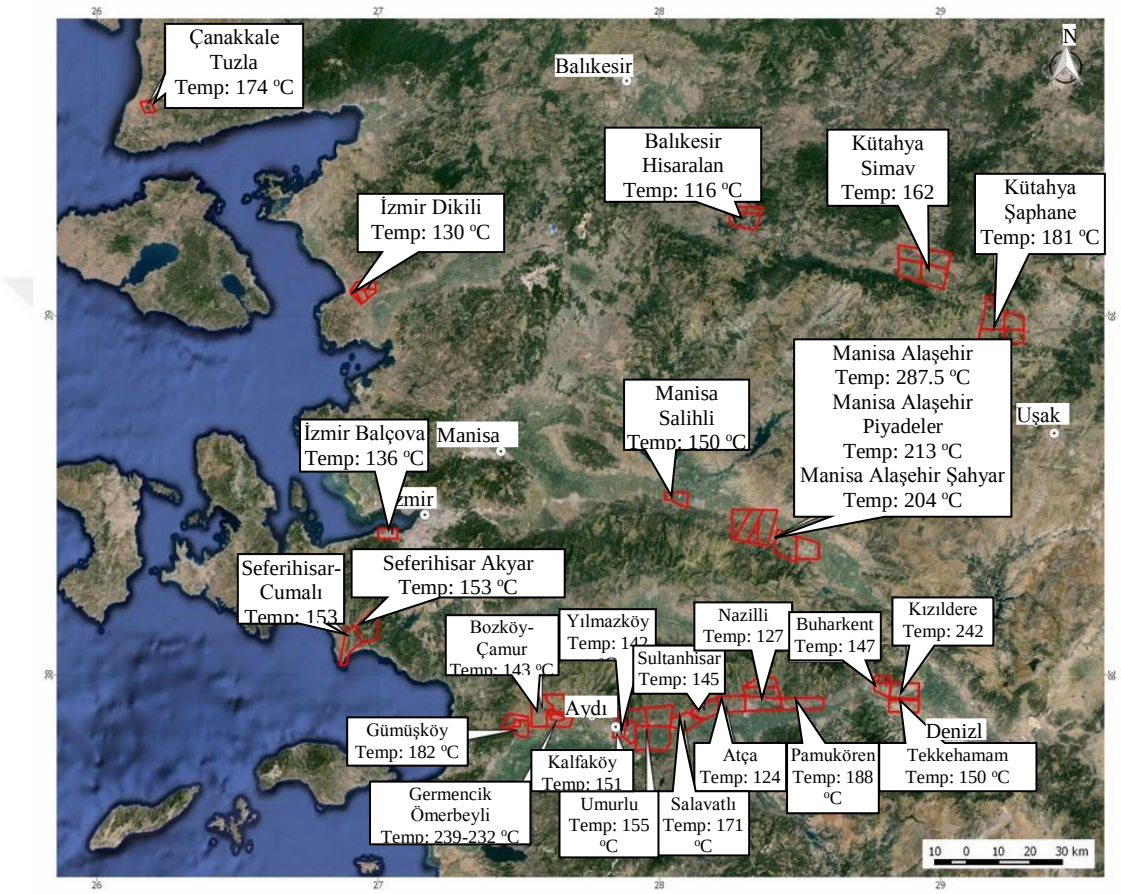

Table 2.4 : 39 geothermal fields amenable to electricity production in Turkey (Akkuş, 2016).

Number	Field Name	Resource Temp (C)
1	Manisa-Alaşehir-Köseali	287.5
2	Aydın-Atça	123.36
3	İzmir-Balçova	143.7
4	İzmir-Dikili	130
5	Aydın-Germencik	239.51
6	Aydın-Gümüş	165
7	Denizli-Kızıldere	242
8	Aydın-Nazilli-Güzelköy	127.36
9	Aydın-Pamukören	188.24
10	Manisa-Salihli-Caferbey	150
11	Aydın-Umurlu-Serçeköy	149.52
12	Aydın-Salavatlı	172.5
13	İzmir-Seferihisar-Cumalı	145
14	Kütahya-Simav-Eynal-Naşa	164
15	Denizli-Sarayköy-Tekkehamam	150
16	Çanakkale Tuzla	175
17	Kütahya-Şaphane-Karamanca	181.2
18	Denizli-Buharkent	144
19	Aydın-Sultanhisar	146
20	Aydın-Kalfaköy	151.52
21	Aydın-Yılmazköy	190
22	Aydın-Nazilli-Bozyurt	140.31
23	Aydın-Hıdırbeyli	141.78
24	Aydın-Sultanhisar-Malgaçemir	128
25	Denizli-Bölmekaya	147
26	Denizli-Sarayköy-Gerali	114
27	İzmir-Aliağa-Güzelhisar	109.54
28	İzmir-Dikili-Hanımçiftliği	145.38
29	İzmir-Seferihisar-Akyar	141.18
30	Manisa-Alaşehir-Kurudere	213.43
31	Manisa-Alaşehir-Türkerler	220
32	Manisa-Alaşehir-Kemaliye	240.3[1]
33	Manisa-Salihli-Kurşunlu	117
34	Manisa-Salihli-Aytemiz	236
35	Manisa-Salihli-Göbekli	182
36	Manisa-Sarıgöl-Alemşahlı	125.21
37	Nevşehir-Derinkuyu-Suvermez	117.5
38	Nevşehir-Göre	183
39	Nevşehir-Kepez	124

[1]Resource temperature value for Manisa-Alaşehir-Kemaliye is estimated by taking the arithmetic average of the recorded temperature values in other Manisa-Alaşehir geothermal fields.

2.4 Geothermal Energy In The World

In the world, tendency to use geothermal energy is increasing because it is a kind of energy that is continuous, renewable, clean and cheap. Low enthalpy geothermal waters having source temperatures lower than 100 ºC is used for direct usage and by the end of 2015, 82 countries are using their low enthalpy geothermal waters for direct use purposes. Direct applications of worldwide geothermal sources in 2015 are presented at Figure 2.13 with distributions by percentage of total installed capacity (MWt) (Lund and Boyd, 2015).

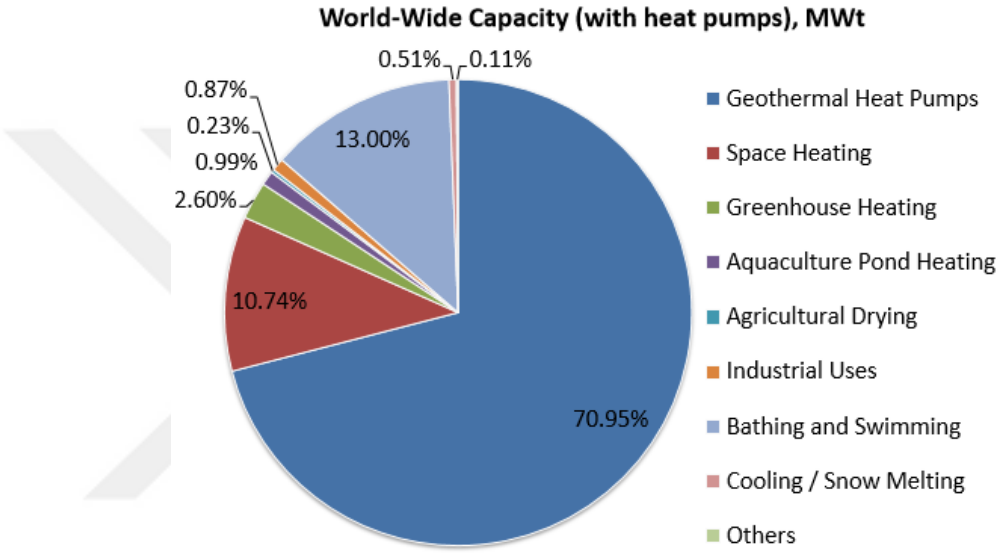

Figure 2.13 : Geothermal direct applications worldwide in 2015 with distributions by percentage of total installed capacity (MWt) (Lund and Boyd, 2015).

Geothermal direct applications worldwide in 2015 is presented at Figure 2.14 with distributions by percentage of total energy used (TJ/yr) (Lund and Boyd, 2015).

Table 2.5 is a summary, by top five countries in the world, of the installed thermal capacity (MWt), annual energy use (TJ/yr and GWh/yr) and the capacity factors by the end of 2015 (Lund and Boyd, 2015).

Turkey is the top 4th country in installed thermal capacity (MWt) in the world by the end of 2015. Also it should be noted that Turkey's installed thermal capacity is increased up to 3272 MWt (Akkuş and Alan, 2016 and Satman, 2016). Moderate to high enthalpy geothermal waters having resource temperatures higher than 100 ºC are used for power generation. The global market is at about 13.3 GW of operating capacity as of January 2016, spread across 24 countries.

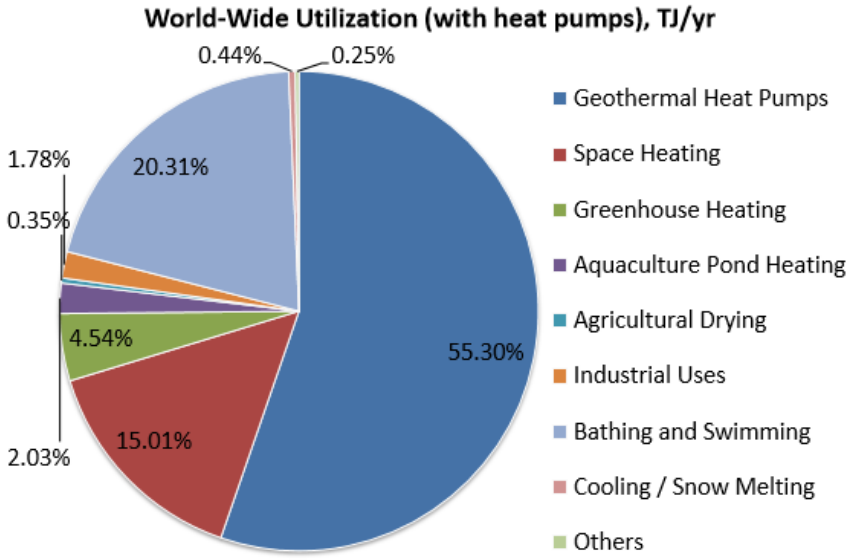

Figure 2.14 : Geothermal direct applications worldwide in 2015 with distributions by percentage of total energy used (TJ/yr) (Lund and Boyd, 2015).

Table 2.5 : Installed thermal capacity (MWt), annual energy use (TJ/yr and GWh/yr) and the capacity factors to the end of 2015, by top five countries, (Lund and Boyd, 2015).

Country	MWt	TJ/yr	GWh/yr	Load Factor
China	17,870	174,352	48,435	0.31
United States	17,416	75,862	21,075	0.14
Sweden	5,600	51,920	14,423	0.29
Turkey	2,886	45,126	12,536	0.5
Germany	2,849	19,531	5,426	0.22
GRAND TOTAL FOR THE WORLD	70,329	587,786	163,287	0.27

Based on current data, the global geothermal industry is expected to reach about 18.4 GW by 2021. Overall, if all countries follow through on their geothermal power development goals and targets the global market could reach 32 GW by the early 2030s (Annual U.S. & Global Geothermal Power Production Report, 2016).

Figure 2.15 presents geothermal power operating capacity in the world including top 21 countries. Today Turkey is located at the 8th order in installed electricity capacity in the world in comparison with the values recorded by the end of March 2016 and February 2015 (Annual U.S. & Global Geothermal Power Production Report, 2016).

Based on Figure 2.15 Turkey has made a remarkable improvement by increasing its installed capacity from 410 MWe in 2015 to 637 MWe in 2016 in comparison to the other top countries producing electricity from their geothermal resources.

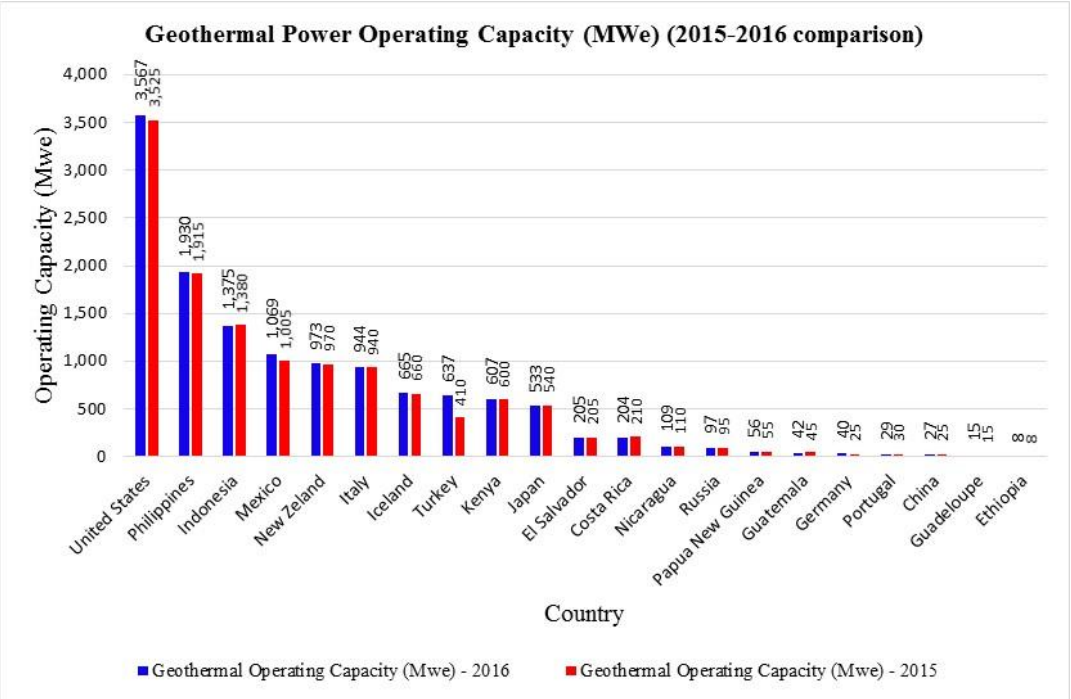

Figure 2.15 : Geothermal Power Operating Capacity by Country in comparison with 2015 and 2016 values (Data obtained from Annual U.S. & Global Geothermal Power Production Report, 2015 and 2016).

3 . GEOTHERMAL POWER PLANTS FOR POWER GENERATION

Electricity is the best energy type to be used by human. Different types of power plants are being constructed to be able to convert geothermal heat into electricity with changeable efficiency ratios. These power plants have been designed by considering the resource temperature of the geothermal water and differ to dry steam, single flash power plants to double flash, triple flash, binary, combined or integrated hybrid type of power plants.

Figure 3.1 shows the Büyük Menderes, Küçük Menderes Grabens with geothermal license areas and installed power plant types in Turkey (modified from Haklıdır, 2016).

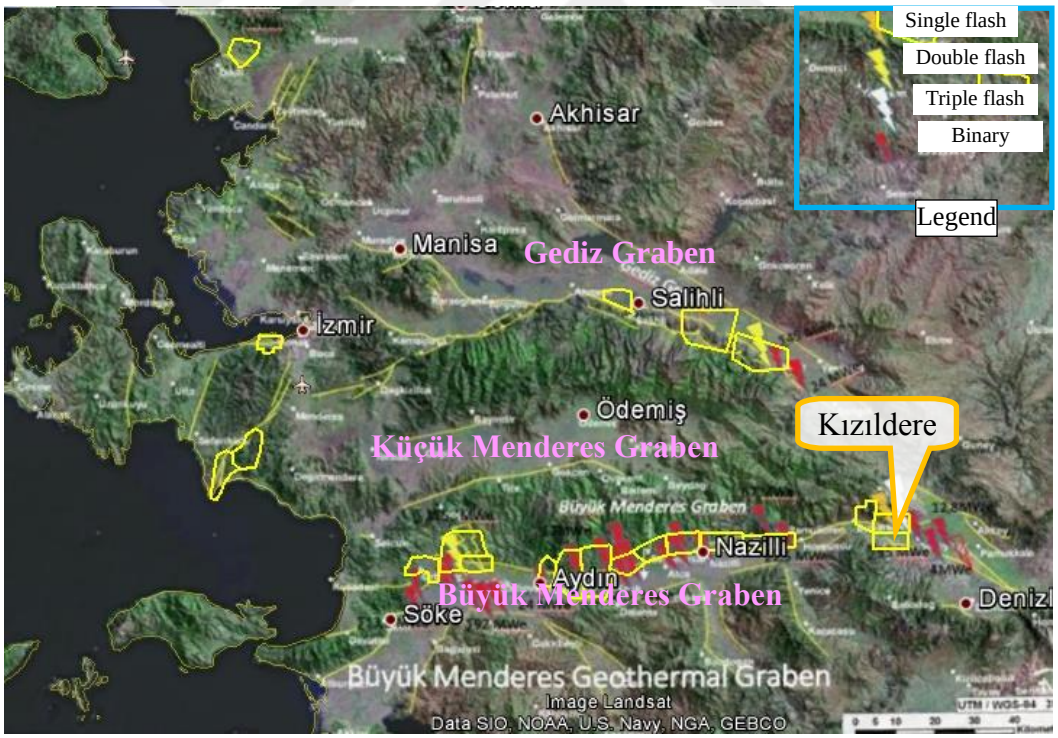

Figure 3.1 : Geothermal power plants in Turkey (modified from Haklıdır, 2016).

As can be seen from Fig. 3.1, nearly all geothermal power plants are binary type in Turkey. By considering 21 geothermal power plants amenable to electricity

production drawn on Figure 3.1, 81% of the power cycles are constructed as binary. On the other hand, by considering that recently we have totally 39 geothermal fields that amenable to electricity production (Akkuş and Alan, 2016) which are not indicated on Figure 3.1 supplied from Haklıdır (2016), 89.7% of the installed geothermal power plants are worked by binary power conversion cycles in Turkey.

3.1 Single-Flash Power Plants

Single-flash power plants are constructed only for liquid-dominated geothermal systems for electricity conversion of geothermal water with resource temperature higher than 180 ºC, which is known as the most efficient power cycle to produce energy with maximum efficiency (Zarrouk and Moon, 2014). In a single-flash power plant, the geothermal water loses pressure while rising to the surface inside wellbores from a few kilometers depth of the earth against the gravitation and frictions inside the pipes, and some of the water turns into steam by reduction of pressure at the upper elevation of the wellbore. Steam and hot water are separated by a separator, and the steam is sent to turbine to run the electricity generator. The leftover hot water is condensed by a condenser, and the cooled water is re-injected into the same reservoir level by an injection well to be able to avoid the reservoir pressure drop.

Figure 3.2 presents a schematic of a single-flash power plant (Kagel, 2008).

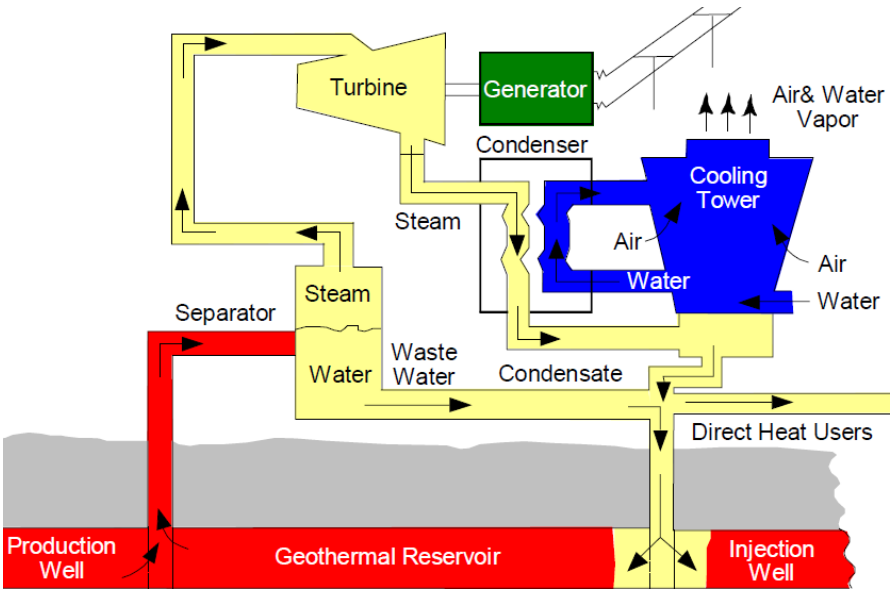

Figure 3.2 : Single-flash power plant (Kagel, 2008).

3.2 Binary Power Plants

Binary power plants are constructed for geothermal reservoirs having resource temperatures between 73-180 ^{o}C (Zarrouk and Moon 2014). In some references, the lower temperature limit to use a binary plant is given as low as 57 ^{o}C (see Url 7). In some references, the lower temperature limit is reported as 90 ^{o}C (see Url-14). It seems that there is no consensus on the working lower temperature value for binary systems in the literature. In binary power plant cycles, a second working fluid, usually a hydrocarbon (see Table 3.1), with much lower boiling temperature than the geothermal water is used to be able to generate electricity. The candidate second working fluid list is given at Table 3.1 below (DiPippo, 2012). Figure 3.3 is a schematic presentation of a binary power plant (Kagel, 2008).

Table 3.1 : Candidate second working fluid list (DiPippo, 2012).

Fluid	Formula	T_c °C	T_c °F	P_c MPa	P_c lbf/in^2	P_s @ 300 K MPa	P_s @ 400 K MPa
Propane	C_3H_8	96.95	206.5	4.236	614.4	0.9935	n.a.
i-Butane	i-C_4H_{10}	135.92	276.7	3.685	534.4	0.3727	3.204
n-Butane	C_4H_{10}	150.8	303.4	3.718	539.2	0.2559	2.488
i-Pentane	i-C_5H_{12}	187.8	370.1	3.409	494.4	0.09759	1.238
n-Pentane	C_5H_{12}	193.9	380.9	3.240	469.9	0.07376	1.036
Ammonia	NH_3	133.65	272.57	11.627	1686.3	1.061	10.3
Water	H_2O	374.14	705.45	22.089	3203.6	0.003536	0.24559

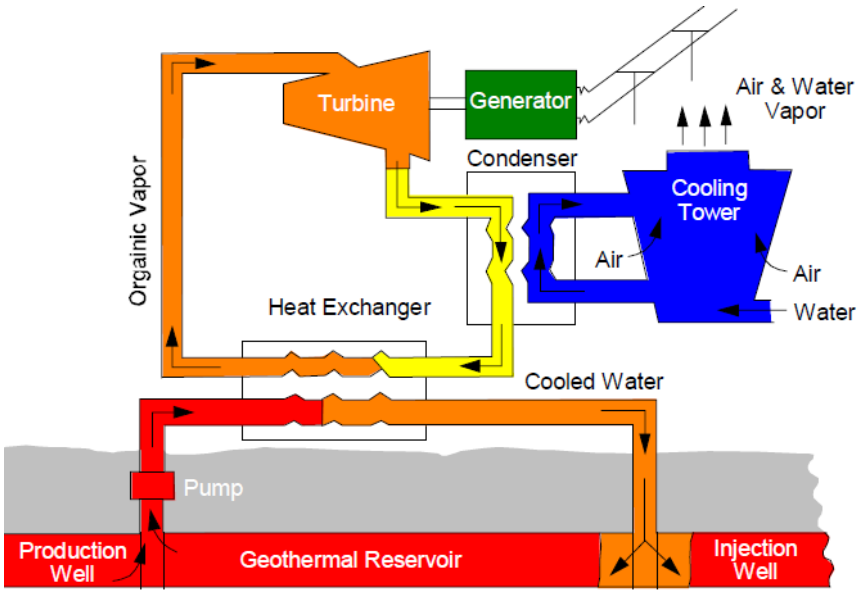

Figure 3.3 : Binary power plant (Kagel, 2008).

In binary power cycles, heat exchangers are used to transfer heat from geothermal brine to the second working fluid without mixing and the vaporized second working fluid goes into turbine to start generator for electricity generation. Cooled water is pumped back into the reservoir level by injection well and the condensed second working fluid returns back into the power cycle system to be heated again by the geothermal water and the process continues.

3.3 Sophisticated/Hybrid Power Plants

Hybrid power plant systems can also be constructed in the form of;

- Combined single and double hybrid power plant systems
- Integrated single and double hybrid power plant systems
- Combined flash-binary hybrid power plant systems
- Integrated flash-binary hybrid power plant systems (DiPippo, 2012).

Hybrid systems have been used effectively to take advantage of the benefits of both technologies. In this type of plant, the flashed steam is first converted to electricity with a steam turbine, and the low-pressure steam exiting the backpressure turbine is condensed in a binary system. This allows for the effective use of air cooling towers with flash applications and takes advantage of the binary process. The flash/binary system has a higher efficiency where the well-fields produce high pressure steam. This type of system has been operating in Hawaii since 1991 at the Puna Geo Venture facility (Kagel 2008).

In early exploration and exploitation phase of geothermal resources one should be careful about choosing just one type of geothermal power plant conversion system due to the lack of the knowledge of detailed contamination and specific character of the resource before enhanced testing of the reservoir by drilled wells. Otherwise the construction of integrated or combined power plants at early stage of exploration makes the situation much more complicated to be solved about the parameters affecting the conversion efficiency of the power plant.

In this work, we will consider the basic two types of power plants, namely single-flash and binary, when determining electricity generation potential of geothermal fields as the hybrid or sophisticated combination of power plants will certainly have higher efficiencies that these two basic types. So, our estimates of electricity

generation potentials to be given in this thesis can be considered as the potentials that would be obtained if one of these two basic power plants is installed for a given geothermal field and hence, it is possible that one can produce higher values of electricity generation potential if a hybrid or combination of these two basic power plants is installed for the geothermal field in consideration.

3.4 Power Plant Energy Conversion Efficiency

The first law of thermodynamics is called as conservation of energy which denotes that existing energy cannot be destroyed or created; it can only be converted to another kind of energy. In fact we use the heat energy of a geothermal system to generate electricity while working with geothermal power conversion systems just as described in the first law of thermodynamics (Çengel and Boles, 2014).

The second law of thermodynamic looks into the energy conversion phenomenon in a different perspective and denotes that energy cannot be converted completely to another type of energy without losses. In geothermal power plant energy conversion process, we lost some amount of energy spread out to surface because of entropy changes of the system. Exergy analysis are done by concerning the entropy changes of the system to predict the conversion efficiency of each individual component of the conversion system and the results of these kind of studies are used for optimization purposes of maximum available energy or availability on a constructed specific type of conversion system (Çengel and Boles, 2014).

Power plant efficiencies differ according to the conversion efficiency of the system related to the power plant type such as single flash, binary flash, double flash, hybrid based on the resource temperature of the geothermal reservoir liquid, the non-condensable gasses such as H_2S, N_2, CO_2, mineralogy such as rich silica content causing silica scaling in the wellbore and pipes, total dissolved solids (TDS), chlorine ion concentration (salinity) and also the atmospheric ambient temperatures changing from one place to another geographically (Çengel and Boles, 2014).

Zarrouk and Moon (2014) made a study based on the installed and working 94 different geothermal power plants around the world by using the enthalpy and disregarding the entropy changes occurs during that conversion of energy and they concluded that geothermal power conversion efficiencies are 12% in average.

However, it should be noted that the conversion efficiencies given by Zarrouk and Moon (2014) is based on the 1st law of thermodynamics and hence, do not account for the exergy analysis based on the 2nd law of thermodynamics.

Hence Zarouk and Moon (2014) states in their paper that exergy analysis which is the maximum output that could theoretically be obtained from a geothermal system relative to the surrounding (ambient temperature) is not considered in their work.

Garg and Combs (2015) states that the conversion efficiency depends on the resource temperature, abandonment temperature, and the type of power plant and such conversion efficiencies range from 70% to 85% based on the 2^{nd} law of thermodynamics exergy analysis.

Exergy analysis are done by concerning the entropy changes of the system to predict the conversion efficiency of each individual component of the conversion system and the results of these kind of studies are used for optimization purposes of maximum available energy or availability on a constructed specific type of conversion system.

4. VOLUMETRIC "HEAT IN-PLACE" ESTIMATION METHODS

In petroleum and natural gas industry it is essential to make some mathematical approaches related to the oil or gas initially in place and recoverable amount of this trapped oil and gas potential during the early phases of the exploitation and development of the field. This enables the decision makers to have a vision and plan for the future target and operation schedule of the assets.

Similarly, in the geothermal sector it is very important to get a reasonable idea about the stored "heat in place" and how much of it could be produced and generated. Due to this purpose different volumetric heat in place approaches have been found in the literature. The USGS method has been developed by the US Geological Survey scientists in 1970's, the MIT method in 2006 (MIT, 2006) and Garg & Combs method in 2015. Garg and Combs (2015) showed that usage of the arbitrary values of the reference (abandonment) temperatures and conversion efficiencies in USGS and MIT methods yields unrealistic (particularly too optimistic) predictions of the electric generation potentials of geothermal reservoirs. Hence, they suggested that the thermodynamic properties of the chosen power plant conversion system such as single, double or binary flash based on exergy analysis (using the 2nd law of thermodynamics) should be considered to predict the proper or realistic values of electric power generation potential of a geothermal reservoir. Onur (2015) gave some applied examples of the Garg and Combs (2015) method for a few geothermal fields in Turkey and showed the realistic values of electric generation potential of these fields in comparison with those predicted from USGS and MIT methods.

Before analyzing these methods in details, we need to look at the common background of all these three methods related to stored heat in place and the recoverable amount of this resource potential.

Subsurface heat in place stored is calculated by using the Eq. 4.1 below (Muffler, 1979);

$$q_R = AH\left(\rho c_p\right)_R\left(T_R - T^r\right) \tag{4.1}$$

where q_R is the stored heat in place (kJ), A = Area (m^2), H = Thickness (m), $(\rho c_p)_R$ =volumetric, isobaric specific heat capacity of the liquid saturated rock, T_R = resource temperature (^oC) and T^r = reference or abandonment temperature (^oC).

$(\rho c_p)_R$ (kJ/m^3-^oC) is calculated by using Eq. 4.2 below;

$$\left(\rho c_p\right)_R = \phi\rho_l c_{pl} + (1-\phi)\rho_s c_{ps} \tag{4.2}$$

where ϕ = porosity (fraction), ρ_l and ρ_s are liquid and solid rock density respectively (kg/m^3), c_{pl} and c_{ps} are liquid and solid rock matrix specific heat capacity respectively (kJ/kg-^oC).

Because in this thesis only single-phase liquid-dominated geothermal reservoirs are considered for predicting the electricity production potential, the steam or gas phase is disregarded in the calculation of the $(\rho c_p)_R$. As noted earlier, existence of any dry steam or gas phase dominated geothermal systems in Turkey has not yet been reported.

One cannot produce all the stored energy in the reservoir, can only produce what is possibly recoverable in the wellhead. The amount that can be recovered is accounted by the recovery factor (denoted by R_g in this thesis) which depends on permeability structure (fracture vs. matrix, permeability anisotropy, faulting etc.), production and injection well depths and patterns, and the thermal (heat and fluid recharge from depth) and hydraulic boundary conditions (recharge/discharge along the ground surface and assumed lateral boundaries of the geothermal reservoir) (see Garg and Combs, 2015). Williams (2014) associated the recovery factor with the fracture permeability and explained that even though we have a good fracture porosity dominated reservoir which is characterized by good fracture permeability, we can have relatively low fracture fluid volumes affected by very changeable rock matrix heterogeneity and anisotropy. Permeability is also related to rapid sedimentary deposition environmental circumstances and in situ geo-mechanical status of the rock such as stress and strain and also the fluid chemistry is another issue in determining permeability distribution inside the rock. Williams (2014) has reported a recovery factor ranging from R_g = 0.08 to 0.20 for naturally fractured geothermal reservoirs whereas R_g = 0.1 to 0.25 for sedimentary type geothermal reservoirs.

Also we could have some losses in the wellbore which includes temperature losses inside the drill pipes into the formation and geothermal gradient. So we cannot produce the liquid in the wellhead with the same reservoir temperature. At that point we need to know that our heat recovery in the wellhead is determined by the recovery factor which is defined by Eq. 4.3 below;

$$R_g = \frac{q_w}{q_R} \tag{4.3}$$

where R_g = thermal recovery factor; q_w = heat produced in the wellhead (kJ), q_R = heat stored in the reservoir (kJ).

So one step further in Eq. 4.3 is,

$q_R = \frac{q_w}{R_g}$; then our first Eq. 4.1 turns into the Eq. 4.4 below;

$$q_w = R_g AH\left(\rho c_p\right)_R \left(T_R - T^r\right) \tag{4.4}$$

Also one should consider the thermal recovery factor as "zero" at the very early phases of exploration and development of geothermal reservoirs due to the lack of detailed and well analyzed formation porosity, permeability, fracture system and fluid chemistry. It is possible that one can drill a well and cannot find permeability to produce the fluid.

Mass could be produced at the wellhead (m_w, kg) can be calculated from Eq. 4.5:

$$m_w = q_w / \left(h_w - h^r\right) \tag{4.5}$$

where q_w is the heat produced at the wellhead (kJ), h_w is the enthalpy of produced water at the wellhead at resource temperature (kJ/kg) and h^r is the enthalpy of liquid at the reference, rejection, dead-state, or abandonment temperature (kJ/kg).

Assuming isenthalpic flow (though it is not a very realistic assumption due to heat losses when fluid is rising in the wellbore) in the wellbore and neglecting the work required to raise water to the wellhead, the enthalpy of produced fluid at the wellhead, h_w, is equal to that of liquid water at the reservoir temperature (Garg and Combs, 2015) as shown in Eq. 4.6.

$$h_w = h_R\left(T_R\right) \tag{4.6}$$

To be able to calculate recoverable energy from the reservoir we need to calculate the maximum available work W_A (kJ) (where $W_A=me$). Neglecting kinetic or potential energy effects, the maximum energy output per unit mass of the substance e (kJ/kg) is given by DiPippo, 2008 by Eq. 4.7:

$$e = h - h^r - T_{rk}(s - s^r) \tag{4.7}$$

where h and s denote the enthalpy and entropy of the substance at turbine inlet conditions with temperature T, T_{rk} is the absolute reference temperature (T_{rK} = 15+273.15=288.15 K (Brook et al., 1979), (in the case of the reference temperature is chosen as 15 ^oC) which is the case mostly used in USGS method) and s^r is the entropy of liquid water at the reference temperature T^r. For mass m of the substance, the available work (W_A) is therefore given by Garg and Combs, 2011 by Eq.4.8:

$$W_A = m\left[h - h_r - T_{rK}\left(s - s_r\right)\right] \tag{4.8}$$

As a next step, recoverable energy from a geothermal reservoir is given by Eq. 4.9 below (Muffler 1979);

$$E_r = \eta_c W_A \tag{4.9}$$

where E_r = recoverable energy at the wellhead (kW), η_c=conversion efficiency (fraction), W_A= maximum available work (kJ).

Again it is certain that we cannot convert all the available work into energy completely; we can just convert it by the power conversion efficiency (η_c).

Then to calculate the electricity production potential (*PW*, MWe) from the reservoir we need to use Eq. 4.10 below;

$$PW = \frac{E_r}{10^3 L_F t_p} \tag{4.10}$$

Using Eq. 4.9 in Eq. 4.10 gives Eq. 4.11 below;

$$PW = \frac{\eta_c W_A}{10^3 L_F t_p} \tag{4.11}$$

where L_F = load factor (indicating the percentage of time spent in working condition for the power plant) (fraction), t_p is the project life (indicates the whole life time of the power plant) (seconds) and the 10^3 is the conversion factor from kW to MWe.

4.1 USGS Method

In the 1970s, researchers at the United States Geological Survey (USGS) developed a methodology to quantify the uncertainty of estimates of the geothermal resources associated with an identified hydrothermal convection system (e.g., Nathenson, 1975a; 1975b; Nathenson and Muffler, 1975; Muffler and Cataldi, 1977; Brook, et al., 1979) (Garg and Combs, 2011).

The main issue in USGS methodology is the available power output from the conversion system. Availability is described as the maximum work or power theoretically could be obtained in certain thermodynamic circumstances from a working power system. To achieve the optimum availability from the system, two certain thermodynamic conditions are mentioned by DiPippo (2008);

1. All processes taking place within the system must be perfectly reversible.

2. The state of all fluids being discharged from the system is in thermodynamic equilibrium with the surroundings.

Reversibility means that the thermodynamic system undergoes a process which changes its state but is perfectly reversible without leaving any trace of the process that the system undergone. In fact for a process to be reversible the system must be in thermodynamic equilibrium with the surroundings; otherwise we cannot talk about a reversible process. On the other hand in the irreversibility phenomenon the system stays just in its state and the surroundings changes causing the irreversibility due to the entropy created by the interaction between the system and the surroundings.

Actually we need to be aware that no real power conversion system is eligible or capable to convert the heat energy to electricity power energy completely. These systems can just convert a portion of the available work to electricity power. This portion is determined by the thermal conversion efficiency (η_{th}) of the system.

The first condition requires us to neglect all the irreversibility sources affecting the system such as friction losses, turbulent flow in the wellbore, gravitational forces and

geothermal gradient. By doing this we neglect all the potential and kinetic energy effects on the isolated system which is in thermodynamic equilibrium with its surroundings.

For mass *m* of the substance, the available work (W_A) is given by (Garg and Combs, 2011) as in Eq. 4.12 below;

$$W_A = m\left[h - h^r - T_{rK}\left(s - s^r\right)\right] \tag{4.12}$$

If we use Eq. 4.4 and Eq. 4.5 in the Eq. 4.12, we get the general USGS formulation for the available power at the wellhead as shown in Eq. 4.13;

$$W_{A,USGS} = R_g \mathrm{A} H\left(\rho c_p\right)_R \left(T_R - T^r\right)\left[1 - T_{rK}\frac{\left(s_R - s^r\right)}{\left(h_R - h^r\right)}\right] \tag{4.13}$$

In this Eq., T_{rK} is the absolute reference temperature (T_{rK} = 15+273.15=288.15 K) (in the case of the reference temperature is chosen as 15 ^{o}C), h_R and h^r represent the specific enthalpy values of the liquid at reservoir temperature value and the reference temperature value respectively (kJ/kg) and the s_R and s^r represent the specific entropy values of the liquid at the reservoir temperature and the reference temperature values (kJ/kg-^{o}C) respectively.

In USGS method the reference temperature values are generally accepted as the ambient temperature value 15 ^{o}C but in some applications it could be seen that 40 ^{o}C or 100 ^{o}C ambient or reference temperature values are used as another choices. If we arbitrarily use any of these three different reference temperatures, we will predict three different electricity production potentials for the same reservoir. It should not be forgotten that the chosen reference temperature value play a big role in determining the resulting energy production potential from the geothermal system.

If we have those kinds of alternative choices related to reference temperature and could use them arbitrarily, this will definitely affect prediction of our electric generation potential calculations and increase the uncertainty largely. It should be realized that the chosen reference temperature value plays a big role in determining the resulting energy production potential from the conversion system. Knowing the power conversion factors such as 0.11, 0.18 and 0.4 are arbitrarily chosen and used

in USGS and MIT methods can help to imagine the dimensions of uncertainty better in the usage and the results of these methods.

An illustrative example covering two different cases with respect to T_R resource temperature (150 ^oC and 220 ^oC) and in each, three separate case for the T^r reference temperature (15 ^oC, 40 ^oC, and 100 ^oC) is designed to see the difference more clearly as below. Table 4.1 lists the input parameters for the calculation of totally six different cases to explore the difference in results of electricity production potential in MWe. The enthalpy and entropy input values are calculated by using IAPWS, 1996 according to the reservoir temperature, pressure and reference temperature values. In Case 1, Case 2 and Case 3, T_R resource temperature was taken as 150 ^oC and the T^r reference temperature was changed as 15, 40 and 100 ^oC respectively. For 15 ^oC reference temperature the electricity power potential according to USGS method (PW_{USGS}) is calculated as 46.5 MWe, for 40 ^oC PW_{USGS} =44.5 MWe and for 100 ^oC PW_{USGS} =26.9 MWe.

It could be said that as the T^r reference temperature increases, the PW_{USGS} decreases and the difference between the calculated PW_{USGS} values between Case 1 and Case 2 is 4.27% where the difference between the calculated PW_{USGS} values between Case 1 and Case 3 is 19.6% related to the arbitrarily chosen reference temperature values.

In Case 4, Case 5 and Case 6, T_R resource temperature was assumed as 220 ^oC and the T^r reference temperature was changed as 15, 40 and 100 ^oC respectively. For 15 ^oC reference temperature the electricity production potential according to USGS method (PW_{USGS}) is calculated as 93.82 MWe, for 40 ^oC reference temperature the electricity production potential (PW_{USGS}) is calculated as 91.66 MWe and for 100 ^oC PW_{USGS} =73.83 MWe. Again it could be said that as the T^r reference temperature increases, the PW_{USGS} decreases and the difference between the calculated PW_{USGS} values Case 4 and Case 5 is 2.3% where the difference between Case 4 and Case 6 is 21.3%. So it could also be said that as a result, as T_R resource temperature value increases, our resultant difference in calculated values of PW_{USGS} increases accordingly as the sensitivity increases.

Table 4.1 : Input parameters for the calculation of PW_{USGS}, MWe.

PW_{USGS} , (MWe) input parameters	Case 1	Case 2	Case 3	Case 4	Case 5	Case 6
Area, (A, MMm^2)	20	20	20	20	20	20
Thickness, (H, m)	500	500	500	500	500	500
Resource Temperature, (T_R, ^{o}C)	150	150	150	220	220	220
Resource Pressure, (p_R, bar)	52	52	52	52	52	52
Reference Temperature, (T^r, ^{o}C)	15	40	100	15	40	100
Recovery Factor, (R_g, fraction)	0.12	0.12	0.12	0.12	0.12	0.12
Porosity (ϕ , fraction)	0.3	0.3	0.3	0.3	0.3	0.3
Specific heat capacity of brine ($c_p)_l$, kJ/kg-^{o}C)	4.29201	4.29201	4.29201	4.59231	4.59231	4.59231
Density of brine (ρ_l , kg/m^3)	919.669	919.669	919.669	842.749	842.749	842.749
Specific heat capacity of rock (c_{pS} , kJ/kg-^{o}C	0.92	0.92	0.92	0.92	0.92	0.92
Density of rock (ρ_s , kg/m^3)	2600	2600	2600	2600	2600	2600
Volumetric specific heat capacity of brine and rock $(\rho c_p)_R$, kJ/m^3-^{o}C)	2858.57	2858.57	2858.57	2835.45	2835.45	2835.45
Absolute reference temperature (T_{rK}, K)	288.15	313.15	373.15	288.15	313.15	373.15
h_R (kJ/kg)	635.107	635.107	635.107	944.378	944.378	944.378
h^r (kJ/kg)	62.9815	167.533	419.166	62.9815	167.533	419.166
s_R (kJ/kg-^{o}C)	1.83656	1.83656	1.83656	2.51235	2.51235	2.51235
s^r (kJ/kg-^{o}C)	0.224463	0.572402	1.30721	0.224463	0.572402	1.30721
Conversion Factor, (η_{th} , fraction)	0.4	0.4	0.4	0.4	0.4	0.4
Load Factor, (L_F, fraction)	0.95	0.95	0.95	0.95	0.95	0.95
Project Life, (t_p, s) (25 years*s)	788940000	788940000	788940000	788940000	788940000	788940000

The result of the calculation is presented at Table 4.2 below;

Table 4.2 : The results of PW_{USGS}, MWe calculation with differences in percentage related to different cases.

Results of PW_{USGS}, MWe for each Case		Difference in percentage (%)	
Case 1	46.48		
Case 2	44.49	4.27	**(Case 1-2)**
Case 3	26.88	19.6	**(Case 1-3)**
Case 4	93.82		
Case 5	91.66	2.3	**(Case 4-5)**
Case 6	73.83	21.3	**(Case 4-6)**

4.2 MIT Method

The MIT method is based on the first law of thermodynamic disregarding the enthalpy and entropy of the system. According to the MIT method, for mass *m* of the substance, the maximum available work (W_A, kJ) is calculated as in Eq. 4.14 below.

$$W_A = m\left[h - h^r\right] \tag{4.14}$$

Using Eqs. 4.4 and 4.5 in 4.14 the resultant Eq. becomes as in Eq. 4.15 as follows;

$$W_{A,MIT} = R_g AH\left(\rho c_p\right)_R \left(T_R - T^r\right) \tag{4.15}$$

According to the MIT method, the thermal conversion efficiency for binary systems is calculated as below in Eq. 4.16 (MIT, 2006);

$$\eta_{th} = 0.09345\ T_R - 2.32657 \tag{4.16}$$

where T_R is the resource temperature in ^{o}C.

Table 4.3 presents computed values of the conversion efficiencies used in the method, computed from Eq. 4.16 as a function of the geothermal resource temperature T_R. In the MIT report (MIT, 2006), it is stated that Eq. 4.16 is obtained based on binary type power plants.

Başel (2010), in her PhD dissertation, while determining the producible electricity potential of Turkey, used the MIT method (Eq. 4.15) based on the first law of thermodynamics and calculated the conversion efficiencies by using Eq. 4.16 regardless of the power plant type, whether it is a single-flash or binary power plant.

Table 4.3 : Thermal conversion efficiency as a function of reservoir temperature (computed from Eq. 4.16) for the MIT method.

Reservoir Temperature T_R (^{o}C)	**Thermal Conversion Efficiency η_{th} (%)**
70	4.2
80	5.1
90	6.1
100	7.0
150	11.7
200	16.3
250	21.0
300	25.7
350	30.4

4.3 Garg and Combs Method

Garg and Combs (2015) have stated that in the usage of USGS volumetric method, arbitrarily chosen T^r reference temperature values (15 or 40 ^oC) and inappropriate usage of the conversion efficiencies cause divergence from the realistic values of recoverable heat q_w(kJ) at the wellhead and electricity production (*PW*, *MWe*) results.

They suggest that turbine inlet pressure should be set equal to separator pressure (Garg and Combs, 2015). They introduce the concept of an "abandonment temperature", which is defined as the temperature below which a geothermal reservoir will not be produced. Values of abandonment temperature depend on the specific power cycle.

Garg and Combs (2015) suggest that the reference temperature values should not be chosen arbitrarily, they must be based on the power plant type.

4.3.1. Single-flash power plant

For a flash type power plant, the lower limit for the abandonment temperature is equal to the saturation temperature T_{sep} (^oC) corresponding to the saturation pressure p_{sep} (bar) at the seperator ($T_{abn} = T^r = T_{sep}$).

In flash type power plants the reservoir fluid with the average reservoir temperature is separated by separators at a separator temperature. The separated brine is re-injected to the reservoir while the steam is used for electricity production (Garg and Combs, 2015).

Garg ve Combs (2015) gave the Eq. 4.17 below for the calculation of available work ($W_{A,FLASH}$) for flash type power conversion systems;

$$W_{A,FLASH} = \frac{R_g A H (\rho c_p)_R (T_R - T_{sep})}{h_{gl}(T_{sep})} \left\{ h_{stm}(T_{sep}) - h_w(T_c) - T_{cK} \left[s_{stm}(T_{sep}) - s_w(T_c) \right] \right\} \tag{4.17}$$

where $h_{gl}(T_{sep})$ denotes the heat of vaporization (kJ), h_{stm} and s_{stm} denote the enthalpy (kJ/kg) and entropy values (kJ/kg-^oC) of the steam at T_{sep} respectively, h_w and s_w denote the enthalpy (kJ/kg) and entropy (kJ/kg-^oC) values of liquid phase at

condenser temperature T_c respectively, T_{cK} denotes the absolute condenser temperature (K).

All liquid and steam properties are evaluated along the saturation line. The values given by the International Association for the properties of Water and Steam (IAPWS, 1996) should be used for this purpose.

4.3.2 Binary power plant

The produced brine at an average wellhead temperature is used to heat the working secondary fluid (e.g., iso-butane, iso-pentane) and the spent brine is re-injected back into the reservoir.

For a binary type power plant, the abandonment temperature equals to the, so called, pinch point temperature, T_p, which is a temperature corresponds to a location in the heat exchanger with the least temperature difference, ΔT, between the primary (geothermal water) and the secondary (usually iso-butane) fluid and the bubble point temperature, T_b, of the secondary fluid as shown in Eq. 4.18 below (Garg and Combs, 2015).

$$T_p = T_b + \Delta T \tag{4.18}$$

Hence for a binary power plant it is more appropriate to set $T^r = T_p$. The turbine inlet pressure p_{in}, the corresponding saturation temperature of the secondary fluid T_b can be determined from thermodynamic data for the fluid (NIST, 2010).

The available work for a binary power plant is given by the Eq. 4.19 below (Garg and Combs, 2015);

$$W_{A,BINARY} = \frac{R_g \mathrm{A} H \left(\rho c_p\right)_R \left(T_R - T_p\right)}{h_{sfgl}(T_b)} \left\{ \begin{matrix} h_{sfg}(T_b) - h_{sfl}(T_c) - T_{cK}\left[s_{sfg}(T_b) - s_{sfl}(T_c)\right] \\ -V_{sf}(T_c, p_{sfb})\left[p_{in} - p_{sfb}(T_c)\right] \end{matrix} \right\} \tag{4.19}$$

where $h_{sfgl}(T_b)$ denotes the heat of vaporization for the secondary fluid at its bubble point temperature T_b, $h_{sfl}(T_c)$ and $s_{sfl}(T_c)$ denote the enthalpy and entropy values of the secondary fluid in liquid phase at condenser temperature respectively (kJ/kg), (kJ/kg-^{o}C), $h_{sfg}(T_b)$ and $s_{sfg}(T_b)$ denote the enthalpy and entropy values of the secondary fluid in gas phase at bubble point temperature respectively (kJ/kg), (kJ/kg-^{o}C), $V_{sf}(T_c, p_{sfb})$ (m^3/kg) is the specific volume of the secondary fluid at the

condenser temperature at liquid phase and the bubble point pressure, p_{in} denotes the turbine inlet pressure (bar) and $p_{sfb}(T_c)$ denotes the bubble point pressure of the secondary fluid at condenser temperature (bar). The subscripts "*g*" and "*l*" refer to gas and liquid. Given the turbine inlet pressure, the secondary fluid properties or saturation temperature can be evaluated by using NIST tables (NIST, 2010).

Garg and Combs, 2015 suggested conversion efficiency value should be used as η_c =0.7-0.8; 0.75 as average for flash and binary power cycles.

As an illustrative example, two geothermal resources with 150 ^{o}C and 220 ^{o}C are considered. The geothermal resource having 150 ^{o}C resource temperature is proper for a binary power conversion system and pentane is assumed to have been used as the secondary fluid while the other geothermal field having 220 ^{o}C resource temperature is proper for a single flash power conversion system.

The purpose of this illustrative example is to correlate the available work outputs of these two geothermal power plants by using the Garg and Combs, flash and binary methods in comparison to the USGS and MIT methods results.

For the geothermal fluid having 220 ^{o}C resource temperature (T_R) which is proper for single flash conversion system, the turbine inlet pressure is assumed at 4 bars so the corresponding saturation temperature is 143.608 ^{o}C. Thermodynamic properties are determined as assuming that the turbine inlet pressure is equal to the separator pressure and the condenser temperature (T_c) is 40 ^{o}C.

For the liquid having 150 ^{o}C resource temperature (T_R) which is proper for binary type conversion system, it is assumed that the second working fluid is pentane and there are 5 ^{o}C differential temperature between the original geothermal fluid and the secondary fluid. Assuming the turbine inlet pressure (p_{in}) is equal to 7.5 bars the saturation temperature of pentane at this pressure is equal to 110.81 ^{o}C. Then the pinch point temperature (T_p) of the brine is 115.81 ^{o}C and the condenser temperature (T_c) is 40 ^{o}C. Thermodynamic properties of the secondary fluid is taken from NIST, 2000 HTML table which is given in Appendix A Table A.1 and Table A.2 as listed according to the saturation temperature for liquid and vapor phase respectively and in Appendix B, Table B.1 and Table B.2 as listed according to the saturation pressure for pentane as the secondary working fluid in the system for liquid and vapor phase respectively. Input parameters are presented at Table 4.4 below;

Table 4.4 : Input parameters for calculation of normalized work output from USGS, MIT, Garg and Combs Flash and Binary methods.

Input Parameters for Normalized Work (WA)n, kJ	USGS			MIT	GARG & COMBS FLASH	GARG & COMBS BINARY
Resource Temperature, (T_R, °C)	150	150	150	150-220	220	150
Resource Pressure, (p_R, bar)	52	52	52	-	-	-
Reference Temperature, (T^r, °C)	15	40	100	15-40-100	-	-
Absolute reference temperature (T_{rK}, K)	288.15	313.15	373.15	-	-	-
h_R (kJ/kg)	635.107	635.107	635.107	-	-	-
h^r (kJ/kg)	62.9815	167.533	419.166	-	-	-
s_R (kJ/kg-°C)	1.83656	1.83656	1.83656	-	-	-
s^r (kJ/kg-°C)	0.224463	0.572402	1.30721	-	-	-
Condenser temperature (T_c, °C)	40	40	40	-	40	40
Plant seperator temperature (T_{sep}, °C)	-	-	-	-	143.608	-
Plant seperator pressure (p_{sep}, bar)	-	-	-	-	4	-
h_{stm} (T_{sep}=143.608 °C) (kJ/kg)	-	-	-	-	2738.05	-
s_{stm}(T_{sep}= 143.608 °C) (kJ/kg-°C)	-	-	-	-	6.89549	-
h_w (T_c=40 °C) (kJ/kg)	-	-	-	-	167.533	-
s_w(T_c=40 °C) (kJ/kg-°C)	-	-	-	-	0.572402	-
h_{gl} (T_{sep}= 143.608 °C) =(h_{stm}-h_w)	-	-	-	-	2133.397	-
T_{cK}, K @ (T_c=40 °C)	-	-	-	-	313.15	313.15
Secondary fluid	-	-	-	-	-	**Pentane**
Turbine inlet pressure (p_{in}, bar)	-	-	-	-	-	7.5
Saturation temperature of secondary fluid (T_b, °C) @ p_{in}, bar	-	-	-	-	-	110.81
Assumed temperature differential (°C) between original and secondary fluid	-	-	-	-	-	5
Pinch point temperature (T_p, °C)	-	-	-	-	-	115.81
Plant seperator pressure (p_{sfb}, bar) @ T_c	-	-	-	-	-	1.1567
Heat of vaporization of secondary fluid (h_{sfgl}, kJ/kg) @ T_b	-	-	-	-	-	283.27
h_{sfl}(T_c=40 °C) (kJ/kg)	-	-	-	-	-	9.3689
s_{sfl} (T_c=40 °C) (kJ/kg-°C)	-	-	-	-	-	0.030032
h_{sfg} (T_b= 110.81°C) (kJ/kg)	-	-	-	-	-	476.35
s_{sfg} (T_b= 110.81°C) (kJ/kg-°C)	-	-	-	-	-	1.2903
V_{sf} (@ Tc= 40 °C and p_{sfb}= bar	-	-	-	-	-	0.001651

Normalized available work outputs computed by using USGS (by assuming three different reference temperatures as 15, 40 and 100 ^{o}C arbitrarily) by using Eq. 4.13, MIT using Eq. 4.15, Garg and Combs flash (Eq. 4.17) and binary (Eq. 4.19) are presented at Table 4.5 below; For simplicity W_A work values are normalized as in Eq. 4.20 below;

$$(W_A)_n = W_A / R_g AH(\rho c_p)_R \tag{4.20}$$

Table 4.5 : Normalized available work $(W_A)_n$ for USGS, MIT, Garg and Combs single flash and binary power cycles as a function of resource and reference temperatures.

Resource Temperature T_R (^{o}C)	**Reference Temperature T^r (^{o}C)**	**Normalized Work $(W_A)_n$, ^{o}C**			
		$(W_{A,USGS})_n$	$(W_{A,MIT})_n$	$(W_{A,FLASH})_n$	$(W_{A,BINARY})_n$
150	15	25.39	135	-	8.73
	40	16.87	110		
	100	4.26	50		
220	15	51.67	205	21.14	-
	40	39.24	180		
	100	17.25	120		

Based on the results presented on Table 4.5, the normalized available work obtained from the Garg and Combs method for the single flash is 40.9% of that computed by using USGS method with 15 ^{o}C reference temperature, 53.9% of that computed by USGS method with 40 ^{o}C reference temperature and 122.5% of that computed by USGS method with 100 ^{o}C reference temperature.

In comparison to the MIT method results, the normalized available work obtained from single flash Garg and Combs method is 10.3% of that computed by using the MIT method with 15 ^{o}C reference temperature, 11.7% of that computed by the MIT method with 40 ^{o}C reference temperature and 17.6% of that computed by the MIT method with 100 ^{o}C reference temperature.

By looking at binary power cycle results, the obtained normalized available work value from Garg and Combs method is 33.5% of that computed by using USGS method with 15 ^{o}C reference temperature, 50.4% of that computed by USGS method with 40 ^{o}C reference temperature and 199.4% of that computed by USGS method with 100 ^{o}C reference temperature. In comparison to the MIT method results, the

obtained normalized available work value from Garg and Combs method is 6.5% of that computed by using MIT method with 15 ^{o}C reference temperature, 7.9% of that computed by MIT method with 40 ^{o}C reference temperature and 17.5% of that computed by MIT method with 100 ^{o}C reference temperature.

These results obviously show that both USGS and MIT methods overestimate the available work if we do not take into account the power plant type used in predicting the electricity potential of a geothermal reservoir as well as the abandonment temperature as the reference temperature for which the chosen power plant will not be operated.

Normalized available work is calculated as 21.14 ^{o}C by using Eq. 4.17 for single flash power conversion system where resource temperature is 150 ^{o}C and 8.73 ^{o}C available normalized work by using Eq. 4.19 for binary power conversion system where resource temperature is recorded as 220 ^{o}C with the input parameters given in Table 4.4. Because of mechanical losses in the generator, only 75% (in average) of the available work could be converted to electricity. 75% conversion efficiency value determines how much of the produced work on the wellhead could be converted into energy. Garg and Combs (2015) recommended taking the conversion efficiency value to be assumed as 75% in the usage of their approximation. So at the wellhead, only 15.85 ^{o}C normalized energy could be obtained out of the total available normalized work (21.14) for single flash system and only 6.54 ^{o}C energy output could be obtained out of the total available normalized work (8.73 ^{o}C at the wellhead) for binary cycle considering 75% conversion efficiency for the power plant. To be able to get approximate results to the Garg and Combs outputs from USGS method for the producible electricity, one needs to use approximately 40% conversion efficiency value with 40 ^{o}C reference temperature and if one uses MIT method for producible electricity potential then 11% conversion efficiency should be used with 40 ^{o}C reference temperature (see also Table 7.4 and Table 7.5) regardless from the resource temperature value. But the best way of estimation of electricity potential is the Garg and Combs (2015) method which gives the most approximate results to reality by considering the real thermodynamic condition of the power plant conversion cycle with changing approximations accordingly to resource temperature.

5. PROBABILITY BASED VOLUMETRIC HEAT IN-PLACE METHODS

Exploration is the first step in search of producible amount of accumulations in reservoirs under the ground. During this phase several kinds of geological, geophysical, geochemical and petrophysical work conducted to determine production well locations.

Once a field is discovered, the exploitation and early stage of development work are to be conducted to better understand and delineate the reservoir properties such as total and effective formation porosity, matrix, fracture, relative permeability values, water saturation with irreducible and free producible percentages, the thickness of the reservoir and its areal extension, temperature and geochemical properties, existence of structural and stratigraphical complexity including different kinds of faults, pinch outs, fractures, the orientation of these cracks with stress to strain ratios etc. In addition to these uncertain reservoir characterization parameters, the researchers should have some ideas about the distribution of these petrophysical parameters related to the heterogeneity and anisotropy existent inside the reservoir itself. Also to be able to conduct the exploitation work, decision makers should have some ideas about the producibility and recovery factor of the reservoir. These are essential parameters to have an understanding of the reservoir and it is a hard work to determine how much heat is stored in the reservoir. This uncertainty about reservoir parameters should be reflected to probabilistic mathematical simulation studies for predicting the heat-in place and also the potential of the electricity generation of the geothermal system of interest with uncertainty in the used reservoir data during the calculations which are obtained from field observations, geology, geophysics, well logs and well tests if available.

For geothermal exploration studies it is essential to determine stored heat in place (q_R) (Eq. 4.1) and the producible power potential (PW) (Eq. 4.11) of the geothermal reservoir.

One can use either the MCM or the AUPM to characterize and quantify uncertainty in the estimated power potential from the volume method. The MCM is the most

general approach to assess the uncertainty (Onur et al., 2010). In the MCM, one should decide a proper distribution for each sort of data such as triangular, uniform, normal or log-normal. Deciding the distribution type is closely related to field experience and the assurance on the parameters will be used in a probabilistic manner in the MCM. The MCM creates probability density functions (PDFs) for given distribution types; it generates random numbers inside the given maximum and minimum values by using the PDFs and after a large number of iterations it generates a PDF for the *PW*, MWe. The results are presented as a histogram of the generated PDF and the cumulative distribution function (CDF) with the estimations of mean, variance, Proved (P10), Probable (P50) and Possible (P90) estimates of power generation potential of the geothermal reservoir (*PW*). P10 referring to proved value of *PW* corresponds to 10^{th} percentile of the generated CDF and that means the proved *PW* value is equal or higher than that value with a probability of 90%. Similarly P50 referring to probable estimate of *PW* corresponds to 50^{th} percentile of CDF meaning that the probable *PW* value is equal or higher than that value with 50% probability. P90 referring to possible estimated value of *PW* corresponds the 90th percentile of CDF meaning that the real *PW* value of possible reserve is equal or higher than that value with 10% probability.

However, there is a simple, accurate and fast alternative method which is AUPM for characterizing uncertainty (Onur et al. 2010) which will be explained in the next chapter in details.

5.1 Sources Of Uncertainty In Power Generation Potential By Volumetric Methods

In fact, no researcher can ever know or calculate exactly the real amount of stored heat in-place or electricity production capability of a geothermal reservoir; researchers can just make some approximations to the true value about the reservoir characteristics and the resultant production profile by using different approaches.

Data have been used to make an approximation for the electricity production potential of a liquid-dominated geothermal reservoir (Eq. 4.11, *PW*) includes also uncertainties in the input parameters. But it could be said that some parameters used in this approximation have much larger uncertainty ranges in comparison to the other used parameters in some relationship with them.

Table 5.1 classifies the input parameters as “data with large uncertainty ranges” and parameters as “data with very less or no uncertainty” when predicting the stored heat-in place and electric power potential of a geothermal system.

5.1.1 Most uncertain input parameters and their distributions

Based on Table 5.1, reservoir area, thickness, temperature and thermal recovery factor are the most uncertain input parameters while calculating the electricity production potential of a geothermal reservoir by using volumetric USGS method with MCM simulations.

Table 5.1 : Classification of input parameters of PW, MWe, with respect to uncertainty (Onur, 2015).

Data with large uncertainty	Data with less or no uncertainty
Reservoir Area (A, m^2)	Reference Temperature (T^r, ^oC)
Reservoir Thickness (H, m)	Conversion efficiency (η_c, fraction)
	Volumetric heat capacity of rock ($(\rho c_p)_R$, kJ/m^3-^oC)
Reservoir Temperature (T_R, ^oC)	
Thermal Recovery Factor (R_g, fraction)	Plant load factor (L_F, fraction)
	Plant or project life, (t_p, seconds)

During exploration phase, seismic evaluations are done and structural and stratigraphical interpretation maps are produced but it is well known that companies have seismic interpreters qualified as first opinion, second opinion and a third opinion. In fact it is necessary to get different opinions with different subjective interpretations for seismic. Besides, seismic data has processing uncertainty itself to some degree and need re-processing sometimes and time to depth conversions could be substantially subjective based on different personal field knowledge and believes about the field. This situation affects and amplifies the uncertainty of area and thickness input data inevitably.

Especially in the early phases of exploration or development of the field, the uncertainty is also large for temperature and recovery factor due to the lack of very detailed practical field experience related to reservoir characterization via well log and test data.

In any application in the early phase of exploration, the lower limit of the recovery factor (R_g) should be considered as “0” (zero) because it is one of the possible

outcomes that there may be no permeability in the prospective formation. Formation temperature data should definitely be obtained from the recorded well temperature data during drilling operation or if there was a problem in measuring the well temperature during drilling due to operational issues, after the drilling operation, temperature logs should be run in open hole condition in geothermal wells, but considering the measuring accuracy of tools after cooling the wellbore by short trips while preparing the well for log operation.

Researchers, while working to be able to make some approximations to PW (MWe) of a geothermal reservoir, should use a triangular data distribution if they have a strong idea of what the mostly represented value may be for the uncertain parameter they are evaluating; then the maximum and minimum values should be estimated as the top and base limits would be used by the software in random number generation process. But if the researchers do not have any idea about the mostly represented value of the uncertain input parameter, they should use a uniform distribution by just giving the same chance or probability to each value to happen in between the top and base limits. Normal or lognormal distributions also could be used if the decision makers have strong ideas about the mean and standard deviation of the uncertain input parameter.

5.1.2 Almost certain input parameters

Almost certain parameters are sourced by engineering or operational concepts. Plant load factor (L_F) defines the operational duration of the geothermal power plant, as a fraction, recorded as "working" excluding the time intervals spended by repairments or operational problems. Plant project life (t_p) is nearly a certain parameter for it is decided certainly for the geothermal power plant. The (thermal) conversion efficiency (or utilization factor) is a strong function of the reference temperature and the constructed power cycle (binary or single) based on Garg and Combs (2015) approach, as discussed in Chapter 4, which gives much more realistic results. For the usage of the USGS method, without considering the power cycle or reference temperature which is accepted as arbitrarily as 15 or 40 ^{o}C, one should accept a conversion efficiency value as 40% to get closer results to Garg and Combs (2015) method as illustrated in Chapter 4. Also the volumetric heat capacity of the rock is in the class of data with less uncertainty, because geothermal reservoir rocks are

massive successions having hundreds of meters thickness and kilometers of areal extension under hundreds of meters depth in which the density and specific heat capacity of the rock do not change substantially and also the most of the heat stored in the solid matrix of the rock and hence if we have uncertainty in the porosity is significantly reflected in the estimate of the volumetric heat capacity of the total system Nevertheless, if desired, we can associate uncertainty in the parameters, if data available, when predicting stored heat-in place and electricity potential.

5.2 Workflow for Probabilistic Prediction of Power Generation Potential

Probabilistic prediction of power generation potential of a geothermal field could be made by using MCM or AUPM methods. In both methods the data distribution type must be known. Characterizing uncertainty with AUPM is done by using the mean and variance of input data based on the Central Limit Theorem (CLT) (Parzen, 1962). AUPM will be described in the following section in details.

Figure 5.1 shows the general workflow to be followed while working with the MCM to make a probabilistic approach to potential of electricity production potential of a geothermal system.

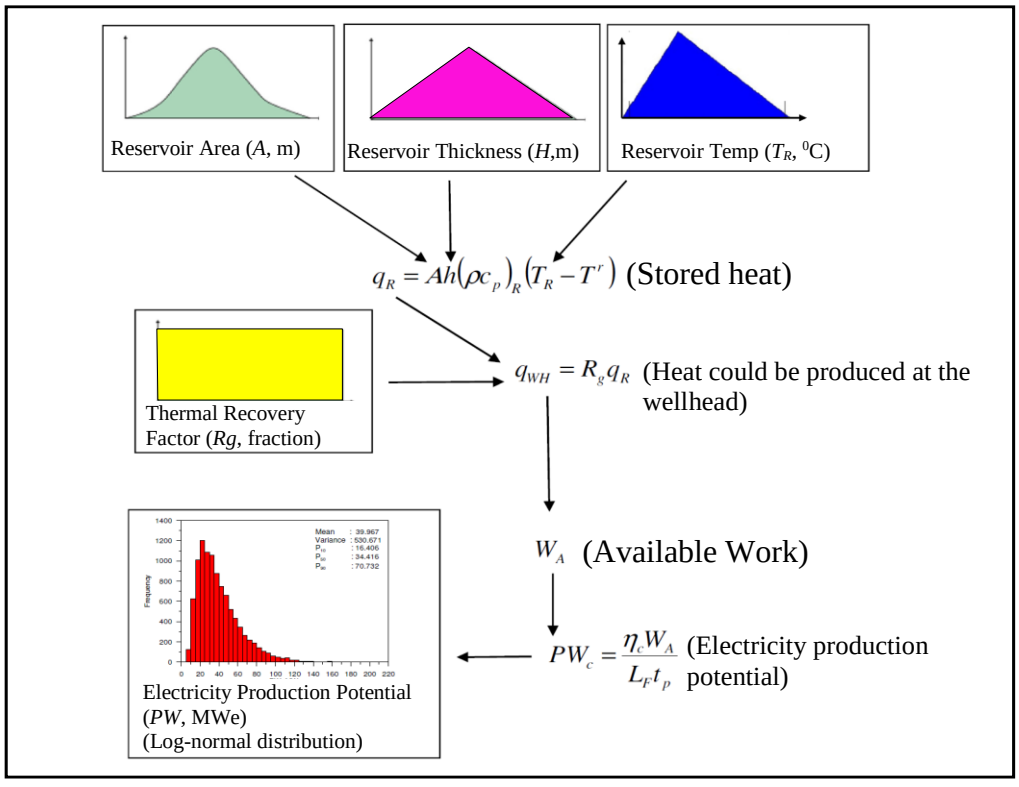

Figure 5.1 : Workflow of the MCM for the volumetric probabilistic approach

The MCM as being a statistical probabilistic and volumetric method, it does not matter whichever the input data distribution (triangular, uniform, normal) comes from, the resultant *PW* will log-normally distributed after a sufficient number of iterations. This result simply follows from the fundamental theorem of statistics and probability – the Central Limit Theorem (CLT, Parzen, 1962). As a consequence of this theorem and the functional relationship of the volumetric method which involves products and quotients of several random input parameters for computing the electric generation potential, resulting distribution of the potential is to be nearly log-normal (Onur et. al., 2010). This result is in fact valid no matter what the form of the uncertainty the input parameters are assumed (Onur et. al., 2010).

Germencik geothermal field is used as an illustrative example to get some ideas of relationship and sensitivity of input data to the MCM in four different cases as follows.

Table 5.2 lists four different cases with different distribution types. MCM method is applied by using Garg and Combs, 2015 USGS based electricity production potential method of a double flash power cycle system for the maximum reservoir temperature recorded in drilled wells is 239.5 ^{o}C. We have chosen a conversion of efficiency of 87.4% as it is a double flash power conversion system. Because the uncertainty is much stronger in input parameters such as reservoir thickness and recovery factor, volumetric methods is generally applied especially in discovery and early development stages of a geothermal field. So it is not necessary to consider complex power conversion systems such as double or triple flash, binary, double binary, flash plus binary in volumetric producible reserve estimations. Furthermore, in volumetric estimations of producible electricity potential of a geothermal field with a binary power plant conversion system, additional available work caused by Low Pressure Steam – LPS system could be added to the output of Eq. 4.19 or power conversion efficiency value could be assumed in between 80%-90% while using Eq. 4.19 because binary power conversion systems could convert power into usable energy with 10%-20% higher conversion efficiency in comparison to single flash type.

The other important point to be highlighted in here is that Germencik geothermal field having 47.4 MWe installed capacity has a binary power conversion system and the same approach mentioned above is assumed for power conversion efficiency and

87.4% efficiency value was determined by Unverdi and Cerci (2013) was used for conversion efficiency.

In Germencik geothermal field the produced geothermal liquid enters the turbine after being separated in High Pressure Steam – HPS system with 5.972 bar absolute pressure (Unverdi and Cerci, 2013). If pressure loss between high pressure separator and the turbine inlet is neglected, then separator temperature could be accepted as 158.644 ^{o}C and the turbine inlet pressure could be assumed as equal to the separator pressure. Condenser temperature is accepted as 40 ^{o}C (Unverdi and Cerci, 2013).

The MCM is made by using Palisade@RISK software free trial version by making 25000 iterations and by using the flash method of Garg and Combs, 2015.

In Case 1, the probability distribution of all input parameters are assumed to be triangular, in Case 2, the minimum and maximum limits of all input parameters are the same as for Case 1, but uniform distribution is assumed for each input parameter.

In Case 3, a mix of uniform and triangular distributions is estimated with the same input parameters as Case 1; the only difference is estimation of the minimum value of recovery factor (R_g) as "zero" with a uniform distribution. Case 4 was designed to be correlated with Case 1 to be able to determine the effect of distribution types of the input parameters where the input values are different but the mean and variance values of the input parameters are the same in Case 1 and Case 4.

The comparison of mean and variance of input parameters including uncertainty as calculated analytically by using Matlab software and obtained by 25000 random sampling by using the given probability distribution in Palisade@RISK is presented at Table 5.3 below.

Based on the results of Case 1 and Case 2, it can be stated that changing distribution type from triangular to uniform does not significantly affect the value of P50; nearly the same result is recorded for P50.

The reason for that is the mean values of the distributions do not change much due to the fact that the minimum and maximum values of the input parameters are the same for Case 1 and Case 2, though the distribution types are different. So the calculated mean value of P50 did not change much. However, we see some differences in the values of P10 and P90 for the parameters from Case 1 to Case 2 cause the P10 and P90 estimates change. For Case 2, where all input parameter distributions are

assumed to be uniform, the estimated value of P10 is less and the value of P90 is higher, as compared the corresponding values estimated for Case 1.

Table 5.2 : Four different cases with different distribution types used in MCM to estimate PW, MWe.

Input parameters	Case 1		Case 2		Case 3		Case 4	
A, km^2	Min:	15	Min:	15	Min:	15	Min:	15
	Mode:	20	Max:	25	Mode:	20	Mode:	20
	Max:	25			Max:	25	Max:	25
H, m	Min:	750	Min:	750	Min:	750	Min:	813.3
	Mode:	1000	Max:	1500	Max:	1500	Max:	1353.3
	Max:	1500						
T_R, °C	Min:	237.5	Min:	237.5	Min:	237.5	Min:	237.5
	Mode:	239.5	Max:	241.5	Mode:	239.5	Mode:	239.5
	Max:	241.5			Max:	241.5	Max:	241.5
R_g, fraction	Min:	0.1	Min:	0.1	Min:	0	Min:	0.115
	Mode:	0.15	Max:	0.2	Max:	0.2	Max:	0.185
	Max:	0.2						
T_{sep}, °C	Constant:	158.644						
T_c, °C	Constant:	40						
$(\rho c_p)_R$, kJ/m^3-°C	Constant:	2470	Same as Case 1		Same as Case 1		Same as Case 1	
η_C, fraction	Constant:	0.874						
L_F, fraction	Constant:	0.95						
t_p, years	Constant:	30						

Table 5.3 : The comparison of mean and variance of input parameters including uncertainty as calculated analytically by using Matlab software and obtained by 25000 random sampling by using the given probability distribution in Palisade@RISK software for four different Cases.

		Case 1 (Triangular)		Case 2 (Uniform)		Case 3 (Mixed)		Case 4 (Mixed)	
X_i	Method	μ_{X_i}	$\sigma^2_{X_i}$	μ_{X_i}	$\sigma^2_{X_i}$	μ_{X_i}	$\sigma^2_{X_i}$	μ_{X_i}	$\sigma^2_{X_i}$
A, m^2	Analytical	2.00E+07	4.17E+12	2.00E+07	8.33E+12	2.00E+07	4.17E+12	2.00E+07	4.17E+12
	MCM	2.00E+07	4.19E+12	2.00E+07	8.31E+12	2.00E+07	4.19E+12	2.00E+07	4.16E+12
H, m	Analytical	1.08E+03	2.43E+04	1.13E+03	4.69E+04	1.13E+03	4.69E+04	1.08E+03	2.43E+04
	MCM	1.08E+03	2.45E+04	1.12E+03	4.73E+04	1.12E+03	4.63E+04	1.08E+03	2.44E+04
T_R °C	Analytical	2.40E+02	6.67E-01	2.40E+02	1.33E+00	2.40E+02	6.67E-01	2.40E+02	6.67E-01
	MCM	2.39E+02	6.61E-01	2.40E+02	1.35E+00	2.40E+02	6.61E-01	2.40E+02	6.64E-01
R_g	Analytical	1.50E-01	4.17E-04	1.50E-01	8.33E-04	1.00E-01	3.33E-03	1.50E-01	4.08E-04
	MCM	1.50E-01	4.12E-04	1.50E-01	8.33E-04	1.00E-01	3.33E-03	1.50E-01	4.06E-04

The results are presented at Table 5.4 for four different cases by 25000 iterations made in Matlab;

Table 5.4 : MCM results for 4 different Cases by 25000 iterations.

***PW*, MWe**	**Case 1**	**Case 2**	**Case 3**	**Case 4**
P10	139	127	26	142
P50	191	203	136	196
P90	250	293	256	257

These results indicate that more uncertainty with a wider range between proved (P10) and possible (P90) for Case 2 occurs because the variances of the input parameters used for Case 2 is larger than those used for Case 1, though the minimum and maximum values of the input parameters are the same for Cases 1 and 2.

Case 3 was designed as a mix of distributions of uniform and triangular with the same minimum and maximum values of Case 1 and Case 2 except from recovery factor (R_g) base limit which is estimated as "zero" with a uniform distribution. So changing the base limit changed the mean value of the estimation and P50 recorded as lower than that obtained in Case 1 and 2. Decreasing minimum value of the recovery factor to zero affected only the P10 and P50 estimate decreasing the estimated values of reserves but it had no significant effect on P90 estimate which is estimated as nearly the same value that estimated in Case 1.

Case 4 was designed to be correlated with Case 1. In Case 4 the input parameters were different in comparison to Case 1 but the mean and variance values of the input parameters were the same. As a result of the MCM simulation based and analytical interpretation it could be seen that the obtained producible electricity potential values are calculated and simulated nearly the same in Case 1 and Case 4. So one could say, from case to case, different distribution type and input parameter values do not affect the resultant producible electricity potential if the mean and variance of input parameters are kept the same.

6. NEW ANALYTIC UNCERTAINY PROPOGATION METHOD

The analytic uncertainty propagation method of Onur et al. (2010) is a very simple, accurate and quick alternative to the MC method in estimation of producible electricity potential from a geothermal reservoir.

The AUPM uses the mean (μ) and variance (σ^2) of the input parameters calculated analytically. The AUPM provides an exact result for the mean and variance of a random function *f* to be predicted if it is linear with respect to the input random variables. Otherwise, if *f* is nonlinear, then the AUPM provides approximate estimates of the mean and variance of the function *f*. The approximation becomes better if the nonlinear *f* can be well approximated by a linear function near the means of the input random variables (Onur et al, 2010).

The validity of the AUPM for characterizing uncertainty results from the fact that the distributions of stored heat and power generation potential to be computed from the volumetric method tend to be log-normal. This is a result of the well-known theorem of central limit (CLT) in statistics (Barlow, 1989). Hence the estimated *PW* will tend to be log-normal because the CLT indicates that natural logarithm of *PW* (ln*PW*) be normally distributed in both cases where the input parameters are independent. Actually, Sarak et al. (2009) also shows that the premise of the CLT holds even if the some of the input variables are correlated. In this thesis, we will assume that all input parameters are independent for simplicity, though the main conclusions to be drawn based on this assumption will also hold for the cases some of the input parameters may be correlated with each other (see Sarak et al., 2009 for details).

As mentioned earlier, the producible power potential of a geothermal reservoir is estimated by using Eq. 6.1 given below;

$$PW = \frac{\eta_c W_A}{10^3 L_f t_p} \tag{6.1}$$

6.1 Derivation of the AUPM

The AUPM is based on taking the natural logarithm of the parameters used while calculationg *PW* individually as follows in Eq. 6.2;

$$\ln PW = \ln \eta_c + \ln W_A + \ln\left(\frac{1}{10^3 L_F t_p}\right) \tag{6.2}$$

Considering the estimation of the *PW* based on the most realistic approach given by Garg and Combs (2015), we take the natural logarithm of W_A is calculated as follows for single-flash (Eq. 6.3) and binary (Eq. 6.4) systems, respectively, as follows:

$$W_{A,FLASH} = \frac{R_g \mathrm{A} H (\rho c_p)_R (T_R - T_{sep})}{h_{gl}(T_{sep})} \left\{ h_{stm}(T_{sep}) - h_w(T_c) - T_{cK}\left[s_{stm}(T_{sep}) - s_w(T_c) \right] \right\} \tag{6.3}$$

$$W_{A,BINARY} = \frac{R_g \mathrm{A} H (\rho c_p)_R (T_R - T_p)}{h_{sfgl}(T_b)} \left\{ \begin{matrix} h_{sfg}(T_b) - h_{sfl}(T_c) - T_{cK}\left[s_{sfg}(T_b) - s_{sfl}(T_c) \right] \\ -V_{sf}(T_c, p_{sfb})\left[p_{in} - p_{sfb}(T_c) \right] \end{matrix} \right\} \tag{6.4}$$

The natural logarithm of W_A for a single-flash power cycle is given by Eq. 6.5 below;

$$\ln W_{A,FLASH} = \ln R_g + \ln A + \ln H + \ln\left[(\rho c_p)_R \right] + \ln(T_R - T_{sep}) + \ln \frac{\left\{ h_{stm}(T_{sep}) - h_w(T_c) - T_{cK}\left[s_{stm}(T_{sep}) - s_w(T_c) \right] \right\}}{h_{gl}(T_{sep})} \tag{6.5}$$

The natural logarithm of W_A for a binary power cycle is given by Eq.6.6 below;

$$\ln W_{A,BINARY} = \ln R_g + \ln A + \ln H + \ln\left[(\rho c_p)_R \right] + \ln(T_R - T_p) + \ln \frac{\left\{ \begin{matrix} h_{sfg}(T_b) - h_{sfl}(T_c) - T_{cK}\left[s_{sfg}(T_b) - s_{sfl}(T_c) \right] \\ -V_{sf}(T_c, p_{sfb})\left[p_{in} - p_{sfb}(T_c) \right] \end{matrix} \right\}}{h_{sfgl}(T_b)} \tag{6.6}$$

If the volumetric, isobaric, specific heat capacity $(\rho c_p)_R$ of the liquid saturated rock (kJ/m^3-is not treated as a certain parameter, though as discussed in Chapter 4, it is a nearly exactly certain parameter, then the natural logarithm of $(\rho c_p)_R$ is evaluated as follows in Eq. 6.7 below;

$$\ln\left(\rho c_p\right)_R = \ln(\phi\rho_l c_{pl} + (1-\phi)\rho_s c_{ps}) \tag{6.7}$$

It should be noted that according to Sarak et. al. (2009), Eq. 6.7 cannot be written as the summation of the natural logarithms of each individual parameters, as in Eq. 6.8 below,

$$\ln(\phi\rho_l c_{pl} + (1-\phi)\rho_s c_{ps}) \neq \ln\phi + \ln\rho_l + \ln c_{pl} + \ln(1-\phi) + \ln\rho_s + \ln c_{ps} \tag{6.8}$$

In fact the three different approximations of a nonlinear function f (e.g., in our case $f \equiv PW$) can be obtained by using the AUPM (see Sarak et al. 2009). In this thesis, we will consider the third approach described by Sarak et al. (2009) and Onur et al. (2010) as this approach is shown to provide a better approximation for the random nonlinear function f as compared to the other two approximate AUPMs by comparisons made with the more rigorous, but time consuming MCM. This third approximate AUPM is based on Taylor series expansion of $\ln PW$ around the mean values of the natural logarithm of input variables ($\mu_{\ln X_i}s$) (Sarak et al. (2009) and Onur et al. (2010)).

The third approximate AUPM method of Onur et al. (2010) considers the natural logarithm of a random function f of M variables, $\ln X_i$, i=1,2,…,M, $\ln f = \ln f(\ln X_1, \ln X_2, \ln X_3, \ldots, \ln X_M)$. Then, expanding $\ln f$ around the mean (or true) values of $\ln X_i$s (denoted by $\mu_{\ln x_i}$, i=1,2, ..,M by using a Taylor series up to first derivatives as in Eq. 6.9, (Onur et al, 2010):

$$\ln f(\ln X_1, \ln X_2, \ldots, \ln X_M) = f(\mu_{\ln X_1}, \mu_{\ln X_2}, \ldots, \mu_{\ln X_M}) + \sum_{i=1}^{M} (\ln X_i - \mu_{\ln X_1}) \left(\frac{\partial \ln f}{\partial \ln X_i} \right)\Bigg|_{\ln X_i = \mu_{\ln Xi}, i=1,\ldots,M} \tag{6.9}$$

The mean and variance of $\ln PW$ (($\mu_{\ln PW}$) and ($\sigma^2_{\ln PW}$)) is approximated by Eq. 6.10 and Eq. 6.11 below;

$$\mu_{\ln PW} = \ln PW(\mu_{\ln X_1}, \mu_{\ln X_2}, \ldots, \mu_{\ln X_M}) \tag{6.10}$$

$$\sigma^2_{\ln PW} = \sum_{i=1}^{M} \theta_i^2 \sigma^2_{\ln X_i} + 2\sum_{i=1}^{M-1}\sum_{j=i+1}^{M} \theta_i\theta_j \rho_{\ln X_i, \ln X_j} \sigma_{\ln X_i}\sigma_{\ln X_j} \tag{6.11}$$

where θ represents the sensitivity of ln$f$ to the variable lnXi evaluated at the mean values of all the variables as in Eq. 6.12 below;

$$\theta = \left(\frac{\partial \ln PW}{\partial \ln X_i} \right) \Bigg|_{\ln X_i = \mu_{\ln Xi}, i=1,\ldots,M} \tag{6.12}$$

where ρ represents the correlation coefficient of the natural logarithm of the random input pairs and σ is the standard deviation from the mean value. As stated before, in this thesis no correlation will be assumed between input data pairs of lnX_i so that Eq. 6.8 reduces to Eq. 6.13 below:

$$\sigma^2_{\ln PW} = \sum_{i=1}^{M} \theta_i^2 \sigma^2_{\ln X_i} \tag{6.13}$$

and the sensitivity of lnPW with respect to natural logarithm of input parameters that can be treated as uncertain for single-flash and binary power cycles are presented at Table 6.1. It should be noted the last logarithm terms in the right-hand sides of Eq. 6.2 and Eq. 6.3 are just constants and certain. These values depending on the power cycle chosen are computed from thermodynamic fluid packages (NIST, 2010). Also note that T^r in Table 6.1 represents T_{sep} for the single-flash system and T_p for the binary system.

Table 6.1 : Sensitivity of lnPW with respect to natural logarithm of input parameters (Onur et al, 2010).

Variable X_i	$\theta_i = \partial \ln PW / \partial \ln X_i^*$
ϕ	$(-\mu_{cp_s}\mu_{\rho_s} + \mu_{cp_l} + \mu_{\rho_l})$
c_{ps}	$(1-\mu_\phi)\mu_{\rho_s}$
ρ_s	$(1-\mu_\phi)\mu_{c_{ps}}$
c_{pl}	$\mu_{\rho_l}\mu_\phi$
ρ_l	$\mu_\phi\mu_{c_{pl}}$
A	1
H	1
T_R	$T_R/(T_R-T^r)$
R_g	1
t_p	-1
L_F	-1

*****evaluated at the mean values of the variables Xis

Similar to the Garg and Combs method, the AUPM method is also applied to predict the uncertainty in the electricity generation potential for USGS (Eq. 4.13) and MIT (Eq. 4.15) methods. For lnW_A functions to be used in Eq. 6.1 for the USGS and MIT

methods are obtained by taking the natural logarithms of Eq. 4.13 and Eq. 4.15 and are given, respectively, by Eq. 6.14 and Eq. 6.15:

$$\ln W_{A,USGS} = \ln R_g + \ln \mathrm{A} + \ln H + \ln\left(\rho c_p\right)_R + \ln\left(T_R - T^r\right) + \ln\left[1 - T_{rK}\frac{\left(s_R - s^r\right)}{\left(h_R - h^r\right)}\right] \tag{6.14}$$

and,

$$\ln W_{A,MIT} = \ln R_g + \ln A + \ln H + \ln\left(\rho c_p\right)_R + \ln\left(T_R - T^r\right) \tag{6.15}$$

Here, the sensitivities to be used in Eq. 6.13 to compute variance of ln*PW* for all parameters to be used are the same as those in given in Table 6.1 for both the USGS and MIT methods. However, it should be noted the last term in the right-hand side of Eq. 6.14 is also dependent on the geothermal resource temperature T_R through the enthalpy [$h_R = h(T_R,p_R)$] and entropy [$s_R = s(T_R,p_R)$] of the geothermal reservoir. As we treat the geothermal reservoir temperature T_R as uncertain, then h_R and s_R are also uncertain. Hence when we compute the variance of ln*PW* with respect to T_R for the USGS method, we account for the uncertainty in h_R and s_R by computing the variance of ln*PW* with respect to T_R. In Eq. 6.16 below, h'_R and s'_R are the derivative of the enthalpy and entropy with respect to reservoir temperature and they are given in Eq. 6.17 and Eq. 6.18 respectively below (Url 18):

$$\frac{\partial \ln PW}{\partial \ln T_R} = \frac{T_R}{T_R - T^r} - \frac{T_R T_{rK}}{1 - T_{rK}\dfrac{\left(s_R - s^r\right)}{\left(h_R - h^r\right)}}\left[\frac{s'_R\left(h_R - h^r\right) - h'_R\left(s_R - s^r\right)}{\left(h_R - h^r\right)^2}\right] \tag{6.16}$$

$$h'_R = \left(\frac{\partial h_R}{\partial T_R}\right)_{p_R} = c_{pl} \tag{6.17}$$

and,

$$s'_R = \left(\frac{\partial s_R}{\partial T_R}\right)_{p_R} = \frac{c_{pl}}{T_R} \tag{6.18}$$

Note that throughout this study, we consider reservoir pressure p_R as constant and known (or certain). Using the thermodynamic relationships given in Eq. 6.16 gives Eq. 6.19 below:

$$\frac{\partial \ln PW}{\partial \ln T_R} = \frac{T_R}{T_R - T^r} - \frac{T_R T_{rK}}{1 - T_{rK} \dfrac{\left(s_R - s^r\right)}{\left(h_R - h^r\right)}} \left[\frac{\dfrac{c_{pl}}{T_R}\left(h_R - h^r\right) - c_{pl}\left(s_R - s^r\right)}{\left(h_R - h^r\right)^2} \right] \tag{6.19}$$

6.2 Computation Of Statistical Markers; P10, P50, and P90 For The AUPM

As Central Limit Theorem (CLT) promises that the data distribution of power capacity of a geothermal reservoir (*PW*) is tend to be log-normal as being independent from different data distribution diversity such as uniform, triangular, normal, lognormal where the natural logarithm of power capacity (ln*PW*) will tend be normally distributed.

Mean and variance of *PW* and ln*PW* for log-normal distributions are as follows in Eq. 6.20 and Eq. 6.21;

$$\mu_{PW} = \exp\left(\mu_{\ln PW} + \frac{\sigma^2_{\ln PW}}{2} \right) \tag{6.20}$$

and,

$$\sigma^2_{PW} = \mu^2_{PW} \left[\exp\left(\sigma^2_{PW}\right) - 1 \right] \tag{6.21}$$

Taking Eq. 6.21 gives Eq. 6.22;

$$\begin{aligned} \frac{\sigma^2_{PW}}{\mu^2_{PW}} &= \left[\exp\left(\sigma^2_{\ln PW}\right) \right] - 1 \\ \exp\left(\sigma^2_{\ln PW}\right) &= 1 + \frac{\sigma^2_{PW}}{\mu^2_{PW}} \\ \ln \exp\left(\sigma^2_{\ln PW}\right) &= \ln\left(1 + \frac{\sigma^2_{PW}}{\mu^2_{PW}} \right) \\ \sigma^2_{\ln PW} &= \ln\left(1 + \frac{\sigma^2_{PW}}{\mu^2_{PW}} \right) \end{aligned} \tag{6.22}$$

Taking Eq. 6.20 gives Eq. 6.23 which is the mean of the producible power potential of the field;

$$\begin{aligned}
\mu_{PW} &= \exp\left(\mu_{\ln PW} + \frac{\sigma^2_{\ln PW}}{2}\right) \\
\ln \mu_{PW} &= \mu_{\ln PW} + \frac{\sigma^2_{\ln PW}}{2} \\
\mu_{\ln PW} &= \ln \mu_{PW} - \frac{\sigma^2_{\ln PW}}{2} \\
\mu_{\ln PW} &= \ln \mu_{PW} - \frac{1}{2}(\sigma^2_{\ln PW})
\end{aligned} \tag{6.23}$$

Using Eq. 6.22 in 6.23 gives Eq. 6.24;

$$\mu_{\ln PW} = \ln \mu_{PW} - \frac{1}{2}\ln\left(1 + \frac{\sigma^2_{PW}}{\mu^2_{PW}}\right) \tag{6.24}$$

In any AUPM method described in the previous section for Garg and Combs' single-flash and binary power cycles, USGS, or MIT, after determining $\mu_{\ln PW}$ and $\sigma^2_{\ln PW}$ probabilistic volumetric values of power capacity could be estimated by using the probability Eq. 6.25, Eq. 6.26 and Eq. 6.27 below,

$$P10 = \exp\left(\mu_{\ln PW} - 1.28\sqrt{\sigma^2_{\ln PW}}\right) \tag{6.25}$$

$$P50 = \exp\left(\mu_{\ln PW}\right) \tag{6.26}$$

$$P90 = \exp\left(\mu_{\ln PW} + 1.28\sqrt{\sigma^2_{\ln PW}}\right) \tag{6.27}$$

6.3 Mean and Variance of Natural Logarithm Of Input Parameter X_i

Any AUPM method derived above for estimating the variances of ln*PW* will require us to work with the means and variances of the natural-log of the input model variables, i.e., $\mu_{\ln X_i}$ and $\sigma^2_{\ln X_i}$. This requires deriving analytical formulas to compute the mean $\mu_{\ln X_i}$ and variance $\sigma^2_{\ln X_i}$ from a given distribution of the input variable X_i. In the following subsections, we provide such formulas for uniform, triangular, normal and log-normal distributions.

6.3.1 Mean and variance for uniform distributions based on Taylor series truncated up to first and second derivatives

Assuming X is uniformly distributed random variable with mean μ_X and the variance σ_X^2, it is well-known that the PDF for a uniform random variable is in Eq. 6.28 below (Barlow, 1989):

$$p(x) = \begin{cases} 0, & \text{for } x < a \\ 1/(b-a) & \text{for } a \le x \le b \\ 0, & \text{for } x > a \end{cases} \tag{6.28}$$

where a represents the minimum and b represents the maximum value of the random variable X.

In terms of the Heaviside function (Kreyszing, 1972), this probability distribution function can be expressed as in Eq. 6.29 below:

$$p(x) = \frac{H(x-a) - H(x-b)}{b-a} \tag{6.29}$$

where Heaviside function is defined by Eq. 6.30 below;

$$H(x-\xi) = \begin{cases} 0 & \text{for } x < \xi \\ 1, & \text{for } x > \xi \end{cases} \tag{6.30}$$

The mean and variance of X (μ_X and σ_X^2) are approximated as follows in Eq. 6.31 and Eq. 6.32;

Noting that mean of X (μ_X) is equal to the expectation of X [$\mathrm{E}(x)$] where a represents the minimum and b represents the maximum value of x.

$$
\begin{aligned}
\mu_x = \mathrm{E}(x) &= \int_a^b x\, p(x)\, dx \\
&= \int_a^b x\, \frac{1}{b-a}\, dx \\
&= \frac{1}{b-a}\left[\frac{x^2}{2}\right]_a^b \\
&= \frac{1}{2(b-a)}(b^2 - a^2) \\
&= \frac{(b-a)(b+a)}{2(b-a)} \\
&= \frac{b+a}{2}
\end{aligned}
\tag{6.31}
$$

$$
\begin{aligned}
\sigma_x^2 = \mathrm{Var}(x) &= E(x^2) - E(x)^2 \\
&= \left(\int_a^b x^2\, p(x)\, dx\right) - \left(\frac{(b+a)}{2}\right)^2 \\
&= \left(\int_a^b x^2\, \frac{1}{b-a}\, dx\right) - \left(\frac{(a+b)^2}{4}\right) \\
&= \frac{1}{b-a}\left(\int_a^b x^2\, dx\right) - \left(\frac{(a+b)^2}{4}\right) \\
&= \left(\frac{1}{3(b-a)}\left[x^3\right]_a^b\right) - \left(\frac{(a+b)^2}{4}\right) \\
&= \frac{b^3 - a^3}{3(b-a)} - \frac{(a+b)^2}{4} \\
&= \frac{4(b^3 - a^3) - 3(b-a)(a+b)^2}{12(b-a)} \\
&= \frac{4b^3 - 4a^3 - (3b-3a)(a^2 + 2ab + b^2)}{12(b-a)} \\
&= \frac{(b-a)^2}{12}
\end{aligned}
\tag{6.32}
$$

Derivation of the mean and variance of random function given by the natural logarithm of the uniform random variable *X*, defining this new random by *Z*, defined as Eq. 6.33 below:

$$Z = \ln X \tag{6.33}$$

The mean of the independent variable Z can be derived by using the general definition of the expected value of a continuous random function, which is given by Eq. 6.34 below:

$$\mathrm{E}[g(x)] = \int_{-\infty}^{\infty} g(x)\, p(x)\, dx \tag{6.34}$$

where $g(X)$ is a measurable function of X, and $p(X)$ is the PDF of X. Then, taking $g(X) = Z = \ln X$, and $p(X)$ as given by Eq. 6.28 or 6.29, the mean of the random variable Z defined by Eq. 6.33 is approximated as in Eq. 6.35 below:

$$\begin{aligned}
\mathrm{E}[\ln(X)] &= \int_{-\infty}^{\infty} \ln X \left[\frac{H(X-a) - H(X-b)}{b-a}\right] dx \\
&= \int_{a}^{b} \ln X \left(\frac{1}{b-a}\right) dx \\
&= \left(\frac{1}{b-a}\right) \int_{a}^{b} \ln X \; dx \\
&= \frac{1}{b-a} \left(X \ln X - X\right)_a^b \\
&= \frac{1}{b-a} (b \ln b - b) - (a \ln a - a) \\
If\ a = 0 &\Rightarrow \frac{1}{b}\left(b \ln b - b - \lim_{a \to 0} (a \ln a - a)\right)
\end{aligned}$$

Because $ln0=\infty$, L Hospital's rule should be applied;

$$\left(\lim_{a \to 0} \frac{\ln a - 1}{\frac{1}{a}}\right) = \lim_{a \to 0} \frac{\frac{1}{a}}{-\frac{1}{a^2}} = \lim_{a \to 0} -\frac{a^2}{a} = \lim_{a \to 0} -a = 0$$

Then if a=0,

$$\begin{aligned}
\mathrm{E}[\ln(X)] &= \frac{1}{b} b(\ln b - 1) \\
&= \ln b - 1
\end{aligned} \tag{6.35}$$

If a >0 then the approximation to the expectation of the natural logarithm of input variable X is as follows in Eq. 6.36;

$$
\begin{aligned}
\mathrm{E}[\ln(X)] &= \frac{1}{b-a}(b\ln b - b) - (a\ln a - a) \\
&= \frac{1}{b-a}(b\ln b - b - a\ln a + a) \\
&= \frac{1}{b-a}(\ln b^b - b - \ln a^a + a) \\
&= \frac{1}{b-a}\left(\frac{\ln b^b}{\ln a^a} - (b-a)\right) \\
&= \frac{1}{b-a}\left[\ln\frac{b^b}{a^a} - (b-a)\right]
\end{aligned}
\tag{6.36}
$$

Summarizing the results of E[ln(*X*)] in Eq. 6.37 below;

$$
\mathrm{E}[\ln(X)] = \begin{cases} (\ln b - 1), & \text{if } a = 0 \\ \dfrac{1}{(b-a)}\left[\ln\dfrac{b^b}{a^a} - (b-a)\right], & \text{if } a > 0 \end{cases}
\tag{6.37}
$$

The variance of *Z* defined by Eq. 6.33 cannot be rigorously derived as the expected value of *Z* given above, and the variance of *Z* can be approximated by the following Eq. 6.38;

$$
\sigma_Z^2 = \mathrm{Var}\ (Z) = [Z'[\mathrm{E}(X)]]^2 \mathrm{Var}\ (X) \tag{6.38}
$$

where $Z'[\mathrm{E}(X)]$ denotes the first derivative of *Z* with respect to *X*, which evaluated at the mean value of the random variable *X*. It should be noted that this approximation is valid for "small" errors, and "small" here means that the first differential does not change much over a few small standard variation of *X*.

The derivative of *Z*, evaluated at E(*X*), is given at Eq. 6.39 below;

$$
Z'[\mathrm{E}(X)] = \left.\frac{d(\ln X)}{dX}\right|_{X=\mathrm{E}(X)} = \left.\frac{1}{X}\right|_{X=\mathrm{E}(X)} = \frac{1}{\mathrm{E}(x)} \tag{6.39}
$$

Replacing E(*X*) in the second equality of Eq. 6.39 by the second equality of Eq. 6.31 we reach Eq. 6.40 below;

$$
Z'[\mathrm{E}(X)] = \frac{2}{b+a} \tag{6.40}
$$

Using Eq. 6.32 for the variance of *X* in the second equality of Eqs. 6.31 and 6.38 gives the variance of *Z* as in Eq. 6.41 below;

$$\sigma_Z^2 = \mathrm{Var}(Z) = \left[\frac{2}{(b+a)}\right]^2 \frac{(b-a)^2}{12} = \frac{1}{3}\left(\frac{b-a}{b+a}\right)^2 \quad (6.41)$$

For a given nonlinear function of random variables such as X, $Y = g(X)$, Taylor series expansions around the mean value of X could be used to derive approximate mean and variance of the random function Y.

A Taylor series expansion (TSE) of $g(X)$ around $X = \mu$ is given at Eq. 6.42 below,

$$Y = g(X) = g(\mu) + g'(\mu)(X-\mu) + \frac{g''(\mu)}{2}(X-\mu)^2 + \varepsilon \quad (6.42)$$

where $g'(\mu)$ and $g''(\mu)$ represent the first and second derivatives of $g(X)$ with respect to X, evaluated at $X = \mu$ and ε is the truncation error.

6.3.1.1 Approximations based on first order derivatives

If Y is truncated up to the first derivative term, then Eq. 6.42 can be approximated as in Eq. 6.43 below;

$$Y = g(X) \approx g(\mu) + g'(\mu)(X-\mu) \quad (6.43)$$

or can be expressed as in Eq. 6.44 below;

$$Y \approx g'(\mu)X + g(\mu) - g'(\mu)\mu \quad (6.44)$$

Taking the expected value of Y given by Eq. 6.44 gives Eq. 6.45 below;

$$\begin{aligned} E(Y) &\approx E[g'(\mu)X + g(\mu) - g'(\mu)\mu] \\ &\approx E[g'(\mu)X] + E[g(\mu)] - E[g'(\mu)\mu] \\ &\approx g'(\mu)E[X] + g(\mu) - g'(\mu)\mu \\ &\approx g'(\mu)\mu + g(\mu) - g'(\mu)\mu \\ &\approx g(\mu) \end{aligned} \quad (6.45)$$

In general, the variance of Y or $g(X)$ is given by Eq. 6.46 below,

$$\begin{aligned} \mathrm{var}(Y) &\approx \mathrm{var}[g(X)] = E\left[\{g(X) - E[g(X)]\}^2\right] \\ &\approx E\left[\{g(X) - g(\mu)\}^2\right] \end{aligned} \quad (6.46)$$

From Eq. 6.43 which shows the truncation of Y up to the first derivative term, we reach Eq. 6.47 below,

$$g(X)-g(\mu)=g'(\mu)(X-\mu) \tag{6.47}$$

To be able to approximate the variance of the function *Y*, using Eq. 6.47 in Eq. 6.46 gives Eq. 6.48 below;

$$\begin{aligned}\operatorname{var}(Y) &\approx \operatorname{var}[g(X)] = E\left[\{g(X)-E[g(X)]\}^2\right] \\ &\approx E\left[[g'(\mu)]^2(X-\mu)^2\right] \\ &\approx [g'(\mu)]^2 E\left[(X-\mu)^2\right] \\ &\approx [g'(\mu)]^2 E\left[(X-E(X))^2\right] \\ &\approx [g'(\mu)]^2 \operatorname{var}(X)\end{aligned} \tag{6.48}$$

To be able to see the viability of the mean and variance of *X* generated by using analytically derived solutions (Eq. 6.31, Eq. 6.32, Eq. 6.35 (for $X_{\min}=0$), Eq. 6.36 (for $X_{\min}\neq 0$) and Eq. 6.41 to calculate μ_X, σ_X^2, $\mu_{\ln X}$ and $\sigma_{\ln X}^2$ respectively) in comparison to the mean and variance of the randomly generated 100000 values of *X* and ln*X* as uniformly distributed by using Matlab (2014 version), different input value cases are considered. The results are presented at Table 6.2 below;

As discussed earlier, in the early exploration phase of a geothermal field, one should consider the minimum value of recovery factor (R_g) as "zero" due to the deficiency of detailed information about the reservoir. Uniform distribution is especially used for R_g for having no strong idea about the mostly represented value of the recovery factor or the mean and variance of recovery factors belong to that field. So in the examination given in Table 6.1 the values concerned for different cases are especially chosen as close to "zero" and equal to "zero" to be able to see the comparison of the mean and variance values computed from the analytically derived expressions with those computed from sampling of the distributions generated by using Matlab. As can be seen from the Table 6.1, the computed values of μ_x, σ_X^2, $\mu_{\ln X}$ and $\sigma_{\ln X}^2$ from our analytically derived Eq.s based on the first order approximation of the TSE are in excellent agreement with those from the Matlab based on sampling of the uniform distributions for each case for the cases where the minimum value of the random variable *X* is different from zero. For $\sigma_{\ln X}^2$ the calculated difference was recorded as approximately 66% for minimum value determined for the uniform distribution is equal to the zero case.

Here, we derive an uncertainty propagation Eq. for a function f, where it is treated as a continuous random function due to uncertainties in the input variables. We assume that all uncertainties are due to the random uncertainties in the input variables and ignore the systematic errors in the input variables. The error propagation Eq. we present is based on a Taylor series approximation of the function around the mean values of the variables up to its first derivatives with respect to each of the input variables.

Table 6.2 : Random sampling vs analytical results of μ_X, σ_X^2, $\mu_{\ln X}$, $\sigma_{\ln X}^2$ for uniform distribution by first order expansion of Taylor Series by using Matlab.

Case	Method	μ_X	σ_X^2	$\mu_{\ln X}$	$\sigma_{\ln X}^2$	Difference in $\sigma_{\ln X}^2$ in percentage (%)
Case 1 X_{min}**: 10**	Random Sampling	25.019	74.571	3.1523	0.14554	17
X_{max}**: 40**	Analytical Result	25	75	3.151	0.12	
Case 2 X_{min}**: 0.1** X_{max}**: 0.2**	Random Sampling	0.15002	0.000833	-1.9161	0.039232	5
	Analytical Result	0.15	0.000833	-1.9163	0.037037	
Case 3 X_{min}**: 0.08** X_{max}**: 0.25**	Random Sampling	0.16504	0.002405	-1.8498	0.10172	13
	Analytical Result	0.165	0.002408	-1.8501	0.08846	
Case 4 X_{min}**: 0.05** X_{max}**: 0.22**	Random Sampling	0.13487	0.002402	-2.0792	0.16429	19
	Analytical Result	0.135	0.002408	-2.0784	0.13214	
Case 5 X_{min}**: 0.01** X_{max}**: 0.05**	Random Sampling	0.030023	0.000133	-3.5922	0.19033	22
	Analytical Result	0.03	0.000133	-3.5934	0.14815	
Case 6 X_{min}**: 0** X_{max}**: 0.05**	Random Sampling	0.025052	0.000208	-3.993	0.99582	66
	Analytical Result	0.025	0.000208	-3.9957	0.33333	
Case 7 X_{min}**: 0** X_{max}**: 0.1**	Random Sampling	0.05013	0.000836	-3.3019	0.99779	67
	Analytical Result	0.05	0.000833	-3.3026	0.33333	

As a consequence of this approximation, the uncertainty propagation provides a linearization of the function in terms of its input random variables (Barlow, 1989; Coleman and Steele, 1999; Zeybek et al, 2009).

So it is decided that we may obtain a better approximation if we consider the approximation of the function by expanding it with a Taylor series up to the second derivatives. This may enable us to derive closer $\sigma^2_{\ln X}$ values to randomly generated sampling results in the cases of the minimum value of the uniform distribution are equal to "zero".

6.3.1.2 Approximations based on second order derivatives

If *Y* is truncated up to the second derivative term, then Eq. 6.42 can be approximated as in Eq. 6.49;

$$Y = g(X) \approx g(\mu) + g'(\mu)(X-\mu) + \frac{g''(\mu)}{2}(X-\mu)^2 \tag{6.49}$$

or can be expressed as in Eq. 6.50 below;

$$Y \approx g'(\mu)X + g(\mu) - g'(\mu)\mu + \frac{g''(\mu)}{2}X^2 - g''(\mu)X\mu + \frac{g''(\mu)}{2}(\mu)^2 \tag{6.50}$$

Taking the expected value of *Y* given by Eq. 6.50 gives Eq. 6.51 below;

$$\begin{aligned}
E(Y) &\approx E\left[g'(\mu)X + g(\mu) - g'(\mu)\mu + \frac{g''(\mu)}{2}X^2 - g''(\mu)X\mu + \frac{g''(\mu)}{2}(\mu)^2 \right] \\
&\approx E[g'(\mu)X] + E[g(\mu)] - E[g'(\mu)\mu] + \frac{1}{2}E[g''(\mu)X^2] - E[g''(\mu)\mu X] \\
&\quad + \frac{1}{2}E[g''(\mu)(\mu)^2] \\
&\approx g'(\mu)E[X] + g(\mu) - g'(\mu)\mu + \frac{g''(\mu)}{2}E[X^2] - g''(\mu)\mu E[X] + \frac{1}{2}g''(\mu)E[(\mu)^2] \\
&\approx g'(\mu)\mu + g(\mu) - g'(\mu)\mu + \frac{g''(\mu)}{2}E[X^2] - g''(\mu)(\mu)^2 + \frac{1}{2}g''(\mu)E[(\mu)^2] \\
&\approx g(\mu) + \frac{g''(\mu)}{2}\{E[X^2] - 2(\mu)^2 + E[(\mu)^2]\}
\end{aligned} \tag{6.51}$$

Noting that mean is equal to expection of *X* as shown in Eq. 6.52;

$$\mu = E(X) \tag{6.52}$$

So the term in the curly braces in the right-hand side of Eq. 6.51 can be expressed as in Eq. 6.53 below;

$$
\begin{aligned}
E\left[X^2\right]-2(\mu)^2+E\left[(\mu)^2\right] &= E\left[X^2\right]-2\left(E\left[X\right]\right)^2+E\left[\left(E\left[X\right]\right)^2\right] \\
&= E\left[X^2\right]-2\left(E\left[X\right]\right)^2+\left(E\left[X\right]\right)^2 \\
&= E\left[X^2\right]-\left(E\left[X\right]\right)^2 = E\left[X^2\right]-\mu^2 \\
&= E\left[X^2-\mu^2\right] \\
&= \mathrm{var}(X)
\end{aligned}
\tag{6.53}
$$

To be able approximate the expectaton of the function *Y*, using the last equality of Eq. 6.53 in Eq. 6.51 gives Eq. 6.54 below;

$$
\begin{aligned}
E(Y) &\approx g(\mu)+\frac{g''(\mu)}{2}\left\{E\left[X^2\right]-2(\mu)^2+E\left[(\mu)^2\right]\right\} \\
&\approx g(\mu)+\frac{g''(\mu)}{2}\mathrm{var}(X)
\end{aligned}
\tag{6.54}
$$

As it is shown above (Eq. 6.48), in general the variance of *Y* is given by Eq. 6.55 below;

$$
\mathrm{var}(Y)\approx \mathrm{var}\left[g(X)\right]=E\left[\left\{g(X)-E\left[g(X)\right]\right\}^2\right] \tag{6.55}
$$

From Eq. 6.49 Eq. 6.56 could be written below;

$$
g(X)-g(\mu_X)=g'(\mu)(X-\mu)+\frac{g''(\mu)}{2}(X-\mu)^2 \tag{6.56}
$$

Using Eq. 6.56 in Eq. 6.48 gives Eq. 6.57 below;

$$
\begin{aligned}
\mathrm{var}(Y) &\approx \mathrm{var}\left[g(X)\right]=E\left[\left\{g(X)-E\left[g(X)\right]\right\}^2\right] \\
&\approx E\left[\left\{g'(\mu)(X-\mu)+\frac{g''(\mu)}{2}(X-\mu)^2\right\}^2\right] \\
&\approx E\left[\left\{\left[g'(\mu)\right]^2(X-\mu)^2+g'(\mu)g''(\mu)(X-\mu)^2(X-\mu)+\frac{\left[g''(\mu)\right]^2}{4}(X-\mu)^4\right\}\right] \\
&\approx E\left[\left[g'(\mu)\right]^2(X-\mu)^2\right]+E\left[g'(\mu)g''(\mu)(X-\mu)^3\right]+\frac{1}{4}E\left[\left[g''(\mu)\right]^2(X-\mu)^4\right]
\end{aligned}
\tag{6.57}
$$

It is shown in Eq. 6.58 below that the expectation of derivative of g around the mean values is;

$$E\left[\left[g'(\mu)\right]^2(X-\mu)^2\right] = \left[g'(\mu)\right]^2 \operatorname{var}(X) \tag{6.58}$$

Using Eq. 6.58 in the last equality of Eq. 6.57 gives Eq. 6.59 below;

$$\operatorname{var}(Y) \approx \operatorname{var}[g(X)] \approx \left[g'(\mu)\right]^2 \operatorname{var}(X) + E\left[g'(\mu)g''(\mu)(X-\mu)^3\right] + \frac{1}{4}E\left[\left[g''(\mu)\right]^2(X-\mu)^4\right] \tag{6.59}$$

Eq. 6.59 can be further expressed as Eq. 6.60 below;

$$\operatorname{var}[g(X)] \approx \left[g'(\mu)\right]^2 \operatorname{var}(X) + g'(\mu)g''(\mu)E\left[(X-\mu)^3\right] + \frac{1}{4}\left[g''(\mu)\right]^2 E\left[(X-\mu)^4\right] \tag{6.60}$$

Recalling that the central moment of a real valued random variable X is defined as in Eq. 6.61 below (Rice, 2007);

$$\mu_n = E\left[(X-\mu)^n\right] \tag{6.61}$$

So, Eq. 6.60 can be expressed in terms of the central moments as in Eq. 6.62 below;

$$\operatorname{var}[g(X)] \approx \left[g'(\mu)\right]^2 \operatorname{var}(X) + g'(\mu)g''(\mu)\mu_3 + \frac{1}{4}\left[g''(\mu)\right]^2 \mu_4 \tag{6.62}$$

The third and fourth central moments of a uniform distribution are given by Eq. 6.63 and Eq. 6.64 below; (Url-16):

$$\mu_3 = 0 \tag{6.63}$$

$$\mu_4 = \frac{1}{80}(b-a)^4 \tag{6.64}$$

where b is the maximum and a is the minimum values of the random variable.

To be able to see the viability of the mean and variance of X generated by using analytically derived solutions by using second order derivatives around the mean values, different input value cases are considered for the uniform distribution type and the results are compared to the mean and variance of the randomly generated 100000 values of X by using Matlab (2014 version). The results are presented at Table 6.3 below;

Based on the results of Table 6.3, the second Taylor series expansion gives less difference between the random sampling and analytically calculated $\sigma^2_{\ln X}$ values as

compared to those computed from the first-derivative Taylor series expansion. However, for the cases random variable has a lower limit of zero, the percentage of difference from those computed from samples generated by the Matlab is still around 60%. So it is recommended that when R_g minimum value is equal to zero case, it is better to use samplings of the uniform distribution by the Matlab or Excel from which random numbers could be easily generated and to use the mean and variance values computed from these samples instead of the analytically calculated $\sigma^2_{\ln X}$. As can be seen from the results given in Table 6.2 and Table 6.3, we do not have significant differences from the ones predicted from our analytically derived equations and from the samples generated by the Matlab if the lower limit of the random variable is different from zero and there is not significant difference between the lower and upper limit values of the random uniform distribution.

Table 6.3 : Random sampling vs analytical results of μ_X, σ^2_X, $\mu_{\ln X}$, $\sigma^2_{\ln X}$, for uniform distribution by second order expansion of Taylor Series.

Case	Method	μ_X	σ^2_X	$\mu_{\ln X}$	$\sigma^2_{\ln X}$	Difference in $\sigma^2_{\ln X}$ in percentage (%)
Case 1 X_{min}**: 10** X_{max}**: 40**	Random Sampling	25.019	74.571	3.1523	0.14526	12
	Analytical Result	25	75	3.151	0.12648	
Case 2 X_{min}**: 0.1** X_{max}**: 0.2**	Random Sampling	0.15002	0.000833	-1.9161	0.039243	4
	Analytical Result	0.15	0.000833	-1.9163	0.037654	
Case 3 X_{min}**: 0.08** X_{max}**: 0.25**	Random Sampling	0.16504	0.002405	-1.8498	0.10158	9
	Analytical Result	0.165	0.002408	-1.8501	0.091982	
Case 4 X_{min}**: 0.05** X_{max}**: 0.22**	Random Sampling	0.13487	0.002402	-2.0792	0.16554	15
	Analytical Result	0.135	0.002408	-2.0784	0.14	
Case 5 X_{min}**: 0.01** X_{max}**: 0.05**	Random Sampling	0.030023	0.000133	-3.5922	0.19042	17
	Analytical Result	0.03	0.000133	-3.5934	0.15802	
Case 6 X_{min}**: 0** X_{max}**: 0.05**	Random Sampling	0.025052	0.000208	-3.993	0.99372	61
	Analytical Result	0.025	0.000208	-3.9957	0.38333	
Case 7 X_{min}**: 0** X_{max}**: 0.1**	Random Sampling	0.05013	0.000836	-3.3019	1.005	61
	Analytical Result	0.05	0.000833	-3.3026	0.38333	

6.3.2 Mean and variance for triangular distributions based on Taylor series truncated up to first and second derivatives

Here, the derivations of analytic mean and approximate variance formulas for the natural logarithm of the random parameter *X*, based on its Taylor series expansion of first and second order derivatives are provided.

6.3.2.1 Approximations based on first order derivatives

Assuming *X* is triangularly distributed random variable with mean μ_x and the variance σ_x^2, it is well-known that the PDF for a triangularly distributed random variable is given in Eq. 6.65 below:

$$p(X)=\begin{cases}\dfrac{2(X-a)}{(b-a)(c-a)}, & \text{for } a\le X\le c\\[2ex] \dfrac{2(b-X)}{(b-a)(b-c)} & \text{for } c< X\le b\end{cases} \tag{6.65}$$

where *a* is the minimum, *b* is the maximum, and *c* is the mode value of *X*. The expectation of X is approximated by Eq. 6.66 below;

$$\begin{aligned}\mathrm{E}[X]&=\int_{-\infty}^{\infty} X\ p(X)\,dx=\int_a^c X\ \frac{2(X-a)}{(b-a)(c-a)}\,dx+\int_c^b X\ \frac{2(b-X)}{(b-a)(b-c)}\,dx\\ &=\frac{2}{(b-a)(c-a)}\int_a^c X\ (X-a)\,dx+\frac{2}{(b-a)(b-c)}\int_c^b X\ (b-X)\,dx\end{aligned} \tag{6.66}$$

The first and second integrals of Eq. 6.66 (I_1 and I_2) give Eq. 6.67 and Eq. 6.68 below;

$$\begin{aligned}I_1&=\int_a^c x\,(x-a)\,dx=\int_a^c x^2-ax\,dx=\left[\frac{x^3}{3}-\frac{ax^2}{2}\right]_a^c=\frac{c^3}{3}-\frac{ac^2}{2}-\frac{a^3}{3}+\frac{a^3}{2}\\ &=\frac{c^3-a^3}{3}-\frac{(ac^2-a^3)}{2}=\frac{(c-a)(c^2+ac+a^2)}{3}-\frac{a(c-a)(c+a)}{2}\end{aligned} \tag{6.67}$$

$$I_2 = \int_c^b x\,(b-x)\,dx = -\int_c^b x\,(x-b)\,dx = -\left[\int_c^b x\,(x-b)\,dx = \int_c^b \left(x^2 - bx\right)dx\right]$$

$$= -\left[\left[\frac{x^3}{3} - \frac{bx^2}{2}\right]\Big|_c^b\right] = -\left[\frac{b^3}{3} - \frac{b^3}{2} - \frac{c^3}{3} + \frac{bc^2}{2}\right] = -\frac{b^3}{3} + \frac{b^3}{2} + \frac{c^3}{3} - \frac{bc^2}{2}$$

$$= -\frac{\left(b^3 - c^3\right)}{3} + \frac{b^3 - bc^2}{2} = -\frac{(b-c)\left(b^2 + bc + c^2\right)}{3} + \frac{b(b-c)(b+c)}{2} \tag{6.68}$$

Using Eqs. 6.67 and 6.68 in Eq. 6.66 gives Eq. 6.69 below,

$$\mu_X = \mathrm{E}[X] = \frac{1}{3}(a+b+c) \tag{6.69}$$

And similarly, one can derive the variance (Url-19) as in Eq. 6.70 below;

$$\sigma_x^2 = \mathrm{Var}(X) = \frac{\left(a^2 + b^2 + c^2 - ab - bc - ac\right)}{18} \tag{6.70}$$

Formulas for the mean and variance of random function *Z* given by the natural logarithm of the triangular random variable *X*. Letting this random variable is denoted by *z*, defined as in Eq. 6.71 below;

$$Z = \ln X \tag{6.71}$$

The mean of *Z* can be derived by using the general definition of the expected value of a continuous random function, which is given by Eq. 6.72 below;

$$\mathrm{E}[g(X)] = \int_{-\infty}^{\infty} g(x)\,p(x)\,dx \tag{6.72}$$

where $g(X)$ is a measurable function of X, and $p(X)$ is the PDF of X. Then, taking $g(X) = Z = \ln X$, and $p(X)$ as given by Eq. 6.65, the mean of the random function Z defined by Eq. 6.71 could be find as in Eq. 6.73 below;

$$\mathrm{E}[\ln(X)] = \int_{-\infty}^{\infty} \ln X\ \ p(X)\,dx = \int_a^c \ln X\ \frac{2(x-a)}{(b-a)(c-a)}\,dx + \int_c^b \ln x\,\frac{2(b-X)}{(b-a)(b-c)}\,dx$$

$$= \frac{2}{(b-a)(c-a)}\int_a^c \ln X\ (X-a)\,dx + \frac{2}{(b-a)(b-c)}\int_c^b \ln X\ (b-X)\,dx \tag{6.73}$$

Performing integrations in third equality of Eq. 6.73 as I_1 and I_2 as below gives Eq. 6.74 and Eq. 6.75 below,

$$I_1 = \int_a^c \ln x\,(x-a)\,dx = \left[\frac{(x-a)^2}{2} - \frac{a^2}{2}\right]\ln x - \left(-ax + \frac{x^2}{4}\right)\Bigg|_a^c$$

$$= \left[\frac{(c-a)^2}{2} - \frac{a^2}{2}\right]\ln c - \left(-ac + \frac{c^2}{4}\right) - \left[\frac{(a-a)^2}{2} - \frac{a^2}{2}\right]\ln a + \left(-a^2 + \frac{a^2}{4}\right)$$

$$= \left[\frac{(c-a)^2}{2} - \frac{a^2}{2}\right]\ln c - \left(-ac + \frac{c^2}{4}\right) - \left[-\frac{a^2}{2}\right]\ln a + \left(-\frac{3a^2}{4}\right)$$

$$= \left[\frac{(c^2 - 2ac + a^2)}{2} - \frac{a^2}{2}\right]\ln c - \left(-ac + \frac{c^2}{4}\right) - \left[-\frac{a^2}{2}\right]\ln a + \left(-\frac{3a^2}{4}\right)$$

$$= \left[\frac{(c^2 - 2ac)}{2}\right]\ln c - \left(-ac + \frac{c^2}{4}\right) - \left[-\frac{a^2}{2}\right]\ln a + \left(-\frac{3a^2}{4}\right)$$

$$= \frac{(c^2 - 2ac)}{2}\ln c + ac - \frac{c^2}{4} + \frac{a^2}{4}(2\ln a - 3)$$

$$= \frac{(c^2 - 2ac)}{2}\ln c - \frac{1}{4}(c^2 - 4ac) + \frac{a^2}{4}(2\ln a - 3) \qquad (6.74)$$

and,

$$I_2 = \int_c^b \ln x\,(b-x)\,dx = -\int_c^b \ln x\,(x-b)\,dx$$

$$= -\left[\left[\frac{(x-b)^2}{2} - \frac{b^2}{2}\right]\ln x - \left(-bx + \frac{x^2}{4}\right)\Bigg|_c^b\right]$$

$$= -\left\{\left[\frac{(b-b)^2}{2} - \frac{b^2}{2}\right]\ln b - \left(-b^2 + \frac{b^2}{4}\right) - \left[\frac{(c-b)^2}{2} - \frac{b^2}{2}\right]\ln c + \left(-bc + \frac{c^2}{4}\right)\right\}$$

$$= -\left\{\left[-\frac{b^2}{2}\right]\ln b - \left(-\frac{3b^2}{4}\right) - \left[\frac{(c^2 - 2bc)}{2}\right]\ln c + \left(-bc + \frac{c^2}{4}\right)\right\}$$

$$= -\left\{-\frac{b^2}{2}\ln b + \frac{3b^2}{4} - \frac{(c^2 - 2bc)}{2}\ln c - \frac{1}{4}(4bc - c^2)\right\}$$

$$= \frac{b^2}{4}(2\ln b - 3) + \frac{(c^2 - 2bc)}{2}\ln c - \frac{1}{4}(c^2 - 4bc) \qquad (6.75)$$

To approximate the expectation of natural logarithm of the function *X*, using Eq. 6.74 and 6.75 in Eq. 6.73 gives Eq. 6.76 below;

$$\mathrm{E}[\ln(X)] = \frac{2}{(b-a)(c-a)}\int_a^c \ln X\ (X-a)\,dx + \frac{2}{(b-a)(b-c)}\int_c^b \ln X\ (b-X)\,dx$$
$$= \frac{2}{(b-a)(c-a)}\left[\frac{c(c-2a)}{2}\ln c - \frac{c}{4}(c-4a) + \frac{a^2}{4}(2\ln a - 3)\right]$$
$$+ \frac{2}{(b-a)(b-c)}\left[\frac{b^2}{4}(2\ln b - 3) + \frac{c(c-2b)}{2}\ln c - \frac{c}{4}(c-4b)\right] \tag{6.76}$$

The variance of *Z* for a triangular distribution cannot be rigorously derived as the expected value of *Z* given above, and the variance of *Z* can be approximated by the following Eq. 6.77:

$$\sigma_Z^2 = \mathrm{Var}\ (Z) = \left[Z'\left[\mathrm{E}\ (X)\right]\right]^2 \mathrm{Var}\ (X) \tag{6.77}$$

where $Z'(\mathrm{E}(X))$ denotes the first derivative of *Z* with respect to *X*, which evaluated at the mean value of the random variable *X*.

The derivative of *Z*, evaluated at E(*X*), is given by Eq. 6.78 below:

$$Z'(\mathrm{E}(X)) = \left.\frac{d(\ln X)}{dx}\right|_{x=\mathrm{E}(x)} = \left.\frac{1}{X}\right|_{x=\mathrm{E}(x)} = \frac{1}{\mathrm{E}(X)} \tag{6.78}$$

Replacing E(*X*) in the second equality of Eq. 6.69 by the second equality of Eq. 6.78 gives Eq. 6.79 below;

$$z'(\mathrm{E}(x)) = \frac{3}{a+b+c} \tag{6.79}$$

Using Eq. 6.70 for the variance of *X* in the second equality of Eq. 6.77 and Eq. 6.79 gives the variance of $Z = \ln X$, where *X* is a random variable based on a triangular distribution as in Eq. 6.80 as below;

$$\sigma_Z^2 = \mathrm{Var}(Z) = \left[\frac{3}{(a+b+c)}\right]^2 \frac{\left(a^2+b^2+c^2-ab-bc-ac\right)}{18}$$
$$= \frac{\left(a^2+b^2+c^2-ab-bc-ac\right)}{2(a+b+c)^2} \tag{6.80}$$

To be able to see the viability of the mean and variance of *x* generated by using analytically derived solutions by using first order derivatives around the mean values, different input value cases are considered for the triangular distribution type

and the results are compared to the mean and variance of the randomly generated 100000 values of x by using Matlab (2014 version). The results are presented at Table 6.4 below;

Based on the results, obtained values by Taylor series approximation around the mean values of the random variable X is in very good convergence in the first four cases with the values obtained from random number generation estimation method done by using Matlab. But again for the last case where minimum value is zero for recovery factor, 42% difference is recorded in comparison the two results. So, deciding that second order Taylor series expansion method may reduce this difference, further estimations were done by analytically in an attempt to derive better approximations in cases where we have the lower limit of the random variable closer to zero or equal to zero. This derivation is provided in the next subsection.

Table 6.4 : Random sampling vs analytical results of μ_X , σ_X^2 , $\mu_{\ln X}$, $\sigma_{\ln X}^2$, for triangular distribution by first order expansion of Taylor Series.

Case	Method	μ_X	σ_X^2	$\mu_{\ln X}$	$\sigma_{\ln X}^2$	Difference in $\sigma_{\ln X}^2$ in percentage (%)
Case 1 X_{min}**: 10** X_{mode}**: 12** X_{max}**: 20**	Random Sampling	13.996	4.6885	2.6271	0.023164	3
	Analytical Result	14	4.6667	2.6274	0.02381	
Case 2 X_{min}**: 10** X_{mode}**: 30** X_{max}**: 100**	Random Sampling	46.669	373.09	3.7512	0.1953	12
	Analytical Result	46.667	372.22	3.7512	0.17092	
Case 3 X_{min}**: 0.1** X_{mode}**: 0.6** X_{max}**: 0.75**	Random Sampling	0.48356	0.019346	-0.77827	0.11808	30
	Analytical Result	0.48333	0.019306	-0.77859	0.08264	
Case 4 X_{min}**: 0.1** X_{mode}**: 0.15** X_{max}**: 0.2**	Random Sampling	0.15001	0.000417	-1.9065	0.019232	4
	Analytical Result	0.15	0.000417	-1.9066	0.018519	
Case 5 X_{min}**: 0** X_{mode}**: 0.1** X_{max}**: 0.2**	Random Sampling	0.099904	0.001661	-2.417	0.28827	42
	Analytical Result	0.1	0.001667	-2.4163	0.16667	

6.3.2.2 Approximations based on second order derivatives

For this purpose the same derived analytical Eq.s were used with different central moments which differ for triangular distribution types given in Eq. 6.81 and Eq. 6.82 below (Url-17);

$$\mu_3 = -\frac{1}{270}(a+b-2c)(a+c-2b)(b+c-2a) \tag{6.81}$$

$$\mu_4 = \frac{1}{135}(a^2+b^2+c^2-ab-ac-bc)^2 \tag{6.82}$$

where *b* is the maximum and *a* is the minimum value, and c is the mode value. The results are presented at Table 6.5 below;

Table 6.5 : Random sampling vs analytical results of μ_X , σ_X^2 , $\mu_{\ln X}$, $\sigma_{\ln X}^2$, for triangular distribution by second order expansion of Taylor Series

Case	Method	μ_X	σ_X^2	$\mu_{\ln X}$	$\sigma_{\ln X}^2$	Difference in $\sigma_{\ln X}^2$ in percentage (%)
Case 1 **X_{min}: 10** **X_{mode}: 12** **X_{max}: 20**	Random Sampling	14.006	4.6814	2.6279	0.023113	1
	Analytical Result	14	4.6667	2.6274	0.023372	
Case 2 **X_{min}: 10** **X_{mode}: 30** **X_{max}: 100**	Random Sampling	46.713	372.63	3.7524	0.1948	10
	Analytical Result	46.667	372.22	3.7512	0.17442	
Case 3 **X_{min}: 0.1** **X_{mode}: 0.6** **X_{max}: 0.75**	Random Sampling	0.48313	0.019319	-0.77907	0.11775	25
	Analytical Result	0.48333	0.019306	-0.77859	0.088718	
Case 4 **X_{min}: 0.1** **X_{mode}: 0.15** **X_{max}: 0.2**	Random Sampling	0.15	0.000418	-1.9066	0.019283	3
	Analytical Result	0.15	0.000417	-1.9066	0.018724	
Case 5 **X_{min}: 0** **X_{mode}: 0.1** **X_{max}: 0.2**	Random Sampling	0.10005	0.001658	-2.4149	0.28653	36
	Analytical Result	0.1	0.001667	-2.4163	0.18333	

Based on the results of Table 6.4 second Taylor series expansion gives less difference between the random sampling and analytically calculated $\sigma_{\ln X}^2$ values but

the percentage of difference is still around 35%. So it is recommended that when the minimum value of the triangular distribution is equal to zero case, it is necessary to make random sampling of the triangular distribution in Matlab and to use that value instead of the analytically calculated $\sigma^2_{\ln x}$. For the other cases there is no problem in usage of analytical solution results as could be seen from the comparison of the consequent values of the two approaches.

6.3.3 Mean and variance for normal (Gaussian) and log-normal distributions

If the distribution of X_i is log-normal with mean μ_{X_i} and variance $\sigma^2_{X_i}$, then lnX_i is normal with the mean $\mu_{\ln X_i}$ and variance $\sigma^2_{\ln X_i}$, given by Eq. 6.83 and Eq. 6.84 respectively below:

$$\mu_{\ln X_i} = \ln \mu_{X_i} - \frac{1}{2}\ln\left(1+\frac{\sigma^2_{X_i}}{\mu^2_{X_i}}\right) \tag{6.83}$$

$$\sigma^2_{\ln X_i} = \ln\left(1+\frac{\sigma^2_{X_i}}{\mu^2_{X_i}}\right) \tag{6.84}$$

If the distribution of X_i is normal with mean μ_{X_i} and variance $\sigma^2_{X_i}$, it is not easy to derive analytical formulas. In such cases, the sampling method can be used; i.e., first a sample of N (say 10000) values of X is generated, then transformed them $g(X)$ = ln$X$, and then the formulas given below is applied to compute mean and variance of ln$X$ as in Eq. 6.85 and 6.86 below:

$$\mu_{\ln X} = \frac{1}{N}\sum_{i=1}^{N} \ln X_i \tag{6.85}$$

and the variance denoted by σ^2 is;

$$\sigma^2{}_{\ln X} = \frac{1}{N}\sum_{i=1}^{N}\left(\ln X_i - \mu_{\ln X}\right)^2 \tag{6.86}$$

7. APPLICATIONS TO THREE GEOTHERMAL FIELDS IN TURKEY

In this chapter, applications of the AUP method based on Garg and Combs based on single-flash and binary power cycles, USGS and MIT methods derived in Chapter 6 for three geothermal fields of Turkey; namely Kızıldere, Germencik, and Salavatlı are presented.

7.1 Kızıldere Field

Resource temperature value of Kızıldere geothermal field is recorded as maximum temperature value in field as 242 ºC (Akkuş, 2016, Table 4.2) and in this examination of probabilistic volumetric reserve estimation examination this value is used as mostly represented value; so Kızıldere geothermal field is amenable to flash power cycle due to resource temperature value above 180 ºC and in Kızıldere, one single and one triple combined flash type are operating currently (Haklıdır, 2016, Figure3.1). The input parameters used for Kızıldere geothermal field by using the approximation of Garg and Combs, 2015, for MCM is given at Table 7.1 below where Table 7.2 shows the input parameters used for USGS and MIT methods.

Table 7.1 : Input parameters used for Garg and Combs, 2015 flash power cycle

Parameter	Distribution Type	Minimum	Mode	Maximum
Reservoir Area (A, m^2)	Triangular	35000000	40000000	45000000
Reservoir Thickness (H, m)	Triangular	750	1000	1500
Resource Temperature (T_R, °C)	Triangular	235	242	250
Porosity (ϕ , fraction)	Triangular	0.03	0.05	0.08
Resource Pressure(p_R, bar)	Constant		52	
Specific heat capacity of brine ($c_p)_f$, kJ/kg-ºC)	Triangular	4.70666	4.77041	4.85357
Density of brine (ρ_f , kg/m^3)	Triangular	822.467	812.387	800.316
Specific heat capacity of rock ($c_p)_R$, kJ/kg-ºC	Constant		0.92	
Density of rock (ρ_R , kg/m3)	Triangular	2500	2600	2700
Volumetric specific heat capacity of rock $\left(\rho C_p\right)_R$, (kg/m^3-ºC)	Triangular	2347	2466	2596
Recovery factor (R_g, fraction)	Uniform	0.05	-	0.15
Separator pressure p_{sep} (bar)	Constant		4.5	
Seperator temperature (T_{sep}, ºC)	Constant		147.903	

Table 7.1 (continued): Input parameters used for Garg and Combs, 2015 flash power cycle method

Parameter	Dist. Type	Minimum	Mode	Maximum
$T_R - T_{sep}$ (°C)	Triangular	87.097	94.097	102.097
Power conversion factor (η_c, fraction)	Constant		0.75	
Plant condenser temperature (T_c, °C)	Constant		40	
Project life (t_p, 25x31557600, sec)	Constant		788940000	
Load factor (L_F, fraction)	Constant		0.95	
h_{stm} (T_{sep}=147.903 °C) (kJ/kg)	Constant		2743.39	
s_{stm}(T_{sep}= 147.903°C) (kJ/kg-°C)	Constant		6.85603	
h_w (T_c=40 °C) (kJ/kg)	Constant		167.533	
s_w(T_c=40 °C) (kJ/kg-°C)	Constant		0.572402	
h_{gl} (T_{sep}= 147.903 °C) =(h_{stm}-h_w)	Constant		2120.253	
T_{cK}, K @ (T_c=40 °C)	Constant		313.15	

Table 7.2 : Input parameters used for USGS and MIT methods.

Parameter	Distribution Type	Minimum	Mode	Maximum
Reservoir Area (A, m^2)	Triangular	35000000	40000000	45000000
Reservoir Thickness (H, m)	Triangular	750	1000	1500
Resource Temperature (T_R, °C)	Triangular	235	242	250
Resource Pressure (p_R, bar)	Constant		52	
Porosity (ϕ , fraction)	Triangular	0.03	0.05	0.08
Specific heat capacity of brine (c_p)$_f$, kJ/kg-°C)	Triangular	4.70666	4.77041	4.85357
Density of brine (ρ_f , kg/m^3)	Triangular	822.467	812.387	800.316
Specific heat capacity of rock (c_p)$_R$, kJ/kg-°C	Constant		0.92	
Density of rock (ρ_R , kg/m3)	Triangular	2500	2600	2700
Volumetric specific heat capacity of rock $\left(\rho c_p\right)_R$ kg/m^3-°C)	Triangular	2347	2466	2596
Recovery factor (R_g, fraction)	Uniform	0.05	-	0.15
Specific enthalpy of the reservoir (h_R, kJ/kg) @ T_R	Triangular	1014.09	1047.25	1085.74
Specific entropy of the reservoir (s_R, kJ/kg-°C) @ T_R	Triangular	2.65159	2.71641	2.79055
Reference temperature (T^r, °C)	Constant		15, 40 or 100	
T_R- T^r (T^r = 15) °C	Triangular	220	227	235
T_R- T^r (T^r = 40) °C	Triangular	195	202	210
T_R- T^r (T^r = 100) °C	Triangular	135	142	150
h_R- h^r (T^r=15) °C	Triangular	951.1085	984.2685	1022.7585
h_R- h^r (T^r=40) °C	Triangular	846.557	879.717	918.207
h_R- h^r (T^r=100) °C	Triangular	594.924	628.084	666.574

Table 7.2 (continued): Input parameters used for USGS and MIT methods.

Parameter	Dist. Type	Min.	Mode	Max.
s_R- s^r (T^r=15) °C	Triangular	2.427127	2.491947	2.566087
s_R- s^r (T^r=40) °C	Triangular	2.079188	2.144008	2.218148
s_R- s^r (T^r=100) °C	Triangular	1.34438	1.4092	1.48334
Thermal conversion factor (η_{th} , fraction)	Constant		0.11, 0.18 or 0.4	
Project life (t_p, 25x31557600, sec)	Constant		788940000	
Load factor (L_F, fraction)	Constant		0.95	
h^r (T^r=15 °C) (kJ/kg)	Constant		62.9815	
s^r (T^r=15 °C) (kJ/kg-°C)	Constant		0.224463	
T_{rK} (T^r=15 °C)	Constant		288.15	
h^r (T^r=40 °C) (kJ/kg)	Constant		167.533	
s^r (T^r=40 °C) (kJ/kg-°C)	Constant		0.572402	
T_{rK} (T^r=40 °C)	Constant		313.15	
h^r (T^r=100 °C) (kJ/kg)	Constant		419.166	
s^r (T^r=100 °C) (kJ/kg-°C)	Constant		1.30721	
T_{rK} (T^r=100 °C), (K)	Constant		373.15	

Table 7.3 below shows the mean and variance of input parameters X_i and $\ln X_i$ calculated analytically by using Matlab-2014 for AUPM approximation.

Table 7.3 : Mean and variance of input parameters X_i and $\ln X_i$ calculated analytically.

X_i	μ_{X_i}	$\sigma^2_{X_i}$	$\mu_{\ln X_i}$	$\sigma^2_{\ln X_i}$
R_g, fraction	1.00E-01	8.33E-04	-2.35E+00	8.65E-02
A, m^2	4.00E+07	4.17E+12	1.75E+01	2.60E-03
H, m	1.08E+03	2.43E+04	6.98E+00	2.06E-02
$\left(\rho c_p\right)_R$	2.47E+03	2.59E+03	7.81E+00	4.24E-04
T_R-T_{sep}, °C	9.44E+01	9.39E+00	4.55E+00	1.10E-03
T_R-T^r (T^r=15), °C	2.27E+02	9.39E+00	5.43E+00	1.82E-04
T_R-T^r (T^r=40), °C	2.02E+02	9.39E+00	5.31E+00	2.29E-04
T_R-T^r (T^r=100), °C	1.42E+02	9.39E+00	4.96E+00	4.63E-04
h_R- h^r (T^r=15) °C	9.86E+02	2.14E+02	6.89E+00	2.20E-04
h_R- h^r (T^r=40) °C	8.81E+02	2.14E+02	6.78E+00	2.75E-04
h_R- h^r (T^r=100) °C	6.30E+02	2.14E+02	6.45E+00	5.40E-04
s_R- s^r (T^r=15) °C	2.50E+00	8.06E-04	9.14E-01	1.29E-04
s_R- s^r (T^r=40) °C	2.15E+00	8.06E-04	7.64E-01	1.74E-04
s_R- s^r (T^r=100) °C	1.41E+00	8.06E-04	3.45E-01	4.04E-04
h_R, kJ/kg @ T_R	1.05E+03	2.14E+02	6.96E+00	1.95E-04
s_R, kJ/kg-°C @ T_R	2.72E+00	8.05E-04	1.00E+00	1.09E-04

19 different cases were considered while doing this illustrative example for Denizli-Kızıldere geothermal field. The results are given at Table 7.4 below;

Table 7.4 : The results of analytic volumetric probabilistic estimations of geothermal reserves by AUPM, MCM (Garg and Combs, 2015 approximation), USGS and MIT methods for Kızıldere geothermal field.

Case	Approximation	Method	Volumetric Probabilistic Reserve Estimations			% difference in each Case			%Difference in P10 in comparison to Case 1 AUPM	%Difference in P50 in comparison to Case 1 AUPM	%Difference in P90 in comparison to Case 1 AUPM
			P10	P50	P90	P10	P50	P90			
C1	**Garg & Combs_Flash**	**AUPM**	179	274	420	**6**	**5**	**0**			
		MCM	168	288	418						
C 2	**USGS (T^r=15 ºC & η_{th} =0.11)**	**AUPM**	60	91	140	7	2	1	66	67	67
		MCM	56	93	141						
C 3	**USGS (T^r =15 ºC & η_{th} =0.18)**	**AUPM**	98	149	229	7	3	1	45	45	45
		MCM	91	154	231						
C 4	**USGS (T^r =15 ºC & η_{th} =0.4)**	**AUPM**	217	332	508	6	3	1	18	17	17
		MCM	205	344	514						
C 5	**USGS (T^r =40 ºC & η_{th} =0.11)**	**AUPM**	46	71	109	7	3	2	74	74	74
		MCM	43	73	111						
C6	**USGS (T^r =40 ºC & η_{th} =0.18)**	**AUPM**	76	116	178	7	4	2	58	58	58
		MCM	71	121	182						
C 7	**USGS (T^r =40 ºC & η_{th} =0.4)**	**AUPM**	169	259	396	7	2	1	**6**	**5**	**6**
		MCM	158	265	401				**1**[1]	**10**[1]	**5**[1]
C 8	**USGS (T^r =100 ºC η_{th} =0.11)**	**AUPM**	22	34	54	9	3	0	88	88	87
		MCM	20	35	54						
C 9	**USGS(T^r =100 ºC& η_{th} =0.18)**	**AUPM**	36	56	89	8	0	1	80	80	79
		MCM	33	56	90						
C 10	**USGS (T^r =100 ºC & η_{th} =0.4)**	**AUPM**	79	125	198	8	1	0	56	54	53
		MCM	73	126	198						
C 11	**MIT (T^r =15 ºC & η_{th} =0.11)**	**AUPM**	220	337	516	6	5	0	19	19	19
		MCM	208	356	517						
C 12	**MIT (T^r=15 ºC & η_{th} =0.18)**	**AUPM**	361	552	844	6	6	1	51	50	50
		MCM	339	584	850						
C 13	**MIT (T^r=15 ºC & η_{th} =0.4)**	**AUPM**	802	1226	1876	6	5	0	78	78	78
		MCM	752	1294	1876						

Table 7.4 (continued) : The results of analytic volumetric probabilistic estimations of geothermal reserves by AUPM, MCM (Garg and Combs, 2015 approximation), USGS and MIT methods.

Case	Method	Approximation	Volumetric Probabilistic Reserve Estimations			% difference in each Case			Difference in P10 in comparison to Case 1 AUPM	Difference in P50 in comparison to Case 1 AUPM	Difference in P90 in comparison to Case 1 AUPM
			P10	P50	P90	P10	P50	P90	%	%	%
C14	MIT (T^r=40 ºC & η_{th} =0.11)	**AUPM**	196	300	459	5	6	1	**9**	**9**	**9**
		MCM	186	320	463				**10**[1]	**10**[1]	**10**[1]
C 15	MIT (T^r =40 ºC & η_{th} =0.18)	**AUPM**	321	491	751	7	5	0	44	44	44
		MCM	300	516	752						
C 16	MIT (T^r =40 ºC & η_{th} =0.4)	**AUPM**	713	1091	1670	7	6	0	75	75	75
		MCM	664	1157	1676						
C 17	MIT (T^r =100 ºC& η_{th} =0.11)	**AUPM**	138	211	323	6	6	1	23	23	23
		MCM	130	224	325						
C 18	MIT (T^r =100 ºC& η_{th} =0.18)	**AUPM**	226	345	529	6	6	1	21	21	21
		MCM	212	366	534						
C 19	MIT (T^r =100 ºC& η_{th} =0.4)	**AUPM**	502	768	1175	7	5	1	64	64	64
		MCM	469	808	1181						

[1]Difference (%) in comparison to Case 1 MCM

It is known that the Garg and Combs (2015) method gives the most realistic results in estimation of volumetric probabilistic reserves of geothermal resources. According to the results of Table 7.4 the closest AUPM approximation to Garg and Combs, 2015 method is Case 7 (USGS T^r=40 ºC and η_{th} =0.4) with 6% difference in comparison to AUPM P10, 5% difference in comparison to AUPM P50 and 6% difference in comparison to AUPM P90 reserves. Also the comparison of difference in percentage to MCM results obtained in Case 1 are added below the AUPM correlation percentages. Based on that correlation made between AUPM result obtained in Case 1 and MCM result obtained in Case 1, the difference is 1% for P10, 10% for P50 ans 5% for P90 reserve estimations.

The comparison of results in each individual case shows that AUPM application to Garg and Combs, USGS and MIT methods work really well. But it is really obvious that Case 2, 3, 5, 6, 8, 9, 10, 12, 13, 15, 16,17, 18 and 19 are so far away from the realistic results of reserves based on resultant values obtained from AUPM in Case 1.

Case 4 (USGS), Case 7 (USGS), Case 11 (MIT) and Case 14 (MIT) (also see Table 7.5 below for details of the cases below) are the ones have given the closest results to AUPM Case 1. Based on Case 7, it could be said that if one has persistence to use USGS method reference temperature value 40 ºC and conversion efficiency value around 0.4 gives the most approximate results to AUPM with around 6% difference and MCM with around 6% difference. Or if one has still want to use MIT method then it could be recommended to use reference temperature value close to 40 ºC and power plant conversion efficiency value around 0.11. Then the resultant reserves from MIT method in this case will have been overestimated with around 10% difference in comparison to MCM and AUPM in Case 1.

At that point, we should point out that the MIT and USGS methods do not consider the real power conversion system as flash and binary, separator temperature, pressure or enthalpy (for MIT) or entropy values designated properly. So logically the best estimation method is Garg and Combs approximation considering the real working system thermodynamic properties and AUPM is a very good and easy analytical approximation to reserves as an alternative to MCM simulations.

So Table 7.5 shows the summary of the results of volumetric probabilistic estimation of geothermal reserve of Kızıldere field by AUPM, MCM approximations using

Garg and Combs (2015), USGS (1970) and MIT (2006) methods giving very close PW values to each other.

Table 7.5 : Summary of the results of volumetric probabilistic estimation of geothermal reserve of Kızıldere field by AUPM, MCM approximations using Garg and Combs (2015), USGS (1970), and MIT (2006), methods giving very close PW values to each other.

Case	Method	Approximation	Volumetric Probabilistic Reserve Estimations (*PW*, MWe)		
			P10	P50	P90
C 1	Garg & Combs_Flash	AUPM	179	274	420
		MCM	168	288	418
C 4	USGS (T^r =15 ºC & η_{th} =0.4)	AUPM	217	332	508
		MCM	205	344	514
C 7	USGS (T^r=40 ºC & η_{th} =0.4)	AUPM	169	259	396
		MCM	158	265	401
C11	MIT (T^r=15 ºC & η_{th} =0.11)	AUPM	220	337	516
		MCM	208	356	517
C14	MIT (T^r=40 ºC & η_{th} =0.11)	AUPM	196	300	459
		MCM	186	320	463

7.2 Germencik Field

Germencik geothermal field is located on the western part of Büyük Menderes Graben in the Egean Region of Turkey. The field is discovered by MREI in 1968 and today it is operated by Gürmat and Maren geothermal companies. Aydın/Germencik/Ömerbeyli field is operated by Gürmat electricity production company with double flash power cycle having the installed capacity 162.3 MWe and Aydın/Germencik/Hıdırbeyli/Bozköy district is operated by Maren geothermal company with a binary power plant having installed capacity 92 MWe for electricity production (Table 2.2; Akkuş and Alan, 2016).

Based on the personal interview was done with Akkuş in 2016, maximum recorded reservoir temperature for Aydın/Germencik double flash operated area is 239.51 ºC measured in drilled geothermal wells in the area. The license coverage of Germencik geothermal field is 21 km^2 based on MREI, 2016 geothermal license areas map (Figure 2.12, Url-13). This temperature and area values are accepted as the mostly represented values in volumetric reserve calculations done in this section by using

AUP method with flash power conversion cycle approach of Garg and Combs, 2015 in comparison to MC, USGS and MIT methods that the ones listed as the methods giving the closest results of AUP and MC methods. It is assumed that the geothermal fluid is separated at 4 bars (therefore the saturation temperature of the fluid is 143.608 ^{o}C). Input parameters used in the calculations for Garg and Combs, 2015 double flash cycle is given in Table 7.6, the parameters used for USGS and MIT methods (cases in which gives the closest results to AUP and MC methods, namely (C4, C7, C11 and C14; see Table 7.5) is given at Table 7.7 and the mean and variance of X_i and lnX_i values are given at Table 7.8 below;

Table 7.6 : Parameters used in the calculations of Garg and Combs, 2015 double flash cycle for Aydın-Germencik field.

Parameter	Distribution Type	Minimum	Mode	Maximum
Reservoir Area (A, m^2)	Triangular	19000000	21000000	23000000
Reservoir Thickness (H, m)	Triangular	750	1500	2000
Resource Temperature (T_R, °C)	Triangular	234.5	239.5	244.5
Porosity (ϕ , fraction)	Triangular	0.01	0.08	0.13
Resource Pressure(p_R, bar)	Constant		52	
Specific heat capacity of brine ($c_p)_f$, kJ/kg-^{o}C)	Triangular	4.70239	4.74676	4.79512
Density of brine (ρ_f , kg/m^3)	Triangular	808.681	816.036	823.171
Specific heat capacity of rock ($c_p)_R$, kJ/kg-^{o}C	Constant		0.92	
Density of rock (ρ_R , kg/m3)	Triangular	2500	2600	2700
Volumetric specific heat capacity of rock $\left(\rho c_p\right)_R$, (kg/m^3-^{o}C)	Triangular	2316	2511	2665
Recovery factor (R_g, fraction)	Triangular	0	0.05	0.15
Seperator pressure (p_{sep}, bar)	Constant		4	
Plant seperator temperature (T_{sep}, ^{o}C)	Constant		143.608	
T_R– T_{sep} (°C)	Triangular	90.892	95.892	100.892
Plant condenser temperature (T_c , ^{o}C)	Constant		40	
Power conversion efficiency (η_c , fraction)	Constant		0.847	
Plant condenser temperature (T_c , ^{o}C)	Constant		40	
Project life (t_p, 25x31557600, **sec)**	Constant		788940000	
Load factor (L_F, fraction)	Constant		0.95	
h_{stm} (T_{sep}=143.608 ^{o}C) (kJ/kg)	Constant		2738.05	
s_{stm}(T_{sep}= 143.608^{o}C) (kJ/kg-^{o}C)	Constant		6.89549	
h_w (T_c=40 ^{o}C) (kJ/kg)	Constant		167.533	
s_w(T_c=40 ^{o}C) (kJ/kg-^{o}C)	Constant		0.572402	

Table 7.6 (continued): Parameters used in the calculations of Garg and Combs, 2015 double flash cycle for Aydın-Germencik field.

Parameter	Distribution Type	Minimum	Mode	Maximum
h_{gl} (T_{sep}= 143.608 ºC) =(h_{stm}-h_w)	Constant		2133.397	
T_{cK}, K @ (T_c=40 ºC)	Constant		313.15	

Table 7.7 : Input parameters used for USGS and MIT methods for Aydın-Germencik geothermal field.

Parameter	Distribution Type	Minimum	Mode	Maximum
Reservoir Area (A, m^2)	Triangular	19000000	21000000	23000000
Reservoir Thickness (H, m)	Triangular	750	1500	2000
Resource Temperature (T_R, °C)	Triangular	234.5	239.5	244.5
Resource Pressure (p_R, bar)	Constant	52	52	52
Porosity (ϕ , fraction)	Triangular	0.01	0.08	0.13
Specific heat capacity of brine (c_p)$_f$, kJ/kg-ºC)	Triangular	4.70239	4.74676	4.79512
Density of brine (ρ_f , kg/m^3)	Triangular	808.681	816.036	823.171
Specific heat capacity of rock (c_p)$_R$, kJ/kg-ºC	Constant		0.92	
Density of rock (ρ_R , kg/m3)	Triangular	2500	2600	2700
Volumetric specific heat capacity of rock $(\rho c_p)_R$ kg/m^3-ºC)	Triangular	2316	2511	2665
Recovery factor (R_g, fraction)	Uniform	0	0.05	0.15
Specific Enthalpy of the reservoir (h_R, kJ/kg) @ T_R	Triangular	1011.73	1035.36	1059.21
Specific entropy of the reservoir (s_R, kJ/kg-ºC) @ T_R	Triangular	2.64696	2.69326	2.73956
Reference temperature (T^r, ºC)	Constant		For USGS: 15, 40 ºC For MIT: 15,40 ºC	
T_R- T^r (T^r = 15) °C	Triangular	219.5	224.5	229.5
T_R- T^r (T^r = 40) °C	Triangular	194.5	199.5	204.5
T_R- T^r (T^r = 100) °C	Triangular	134.5	139.5	144.5
h_R- h^r (T^r=15) °C	Triangular	948.7485	972.3785	996.2285
h_R- h^r (T^r=40) °C	Triangular	844.197	867.827	891.677
s_R- s^r (T^r=15) °C	Triangular	2.422497	2.468797	2.515097
s_R- s^r (T^r=40) °C	Triangular	2.074558	2.120858	2.167158
Thermal conversion factor (fraction)	Constant		For USGS: 0.4 For MIT: 0.11	
Project life (t_p, 25x31557600, sec)	Constant		788940000	
Load factor (L_F, fraction)	Constant		0.95	
T_{rK} (T^r=15 ºC)	Constant		288.15	
h^r (T^r=15 ºC) (kJ/kg)	Constant		62.9815	
h^r (T^r=40 ºC) (kJ/kg)	Constant		167.533	
s^r (T^r=15 ºC) (kJ/kg-ºC)	Constant		0.224463	
s^r (T^r=40 ºC) (kJ/kg-ºC)	Constant		0.572402	
T_{rK} (T^r=40 ºC)	Constant		313.15	

Table 7.8 below shows the mean and variance of input parameters X_i and $\ln X_i$ calculated analytically and generated randomly by sampling for AUPM approximation.

Table 7.8 : Mean and variance of input parameters X_i and $\ln X_i$ calculated analytically and generated randomly.

X_i	μ_{X_i}	$\sigma^2_{X_i}$	$\mu_{\ln X_i}$	$\sigma^2_{\ln X_i}$
R_g, fraction	6.67E-02[1]	9.72E-04[1]	2.85E+00[1]	3.50E-01[1]
	6.67E-02[11]	9.72E-04[11]	2.85E+00[11]	2.35E-01[11]
A, m^2	2.10E+07[1]	6.67E+11[1]	1.69E+01[1]	1.52E-03[1]
	2.10E+07[11]	6.67E+11[11]	1.69E+01[11]	1.51E-03[11]
H, m	1.42E+03[1]	6.60E+04[1]	7.24E+00[1]	3.65E-02[1]
	1.42E+03[11]	6.60E+04[11]	7.24E+00[11]	3.38E-02[11]
$\left(\rho c_p\right)_R$	2.50E+03[1]	5.10E+03[1]	7.82E+00[1]	8.22E-04[1]
	2.50E+03[11]	5.10E+03[11]	7.82E+00[11]	8.19E-04[11]
T_R-T_{sep}, °C	9.59E+01[1]	4.17E+00[1]	4.56E+00[1]	4.54E-04[1]
	9.59E+01[11]	4.17E+00[11]	4.56E+00[11]	4.53E-04[11]
T_R-T^r (T^r=15), °C	2.25E+02[1]	4.17E+00[1]	5.41E+00[1]	8.27E-05[1]
	2.25E+02[11]	4.17E+00[11]	5.41E+00[11]	8.27E-05[11]
T_R-T^r (T^r=40), °C	2.00E+02[1]	4.17E+00[1]	5.30E+00[1]	1.05E-04[1]
	2.00E+02[11]	4.17E+00[11]	5.30E+00[11]	1.05E-04[11]
T_R-T^r (T^r=100), °C	1.40E+02[1]	4.17E+00[1]	4.94E+00[1]	2.14E-04[1]
	1.40E+02[11]	4.17E+00[11]	4.94E+00[11]	2.14E-04[11]
h_R- h^r (T^r=15) °C	9.72E+02[1]	9.39E+01[1]	6.88E+00[1]	9.94E-05[1]
	9.72E+02[11]	9.39E+01[11]	6.88E+00[11]	9.93E-05[11]
h_R- h^r (T^r=40) °C	8.68E+02[1]	9.39E+01[1]	6.77E+00[1]	1.25E-04[1]
	8.68E+02[11]	9.39E+01[11]	6.77E+00[11]	1.25E-04[11]
s_R- s^r (T^r=15) °C	2.47E+00[1]	3.57E-04[1]	9.04E-01[1]	5.86E-05[1]
	2.47E+00[11]	3.57E-04[11]	9.04E-01[11]	5.86E-05[11]
s_R- s^r (T^r=40) °C	2.12E+00[1]	3.57E-04[1]	7.52E-01[1]	7.95E-05[1]
	2.12E+00[11]	3.57E-04[11]	7.52E-01[11]	7.94E-05[11]
h_R, kJ/kg @ T_R	1.04E+03[1]	9.39E+01[1]	6.94E+00[1]	8.76E-05[1]
	1.04E+03[11]	9.39E+01[11]	6.94E+00[11]	8.76E-05[11]
s_R, kJ/kg-°C @ T_R	2.69E+00[1]	3.57E-04[1]	9.91E-01[1]	4.93E-05[1]
	2.69E+00[11]	3.57E-04[11]	9.91E-01[11]	4.93E-05[11]

So Table 7.9 shows the summary of the results of volumetric probabilistic estimation of geothermal reserve of Germencik field by AUPM, MCM approximations using Garg and Combs (2015), USGS (1970) and MIT (2006) methods.

[1] These values are determined by simulation numerically by creating a triangular probability distribution in Matlab

[11] These values are calculated analytically in Matlab.

The results in Table 7.9 are obtained by using the variance of the natural logarithm of recovery factor determined by simulation numerically by creating a triangular probability distribution in Matlab.

Based on the results of volumetric probabilistic estimation of geothermal reserve of Germencik field by AUPM, MCM approximations using Garg and Combs (2015), USGS (1970), and MIT (2006), AUPM Garg and Combs application has 1% difference in comparison to MCM result in P10, 8% difference in comparison to P50 result of MCM and 8% difference to P90 result of MCM. The USGS and MIT applications of AUP method gives closer values to Case 1 with USGS reference temperature values 15 and 40 ^{o}C with 40% conversion efficiency common for both USGS cases (C2 and C3). When correlating between results obtained from AUPM application to MIT method (Cases 4 and 5) it's obvious that very close results have been reached by 15 and 40 ^{o}C reference temperatures with 11% conversion efficiency. The closest result to Case 1 AUPM Garg and Combs application is obtained from MIT Case 5 where zero difference has been recorded for P10 resultant values in between Case 5 itself and also the result of AUPM MIT application has shown only 2% diffeence to the one that calculated by AUPM in Case 1 in P10, P50 and P90 values.

Table 7.10 summarizes the results of volumetric probabilistic estimation of geothermal reserve of Germencik field by AUPM, MCM approximations using Garg and Combs (2015), USGS (1970), and MIT (2006), methods giving very close PW values to each other by using the variance of the natural logarithm of recovery factor determined calculated analytically.

As a conclusion, comparing the results between Table 7.9 and Table 7.10, it could be said that when the variance of natural logarithm of Rg is taken as analytically calculated, then the resultant P10 AUPM values show 13-14% difference in comparison to MCM while this difference is nearly 1-2% for each case when the variance of the natural logarithm of Rg is taken as numerically simulated by using a triangular probability distribution. P50 values didn't show any difference while P90 values show 3-4% difference in AUPM in comparison to MCM results. This difference is recorded as 8-10% in Table 7.9 where the variance of natural logarithm of Rg is taken as numercally simulated. That is, in the usage of analytically calculated variance of natural logarithm of recovery factor where the lower limit is

zero, the resultant P10 values diverges, P50 values stays the same and P90 values gets converges according to the values obtained in the case where the variance of natural logarithm of recovery factor is determined by numerical simulation of a probability distribution.

Table 7.9 : Summary of the results of volumetric probabilistic estimation of geothermal reserve of Germencik field by AUPM, MCM approximations using Garg and Combs (2015), USGS (1970), and MIT (2006), methods giving very close PW values to each other ($\sigma^2_{\ln Rg} = 0.35$).

Case	Method	Approximation	Volumetric Probabilistic Reserve Estimations			% difference in each Case			Difference in P10 in comparison to Case 1 AUPM %	Difference in P50 in comparison to Case 1 AUPM %	Difference in P90 in comparison to Case 1 AUPM %
			P10	P50	P90	P10	P50	P90			
C 1	Garg & Combs_Flash	AUPM	57	127	281	1	8	8			
		MCM	56	138	258						
C 2	USGS (T^r =15 ºC & η_{th} =0.4)	AUPM	61	136	301	3	8	9	7	7	7
		MCM	63	148	275						
C 3	USGS (T^r=40 ºC & η_{th} =0.4	AUPM	48	106	234	2	8	9	16	17	17
		MCM	47	115	214						
C 4	MIT (T^r=15 ºC & η_{th} =0.11	AUPM	63	139	309	0	7	10	10	9	9
		MCM	63	150	278						
C 5	MIT (T^r=40 ºC & η_{th} =0.11	AUPM	56	124	274	0	8	10	2	2	2
		MCM	56	135	248						
C 6*	MIT (T^r=100 ºC & η_{th} =0.2	AUPM	75	166	368	5	3	13	24	23	24
		MCM	71	172	318						

*Case 6 is especially designed to be able to compare the results obtained by the method which Başel (2010) used in her PhD thesis by accepting the reference temperature as 100 ºC and calculating power conversion efficiency by using a correlation given by MIT for binary power plants given in the 4th part of this thesis (Eq. 4.16). Based on the results it is obvious that this method did not work well for flash conversion systems because of the thermal conversion efficicency is calculated by using the Eq. 4.16 proposed for binary power plants.

Table 7.10 : Summary of the results of volumetric probabilistic estimation of geothermal reserve of Germencik field by AUPM, MCM approximations using Garg and Combs (2015), USGS (1970), and MIT (2006), methods giving very close PW values to each other ($\sigma^2_{\ln Rg} = 0.235$).

Case	Method	Approximation	Volumetric Probabilistic Reserve Estimations			% difference in each Case			Difference in P10 in comparison to Case 1 AUPM %	Difference in P50 in comparison to Case 1 AUPM %	Difference in P90 in comparison to Case 1 AUPM %
			P10	P50	P90	P10	P50	P90			
C 1	Garg & Combs_Flash	AUPM	65	127	247	14	8	4			
		MCM	56	138	258						
C 2	USGS (T^r =15 ºC & η_{th} =0.4)	AUPM	70	136	265	10	8	4	8	7	7
		MCM	63	148	275						
C 3	USGS (T^r=40 ºC & η_{th} =0.4	AUPM	54	106	206	13	8	4	17	17	17
		MCM	47	115	214						
C 4	MIT (T^r=15 ºC & η_{th} =0.11	AUPM	72	139	271	13	7	3	10	9	9
		MCM	63	150	278						
C 5	MIT (T^r=40 ºC & η_{th} =0.11	AUPM	64	124	241	13	8	3	2	2	2
		MCM	56	135	248						
C 6	MIT (T^r=100 ºC & η_{th} =0.2	AUPM	85	166	323	17	4	2	24	24	24
		MCM	71	172	318						

Now taking the Germencik geothermal reservoir as the real case, the comparison of Garg and Combs method results belong to the producible potential reserves with the real case data is given.

In 2009, the operator of the field constructed a 47.4 MWe double-flash power plant based on 6 production and 7 reinjection wells and generating electricity since then (Unverdi and Cerci 2013). Currently the operator of the field has new exploration and development studies to extend the power capacity to 232.3 MWe in the near future.In our calculation the data for reservoir area, resource temperature, thickness, and volumetric capacity are taken from Başel (2010) PhD illustrated in Table C.7. Başel considered a maximum resource temperature of 235 ^{o}C, but we consider a maximum resource temperature of 239.5 ^{o}C instead as this is the maximum temperature measured in the field. We define recovery factor with a uniform distribution with the minimum value is "0" and the maximum value is 0.2. Knowing that Germencik geothermal field is not in the early exploration phase, we wanted to make a fair comparison with the current capacity of the field. We used a conversion efficiency of 87.4%, as reported by Unverdi and Cerci (2013) since Germencik field is operated by a double-flash power conversion system.

For this field, she gives a maximum reservoir area of 7 km^2. This value of area seems small as compared to the reported values of 50 km^2 by Unverdi and Cerci (2013) and 36 km^2 by Tureyen et al. (2014). Başel (2010) estimated the reservoir area information from field resistivity measurements and geological cross sections prior to 2010. The reported values of 50 km^2 and 36 km^2 presumably include new concession areas. So we define a triangular area distribution with 25 km^2 as the minimum, 30 km^2 as the mode and 50 km^2 as the maximum value.

In the Germencik double-flash power cycle, the produced fluid entering the high pressure steam system (HPS) is separated at 5.972 bars at the turbine inlet (Unverdi and Cerci 2013). Ignoring any pressure drop between the high-pressure separator and the tribune inlet, the separator temperature (saturation temperature) is 158.644 ^{o}C. The turbine inlet pressure is set equal to the separator pressure. The condenser temperature is 40 ^{o}C (Unverdi and Cerci 2013). Our estimation results are as follows;

- P10 - 44.4 MWe
- P50 - 218 MWe
- P90 - 438 MWe

Based on these results we could say that the Garg and Combs method gives perfectly matching results in comparison to the real operating condition of the field. In 2009

Germencik geothermal field is started to be operated by 47.4 MWe installed capacity which is so much close to our P10 value and today the operator has already extended the installed capacity up to 232.3 MWe (Url 20). Based on the exergy analysis of the power cycle and this value is so much close to our P50 value calculated by Garg and Combs method by using the operating thermodynamic system in Germencik geothermal field.

7.3 Salavatlı Field

Salavatli geothermal field is located in one of the most promising geothermal regions, on the northern flank of Büyük Menderes graben of Menderes Massif. The field was discovered after a regional resistivity survey conducted by MREI Institute of Turkey. Two wells were drilled in 1987 and 1988 to 1500 m and 962 m, with temperatures of 169.5^{o}C and 172.5^{o}C, respectively (Serpen et. al., 2015). 172.5 ^{o}C is the highest resource temperature recorded in drilled wells in Salavatlı geothermal field up until now (Akkuş, 2016, Table 2.4). Today Salavatlı geothermal field is operated by Menderes Geothermal Energy with a 51.451 MWe installed capacity of a binary plant (Table 2.2).

In this illustrative example of Salavatlı geothermal field, pentane is assumed to be the secondary working geothermal fluid and turbine inlet pressure is assumed as 7.5 bars (the saturation temperature of pentane is 110.81 ^{o}C at this pressure value) with a 5 ^{o}C temperature differential between original geothermal hot water and the secondary working fluid pentane at the pinch point. The license coverage of Germencik geothermal field is 34 km^2 based on MREI, 2016 geothermal license areas map (Figure 2.12, Url-13). This temperature and area values are accepted as the mostly represented values in volumetric reserve calculations done in this section by using AUP method with binary power conversion cycle approach of Garg and Combs, 2015 in comparison to MC, USGS and MIT methods applications that the ones listed as the methods giving the closest results (see Table 7.9 and Table 7.10) of AUP method. The other parameters used for this illustrative example of Garg and Combs method, USGS and MIT applications of AUPM in comparison to the MC simulation results is listed at Table 7.11 below for the binary working cycle.

Input parameters used for USGS and MIT methods for Aydın-Salavatlı geothermal field is listed at Table 7.12 below.Table 7.13 below shows the mean and variance of

input parameters X_i and $\ln X_i$ calculated analytically by using Matlab-2014 for AUPM approximation.

Table 7.11 : Parameters used in the calculations of Garg and Combs, 2015 binary cycle for Aydın-Salavatlı geothermal field.

Parameter	Dist.n Type	Minimum	Mode	Maximum
Reservoir Area (A, m^2)	Triangular	32000000	34000000	36000000
Reservoir Thickness (H, m)	Triangular	750	1000	1500
Resource Temperature (T_R, °C)	Triangular	167.5	172.5	177.5
Volumetric specific heat capacity of rock $\left(\rho c_p\right)_R$ (kg/m^3-°C)	Triangular	2350	2450	2550
Recovery factor (R_g, fraction)	Triangular	0.07	0.18	0.24
Condenser temperature (T_c, °C)	Constant		40	
Secondary fluid			Pentane	
Turbine inlet pressure (p_{in}, bar)	Constant		7.5	
Saturation temperature of secondary fluid (T_b, °C) @ p_{in}, bar	Constant		110.81	
Assumed temperature differential (°C) between original and secondary fluid	Constant		5	
Pinch point temperature (T_p, °C)	Constant		115.81	
T_R-T_p (°C)	Triangular	51.69	56.69	61.69
Secondary fluid bubble point pressure (p_{sfb}, bar) @ T_c	Constant		1.1567	
h_{sfl}(T_c=40 °C) (kJ/kg)	Constant		9.3689	
h_{sfl}(T_b=110.81 °C) (kJ/kg)	Constant		193.08	
s_{sfl} (T_c=40 °C) (kJ/kg-°C)	Constant		0.030032	
h_{sfg}(T_b=110.81 °C) (kJ/kg)	Constant		476.35	
s_{sfg} (T_b= 110.81°C) (kJ/kg-°C)	Constant		1.292	
Heat of vaporization of secondary fluid h_{sfgl}(T_b=110.81 °C) (kJ/kg) (h_{sfg}-h_{sfl} @ T_b=110.81 °C)	Constant		283.27	
V_{sf} (@ Tc= 40 °C and p_{sfb}= bar	Constant		0.001651	
T_{cK}, K @ (T_c=40 °C)	Constant		313.15	
Thermal conversion factor (fraction)	Constant		0.75	
Project life (t_p, years)	Constant		25	
Load factor (L_F, fraction)	Constant		0.95	

Table 7.12 : Input parameters used for USGS and MIT methods for Aydın-Salavatlı geothermal field.

Parameter	Distribution Type	Minimum	Mode	Maximum
Reservoir Area (A, m^2)	Triangular	32000000	34000000	36000000
Reservoir Thickness (H, m)	Triangular	750	1000	1500
Resource Temperature (T_R, °C)	Triangular	167.5	172.5	177.5
Resource Pressure (p_R, bar)	Constant		52	
Volumetric specific heat capacity of rock $\left(\rho c_p\right)_R$ kg/m^3-°C)	Triangular	2350	2450	2550
Recovery factor (R_g, fraction)	Uniform	0.07	0.18	0.24
Specific Enthalpy of the reservoir fluid (h_R, kJ/kg) @ T_R	Triangular	710.64	732.393	754.233
Specific entropy of the reservoir fluid (s_R, kJ/kg-°C) @ T_R	Triangular	2.01147	2.06055	2.10929
Reference temperature (T^r, °C)	Constant		For USGS: 15, 40 °C For MIT: 15,40 °C	
T_R- T^r (T^r = 15) °C	Triangular	152.5	157.5	162.5
T_R- T^r (T^r = 40) °C	Triangular	127.5	132.5	137.5
h_R- h^r (T^r=15) °C	Triangular	647.6585	669.4115	691.2515
h_R- h^r (T^r=40) °C	Triangular	543.107	564.86	586.7
s_R- s^r (T^r=15) °C	Triangular	1.787007	1.836087	1.884827
s_R- s^r (T^r=40) °C	Triangular	1.439068	1.488148	1.536888
Thermal conversion factor (fraction)	Constant		For USGS: 0.4 For MIT: 0.11	
Project life (t_p, 25x31557600, **sec)**	Constant		788940000	
Load factor (L_F, fraction)	Constant		0.95	
T_{rK} (T^r=15 °C)	Constant		288.15	
h^r (T^r=15 °C) (kJ/kg)	Constant		62.9815	
h^r (T^r=40 °C) (kJ/kg)	Constant		167.533	
s^r (T^r=15 °C) (kJ/kg-°C)	Constant		0.224463	
s^r (T^r=40 °C) (kJ/kg-°C)	Constant		0.572402	
T_{rK} (T^r=40 °C)	Constant		313.15	

So Table 7.14 shows the summary of the results of volumetric probabilistic estimation of geothermal reserve of Salavatlı field by AUPM, MCM approximations using Garg and Combs (2015) binary, USGS (1970), and MIT (2006), methods giving very close PW values to each other.

Table 7.13 : Mean and variance of input parameters X_i ans lnX_i calculated analytically.

X_i	μ_{X_i}	$\sigma^2_{X_i}$	$\mu_{\ln X_i}$	$\sigma^2_{\ln X_i}$
R_g, fraction	1.63E-01	1.24E-03	-1.84E+00	4.84E-02
A, m^2	3.40E+07	6.67E+11	1.73E+01	5.77E-04
H, m	1.08E+03	2.43E+04	6.98E+00	2.06E-02
$\left(\rho c_p\right)_R$	2.45E+03	1.67E+03	7.80E+00	2.78E-04
T_R-T_p, ºC	5.67E+01	4.17E+00	4.04E+00	1.30E-03
T_R-T^r (T^r=15), ºC	1.58E+02	4.17E+00	5.06E+00	1.68E-04
T_R-T^r (T^r=40), ºC	1.33E+02	4.17E+00	4.89E+00	2.37E-04
h_R- h^r (T^r=15) °C	6.69E+02	7.92E+01	6.51E+00	1.77E-04
h_R- h^r (T^r=40) °C	5.65E+02	7.92E+01	6.34E+00	2.48E-04
s_R- s^r (T^r=15) °C	1.84E+00	3.99E-04	6.08E-01	1.18E-04
s_R- s^r (T^r=40) °C	1.49E+00	3.99E-04	3.97E-01	1.80E-04
h_R, kJ/kg @ T_R	7.32E+02	7.32E+02	6.60E+00	1.48E-04
s_R, kJ/kg-ºC @ T_R	2.06E+00	3.99E-04	7.23E-01	9.39E-05

The USGS application of Garg and Combs method MC simulation gives results that around 20% overestimate of P10, P50 and P90 values in Case 2 in comparison to MCM results and around 10% underestimate of P10, P50 and P90 values in Case 3 that could be acceptable close values to Case 1. But Case 4 and Case 5 which are the applications of Garg and Combs method on MIT and which worked well in flash power cycle potential estimations did not work very well for binary system of power conversion system installed in Salavatlı geothermal field. Case 4 gave 40% overestimated results to P10, P50 and P90 where Case 5 gave 28% overestimated results to P10, P50 and P90 MCM results. Case 6 gave very approximate results to Case 1 which was calculated by 100 ºC reference temperature and the power conversion efficiency value was calculated by using the moderate value of resource temperature in Eq 4.16 which is given by MIT to be used for binary plants which is the only Eq. Başel used in her PhD thesis (2010) without considering whether the power plant is operated or amenable to be operated by a binary or flash power conversion system.

Table 7.14 : Summary of the results of volumetric probabilistic estimation of geothermal reserve of Salavatlı field by AUPM, MCM approximations using Garg and Combs (2015) binary, USGS and MIT methods giving very close PW values to each other.

Case	Method	Approximation	Volumetric Probabilistic Reserve Estimations			% difference in each Case			Difference in P10 in comparison to Case 1 AUPM %	Difference in P50 in comparison to Case 1 AUPM %	Difference in P90 in comparison to Case 1 AUPM %
			P10	P50	P90	P10	P50	P90			
C 1	Garg & Combs_Binary	AUPM	141	199	280	4	2	0			
		MCM	135	204	280						
C 2	USGS(T^r =15 ºC & η_{th} =0.4)	AUPM	168	237	334	0	7	5	20	20	20
		MCM	168	255	352						
C 3	USGS (T^r=40 ºC & η_{th} =0.4	AUPM	117	168	241	0	7	3	13	9	11
		MCM	117	180	249						
C 4	MIT (T^r=15 ºC & η_{th} =0.11	AUPM	224	314	441	0	7	3	40	39	38
		MCM	224	336	455						
C 5	MIT (T^r=40 ºC & η_{th} =0.11	AUPM	189	265	372	0	7	4	28	28	28
		MCM	188	284	387						
C 6*	MIT (T^r=100 ºC & η_{th} =0.138	AUPM	142	200	281	8	3	5	4	4	5
		MCM	130	195	267						

*Case 6 is especially designed to be able to compare the results obtained by the method which Başel (2010) used in her PhD thesis by accepting the reference temperature as 100 ºC and calculating power conversion efficiency by using a correlation given by MIT for binary power plants given in the 4th part of this thesis (Eq 4.16).

Based on the results of volumetric probabilistic estimation of geothermal reserve of Salavatlı field by AUPM, MCM approximations using Garg and Combs (2015) binary, USGS (1970), and MIT (2006), AUPM Garg and Combs application has 4% difference in comparison to MCM result in P10, 2% difference in comparison to P50 result of MCM and no difference to P90 result of MCM in Case 1.

8. ADDITION OF POWER POTENTIAL OF GEOTHERMAL FIELDS

Total power generation potential should be determined after obtaining the results for reserves for each geothermal field individually. The aggregation problem has been studied in the petroleum engineering literature by a number of authors; see for example, Capen (1996, 2001), Carter and Morales (1998), van Elk et al. (2000), Demirmen (2007), and Delfiner and Barrier (2008). However, this problem has not yet received much attention in the geothermal literature. A previous work (Sarak et al, 2009), showed that the simple arithmetic sum may significantly underestimate the P10 and significantly overestimates the P90, relative to the corresponding ones estimated by probabilistic sum and that the statistically proper method of aggregating divers fields' resources is by probabilistic sum (Onur et al, 2010).

8.1 Simple Arithmetic Sum

Supposing n geothermal fields with the uncertainty of total resources (*Xs*) which is the sum of the resources of all X_i, i=1,2, … , n as shown in Eq. 8.1 below;

$$X_s = \sum_{i=1}^{n} X_i \tag{8.1}$$

The arithmetic sum assumes that all fields considered in aggregation are fully correlated (i.e., pair-wise correlation coefficients for all fields is equal to unity). In other words, probabilistic sum will be equal to the arithmetic sum if all fields are fully correlated. On the other hand, if we assume that all fields are independent and apply the probabilistic addition, then the probabilistic sum overestimates the P10 and P90 of the all fields used in aggregation (Onur et al, 2010).

8.2 Probabilistic Sum

Although the probabilistic sum is the most general approach that one should use whether the fields are independent or not, however it requires the knowledge of pair-wise correlation coefficients for the fields, which may be difficult to obtain (Karacaer and Onur, 2012). For example if we aggregate thermal resources of N_f geothermal fields, then we have to consider a total of N_f (N_f -1)/2 pair-wise correlations. For

example, if N_f = 10, then we would need 45 correlation coefficients, if N_f = 20, then we would need 190 correlation coefficients (Onur et al, 2010 and Karacer and Onur, 2012).

Probabilistic sum of reserves is based on the aggregation of mean and variances of P10, P50 and P90s for a total of N_f geothermal PW resources each following a lognormal distribution characterized by its mean $\mu_{PW_j}, j = 1,2,...,N_f$ and and variance $\sigma^2{}_{PW_j}, j = 1,2,...,N_f$ noting that each PW_j is log-normally distributed and each lnPW_j is normally distributed.

Supposing that one is interested in the uncertainty of the total resources (denoted by PW_S) which is equal to the sum of the resources of all PW_j, j = 1,2,…, N_f, given by Eq. 8.2 below (Onur et al, 2010 and Karacer and Onur, 2012);

$$PW_s = \sum_{j=1}^{n} PW_j \tag{8.2}$$

The mean and variance of *PWs* are given below respectively in Eq. 8.3 and Eq. 8.4;

$$\mu_{PW_s} = \sum_{j=1}^{n} \mu_{PW_j} \tag{8.3}$$

and,

$$\sigma^2_{PW_s} = \sum_{j=1}^{n} \sigma^2_{PW_j} + 2\sum_{i=1}^{n-1}\sum_{j=1}^{n} \rho_{PW_i,PW_j} \sqrt{\sigma^2_{PW_i}\,\sigma^2_{PW_j}} \tag{8.4}$$

where ρ_{PW_i,PW_j} represents the pair-wise correlation coefficient between field resources *i* and *j*.

If all fields are independent then Eq. 8.4 reduces to Eq. 8.5 given below;

$$\sigma^2_{PW_s} = \sum_{j=1}^{n} \sigma^2_{PW_j} \tag{8.5}$$

If it is assumed that all pair-wise correlations in Eq. 8.5 are equal to unity, i.e., $\rho_{PW_i,PW_j} = 1$, for all *i* and *j* such that $i \neq j$, then Eq. 8.5 reduces to Eq. 8.6 given below;

$$\sigma^2_{PW_s} = \left(\sum_{j=1}^{n} \sigma_{PW_j} \right)^2 \tag{8.6}$$

Knowing that based on CLT theorem regardless of the distribution type of input data, the resultant PW would be log-normal and the sum of the log-normal distributions of thermal field *PW* resources is normal, then, the P10, P50, and P90 of the PW_S are given by Eq. 8.7, Eq. 8.8 and Eq. 8.9 below (Onur et al, 2010 and Karacer and Onur, 2012);

$$P10_s = \exp\left(\mu_{PWs} - 1.28\sqrt{\sigma^2_{PWs}}\right) \tag{8.7}$$

$$P50_s = \mu_{PWs} \tag{8.8}$$

$$P90_s = \exp\left(\mu_{PWs} + 1.28\sqrt{\sigma^2_{PWs}}\right) \tag{8.9}$$

9. POWER GENERATION POTENTIAL OF TURKEY'S TWENTY FIVE GEOTHERMAL FIELDS AMENABLE TO POWER PRODUCTION

In her PhD study, Başel (2010) considered 25 geothermal fields of Turkey, which have resource temperature values higher than 100 ºC. She used the MIT method coupled with the Monte Carlo simulation to predict the electricity production potentialof these 25 geothermal fields. She referred to this estimation as the Turkey's geothermal electricity potential. She made the summation of production potential values in two different ways: By arithmetic averaging and by probabilistic averaging and at the end she calculated the arithmetic average of the two values obtained from arithmetic and probabilistic method to get a conclusive result for Turkey's electricity production potential. Those fields are listed at Table 1.2 in Chapter I of this thesis.

Başel (2010) used the MIT method while doing her calculations by using a reference temperature value of 100 ºC. For thermal conversion efficiency (η_{th}) she used a relationship for each of the fields which was developed by MIT engineers (2006) for only binary power conversion plants. This Eq. is as in Eq. 9.1 below;

$$\eta_{th} = 0.0935T_R - 2.3266 \quad (9.1)$$

As a result of her study, Başel (2010) estimated the electricity production potential of 25 fields having resource temperatures higher than 100 ºC as 1269 (P10), 1500 (P50) and 1839 MWe (P90) based on probabilistic summation of the field potentials and 840 (P10), 1428 (P50) and 2371 (P90) MWe based on the arithmetic averaging of the fields with electricity production potentials. Then she recommended using the arithmetic average of the probabilistically and arithmetically calculated estimates as the power generation potential of Turkey.

In a later work, Başel et al. (2013) revised her study by using 38 fields which are amenable to electricity production and get the results as 1673 (P10), 2263 (P50) and 3140 (P90) MWe (Table 2.3), but she didn't give any reservoir characteristics information about the fields such as thickness, porosity, recovery factor, area and

even the names of the fields she studied. So, Başel et al. (2013) estimates cannot be reproduced.

Based on a personal communication made with Akkuş in 2016, he states that today Turkey has 39 geothermal fields amenable to electricity production but only mostly represented reservoir temperature values are available data for the fields. Only 18 fields are common fields which Başel studied in her PhD thesis in 2010. So if one intends to make a volumetric reserve estimation by using these 39 fields the results will have huge amount of uncertainty because of the lack of information about reservoir thickness, areal extension etc. The obtained results will be far away from being realistic due to the foundation of the estimations of reservoir parameters so much subjective.

That's why in this section only 25 fields which all needed reservoir information is given in Başel's PhD thesis in 2010 is examined here by using Garg and Combs method in AUP and MC applications and the results are compared with Başel's (2010) results.

In this examination, the geothermal fields having moderate resource temperatures higher than 180 ^{o}C (when there was no mostly represented value estimation, the minimum value is used while deciding the power plant conversion system) are accepted as proper for single flash power conversion systems and the field having moderate (or minimum if there is no moderate value available) resource temperatures below than 180 ^{o}C are accepted as proper for binary type power conversion systems. For the fields, turbine inlet and seperator pressure value is accepted as 4 bars as constant. Also project life and load factor are accepted as constant values because these values are nearly certain for a geothermal plant. Volumetric specific heat capacity of the reservoirs are calculated by using constant values of porosity, density of rock and fluid and specific heat capacities of rock and fluid for minimum, moderate and maximum cases and the resultant probabilistic values are evaluated by using a triangular distribution concept. The results are presented at Table 9.1 below. The detailed reservoir characteristic values used in volumetric probabilistic estimation of reserves are given at Appendix C (which are taken from Başel's PhD thesis (2010).

Table 9.1 : MCM and AUPM results of 25 geothermal fields which are amenable to electricity production in comparison to the results obtained by Başel (2010) PhD thesis by using the same reservoir parameters.

Results of Garg and Combs (2015) method (AUPM, MCM)								**Başel's PhD (2010) Results (Method: MIT, MC, T^r=100 ºC)**			
Field	**Assumed power conversion system**	**Method**	$\mu_{\ln PW}$	$\sigma^2_{\ln PW}$	**P10**	**P50**	**P90**	η_{th}	**P10**	**P50**	**P90**
Alaşehir, Sarıkız-Manisa	Binary	AUP	1.894	0.174	3.89	6.65	11.35	0.13	3.3	6.8	12.8
		MC	1.895	0.187	3.76	6.77	11.49				
Atça-Aydın	Binary	AUP	0.805	0.086	1.53	2.24	3.26	0.11	1.0	1.7	2.7
		MC	0.805	0.093	1.49	2.28	3.27				
Balçova-İzmir	Binary	AUP	0.491	0.265	0.84	1.63	3.15	0.10	0.5	1.1	2.3
		MC	0.491	0.286	0.82	1.64	3.24				
Dikili-İzmir	Binary	AUP	2.697	0.244	7.88	14.83	27.91	0.12	4.6	13.0	33.1
		MC	2.697	0.264	7.51	15.06	28.69				
Germencik-Aydın	Single Flash	AUP	4.060	0.122	37.05	57.98	90.71	0.18	48.9	82.1	128.4
		MC	4.061	0.131	35.76	59.23	91.20				
Gümüşköy-Aydın	Binary	AUP	4.333	0.366	35.10	76.17	165.32	0.10	12.3	48.8	134.1
		MC	4.333	0.409	32.62	77.56	175.51				
Kızıldere 1-Denizli	Single Flash	AUP	3.148	0.063	16.89	23.28	32.09	0.17	109.1	139.4	180.4
		MC	3.149	0.069	16.14	24.06	31.89				
Kızıldere 2-Denizli	Single Flash	AUP	4.301	0.056	54.57	73.80	99.81	0.20			
		MC	4.302	0.063	51.80	76.71	99.01				
Nazilli-Aydın	Binary	AUP	2.535	0.089	8.62	12.62	18.47	0.14	8.3	14.2	22.4
		MC	2.535	0.097	8.35	12.94	18.55				
Pamukören 1-Aydın	Binary	AUP	2.218	0.056	6.78	9.19	12.45	0.15	26.4	33.5	42.4
		MC	2.218	0.063	6.43	9.54	12.31				
Pamukören 2-Aydın	Single Flash	AUP	2.720	0.061	11.08	15.18	20.80	0.17			
		MC	2.725	0.067	10.60	15.79	20.74				

Table 9.1 (continued): MCM and AUPM results of 25 geothermal fields which are amenable to electricity production in comparison to the results obtained by Başel (2010) PhD thesis by using the same reservoir parameters.

Results of Garg and Combs (2015) method (AUPM, MCM)								Başel PhD (2010) Results (Method: MIT, MC, T^r=100 ºC)			
Field	**Assumed power conversion system**	**Method**	$\mu_{\ln PW}$	$\sigma^2_{\ln PW}$	**P10**	**P50**	**P90**	η_{th}	**P10**	**P50**	**P90**
Caferbeyli 1 -Manisa	Binary	AUP	1.783	0.075	4.19	5.95	8.45	0.11	54.6	80.2	121.4
		MC	1.783	0.081	4.04	6.13	8.40				
Caferbeyli 2-Manisa	Single Flash	AUP	3.938	0.114	33.31	51.32	79.06	0.15			
		MC	3.938	0.124	32.01	52.27	80.00				
Umurlu-Aydın	Binary	AUP	3.722	0.146	25.35	41.35	67.45	0.13	22.8	41.6	69.2
		MC	3.722	0.165	23.65	42.99	68.70				
Salavatlı-Aydın	Binary	AUP	4.950	0.228	76.65	141.20	260.11	0.15	78.2	165.1	343.6
		MC	4.950	0.242	73.20	142.26	268.39				
Seferihisar 1-İzmir	Binary	AUP	2.134	0.068	6.05	8.69	11.82	0.11	13.8	19.9	28.5
		MC	2.134	0.076	5.81	8.69	11.82				
Seferihisar 2-İzmir	Binary	AUP	3.201	0.084	16.93	24.55	35.60	0.09			
		MC	3.201	0.093	16.27	25.19	35.81				
Simav-Kütahya	Single Flash	AUP	3.684	0.163	23.77	39.82	66.71	0.16	34.7	59.6	94.9
		MC	3.682	0.183	22.36	41.14	66.98				
Tekkehamam 1-Denizli	Binary	AUP	1.640	0.077	3.62	5.15	7.34	0.11			
		MC	1.640	0.085	3.46	5.32	7.34				
Tekkehamam 2-Denizli	Binary	AUP	1.442	0.073	2.99	4.23	5.98	0.14	15.2	20.1	26.6
		MC	1.442	0.082	2.85	4.38	5.97				
Tekkehamam 3-Denizli	Binary	AUP	2.319	0.074	7.18	10.16	14.40	0.14			
		MC	2.319	0.080	6.90	10.49	14.30				
Tuzla-Çanakkale	Single Flash	AUP	2.055	0.206	4.36	7.80	13.96	0.16	6.1	11.4	20.0
		MC	2.052	0.229	4.14	7.97	14.14				
Salihli Doğu-Manisa	Binary	AUP	3.145	0.150	14.13	23.21	38.11	0.13	12.6	23.1	39.4
		MC	3.145	0.164	13.48	23.80	38.71				

Table 9.1 (continued): MCM and AUPM results of 25 geothermal fields which are amenable to electricity production in comparison to the results obtained by Başel (2010) PhD thesis by using the same reservoir parameters

Results of Garg and Combs (2015) method (AUPM, MCM)								**Başel PhD (2010) Results (Method: MIT, MC, T^r=100 ºC)**			
Field	**Assumed power conversion system**	**Method**	$\mu_{\ln PW}$	$\sigma^2_{\ln PW}$	**P10**	**P50**	**P90**	η_{th}	**P10**	**P50**	**P90**
Hıdırbeyli Kuzey-Aydın	Binary	AUP	3.043	0.128	13.27	20.97	33.13	0.11	9.0	16.9	29.8
		MC	3.043	0.136	12.97	21.32	33.56				
Hıdırbeyli Güney-Aydın	Binary	AUP	3.477	0.095	21.80	32.36	48.03	0.14	20.5	35.2	56.6
		MC	3.477	0.103	21.07	33.15	48.03				
İmamköy, Yılmazköy-Aydın	Single Flash	AUP	4.454	0.265	44.49	85.97	166.12	0.15	79.6	143.4	245.8
		MC	4.446	0.357	38.53	92.85	168.34				
Kavaklıdere-Manisa	Single Flash	AUP	5.743	0.127	197.87	312.15	492.43	0.17	264.3	446.4	695.6
		MC	5.747	0.140	189.38	319.01	501.31				
Ortakçı-Aydın	Binary	AUP	1.677	0.155	3.23	5.35	8.85	0.12	2.6	4.7	8.4
		MC	1.677	0.165	3.12	5.46	8.89				
Salihli Kuzeydoğu-Manisa	Binary	AUP	1.878	0.067	4.70	6.54	9.11	0.14	4.8	7.2	9.9
		MC	1.878	0.074	4.50	6.73	9.05				
Umurlu Güney-Aydın	Binary	AUP	2.309	0.176	5.89	10.07	17.21	0.13	5.3	10.1	17.7
		MC	2.309	0.199	5.42	10.49	17.42				
Erciş, Zilan-Van	Binary	AUP	1.306	0.154	2.23	3.69	6.10	0.16	1.5	2.9	5.4
		MC	1.306	0.166	2.14	3.76	6.16				
			AUPM Total:		696	1134	1875				
			MCM Total:		661	1165	1909		840	1428	2371

According to the results, the Garg and Combs (2015) coupled with the MCM simulation predicts 661 MWe for P10, 1165 MWe for P50 and 1909 MWe for P90, by considering arithmetic summation, whereas Başel (2010)'s corresponding predictions based on the MIT (for a reference temperature of 100 oC and conversion efficiencies computed from binary plant correlation) are 840 MWe for P10, 1428 MWe for P50 and 2371 MWe for P90. Clearly, the Başel's application of the MIT method significantly overestimates the electricity production potential of those 25 geothermal fields. The MIT overestimates the P10 value as 179 MWe higher, the P50 value 263 MWe higher, and the P90 as 462 MWe higher than those computed from the Garg and Combs (2015) method.

10. CONCLUSIONS AND RECOMMENDATIONS

10.1 Conclusions

- USGS and MIT methods use arbitrarily chosen reference temperature (15, 30, 40, 100 ^{o}C) and thermal conversion efficiency values (0.15, 0.3, 0.4 etc).
- In the USGS and MIT methods, there is no logical reason for not to choose the reference temperature and conversion efficiency values arbitrarily. In MIT method, thermal conversion efficiency is calculated by an empirical relationship designed for only binary power conversion systems. But for flash power conversion system there is a big uncertainty in choosing the conversion efficiency value. If the relationship is used for flash power conversion systems MIT method largely overestimate the producible power potential of the geothermal field as shown in Table 7.4. Reference temperature usages in both methods are arbitrary too which is the other source of error.
- Garg and Combs (2015) volumetric probabilistic calculation method of geothermal reserves by considering the second law of thermodynamics and the power conversion system depending to the resource temperature of the reservoir.
- In early exploration phase of geothermal sources the lower limit of recovery factor should be taken into consideration as "0".
- The AUPM is a quite good alternative to the MCM with only 1-5% difference in resultant values. MCM and AUPM both can be used for all cases with perfect match. In this study we propose AUPM based on Garg and Combs technique which is an alternative and simple technique as being not time consuming and regardless of the requirement of commercial software.
- Changing distribution type of the same input parametres does not significantly affect the value of P50 but significantly affected values can be recorded in P10 and P90.

- Different distribution type and input parameter values do not affect the resultant producible electricity potential when the mean and variance of input parameters are kept the same.
- μ_X , σ_X^2 , $\mu_{\ln X}$, $\sigma_{\ln X}^2$ parameters are recorded as nearly and exactly the same in MC and AUP methods where no lower limit of the input parameters is "0".
- When the lower limit of the input parameter is "0", then the difference is recorded in between analytically calculated and randomly generated values of variance of natural logarithm of the input parameter as nearly 35% in triangular distribution and nearly 60% in uniform distribution. But even if the analytically calculated value is used in power generation potential Eq. in AUPM, the resultant difference will be only 10% higher in P10, no difference in P50 and P90 in comparison to the one obtained from Monte Carlo simulation.
- It is shown in Table 7.4 that for Denizli-Kızıldere geothermal field which is operated by a flash power conversion system, when we use USGS method with 40 ^{o}C reference temperature and the thermal power conversion efficiency as 0.4 or 0.11 we get the closest results to the ones we obtained from Garg and Combs method which works considering the 2nd law of thermodynamics with exergy analysis.

  If we use MIT method with a flash power conversion system then the closest result is obtained by taking the reference temperature as 40 ^{o}C and the thermal power conversion efficiency as 0.11 based on Table 7.4. Also as could be seen in Table 9.1, 100 ^{o}C reference temperature should definitely not be used with MIT method due to large overestimations of reserves.

  It is shown in Table 7.14 that for Salavatlı geothermal field which is operated by a binary power conversion system, when we use USGS method with 40 ^{o}C reference temperature and the thermal power conversion efficiency as 0.4 we get closest results to the ones we obtained from Garg and Combs method which works considering the second law of thermodynamics with exergy analysis.

  If we use MIT method with a binary power conversion system then the closest result is obtained by taking the reference temperature as 100 ^{o}C and

the thermal power conversion efficiency is calculated by using the empirical relationship proposed in MIT method based on Table 7.14.

But it should be noted that could be case sensitive and be much more sensitive with the increase of resource temperature. So the safest and best way of estimating potential reserves is to use Garg and Combs method which considers the real operating power conversion system with its thermodynamic condition based on the 2nd law of thermodynamics being far away from any arbitrary usage of input parameters.

- Distribution type has no important effect on the results, as demonstrated by the example cases given in the thesis. Because based on CLT theorem, the summation of the distributions of input parameters will be log-normally distributed. Thus whatever the distributions are used for input parameters, the resultant PW distribution will be log-normal. Of course changing the minimum or maximum values of input parameters will change P10, P50 and P90 statistical confidence values but the distribution type of PW will not be changed.

  Distribution types of input parameters such as thickness, porosity, etc. should be defined by using core or log data if available or some analogy field data could be used for this purpose.

- Considering the pertinent data for the 25 geothermal fields of Turkey as presented in Başel's PhD study in 2010, it is found that the Garg and Combs (2015) coupled with the MCM simulation method predicts 661 MWe for P10, 1165 MWe for P50 and 1909 MWe for P90, by considering arithmetic summation, whereas Başel (2010)'s corresponding predictions based on the MIT (for a reference temperature of 100 ^{o}C and conversion efficiencies computed from binary plant correlation) are 840 MWe for P10, 1428 MWe for P50 and 2371 MWe for P90.

- Clearly, the Başel's application of the MIT method significantly overestimates the electricity production potential of those 25 geothermal fields. The MIT overestimates the P10 value as 179 MWe higher, the P50 value 263 MWe higher, and the P90 value as 462 MWe higher than those computed from the Garg and Combs (2015) method.

10.2 Recommendations For Future Work

- Field reservoir data are so much important while estimating the minimum, moderate and maximum values of reservoir properties which has uncertainty such as thickness, area, resource temperature etc. While trying to make estimations of production potential of reservoir zones recorded field data or reservoir model data should be used so as not to be subjective relying on one field expert's ideas and believes about the field.
- It must be considered that there is possibility of permeablity of reservoir to be "0" or very close to "0" in geothermal fields in exploration phase. So one need to be careful to accept the minimum limit of recovery factor as "0" at this very early stage of exploration to expect more realistic primary results.
- Garg and Combs (2015) method should be used instead of USGS and MIT methods which has a large range of uncertainty and arbitrary acceptions of input parameters to estimate recoverable volumetric probabilistic electricity potential of geothermal reservoirs.
- In Başel's (2010) PhD thesis only 25 fields was considered amenable to electricity production as having resorce temperature values higher than 100 ^{o}C and those 25 fields were used in this thesis for correlation of results purposes. But today, it seems that Turkey has about 39 geothermal fields which are ameanable to electricity production potential etiher by use of at least a single flash or binary power cycle. In addidition, with today's technology, it is possible to generate electricity from geothermal reservoirs having resorce temperature values between 57-180 ^{o}C by installing binary power plants. So to predict a realistic estimation of Turkey's recent electricity generation potential all 39 geothermal fields having resource temperature values of 57 ^{o}C should be considered and evaluated by the Garg and Combs (2015) method. We believe the data for the 39 fields whoever has it should be shared publically for public interest of Turkey.
- MREI geothermal database sould be updated as soon as possible and be open to academic usage for all intents and purposes. For uncertainty propagation, using real recorded data is the inevitable part of trying to make approximations to reserve potential in probabilistic approaches.

- In this study only uniform and triangular input data distributions are studied; their interaction and effects to the resultant prodution potential is discussed in 5^{th} part and some conclusions were made. As a future work it should be recommended that normal, log-normal and gamma input data distribution types also should be additionally used and examined for their interaction between the other distribution types with the same input minimum, (mode), maximum values and also with the values gives the same mean and variance as a result.
- A sensitivity study should be done about choosing the secondary candidate fluid type revealing which candidate has which advantages and disadvantages regarding to the electricity generation potential results of the power plant to be able to state if there is a strong or weak relationship with the volumetric reservoir input parameters and the secondary fluid.

REFERENCES

Akkuş, İ. (2016). Personal Interview. 08 August, İstanbul.

Akkuş, İ. and Alan, H. (2016). Türkiye'nin Jeotermal Kaynakları, Prospeksiyonlar, Sorunlar ve Öneriler Raporu (Rapor No. 123). Ankara: TMMOB Jeoloji Mühendisleri Odası Raporu.

Axelsson, G., V. Stefansson., and G. Bjornsson. (2005). Sustainable utilization of geothermal resources for 100–300 years. Proceedings World Geothermal Congress 2005, Antalya, Turkey, April, 8 pp.

Barlow, R.J. (1989). Statistics: A Guide to the Use of Statistical Methods in the Physical Sciences, John Wiley & Sons, 204p.

Başel, E. D. K. (2010). *Investigation of Turkey's geothermal Potential*, PhD Dissertation (in Turkish), Istanbul Technical University, Graduate School of Science, Engineering and Technology, Istanbul, Turkey, 310 p.

Başel, E. D. K., Serpen U., and Satman A. (2013). Geothermal boom in Turkey: Growth in identified capacities and potentials. Elsevier, Renewable Energy 68 (2014) 314-325.

Bodvarsson, G. (1964). Physical characteristics of natural heat sources in Iceland. Proc. UN Conf. on New Sources of Energy, Volume 2: Geothermal Energy, Rome, August 1961. United Nations, New York, 82-89.

Brook, C. A. Mariner, R.H., Mabey, D.R., Swanson, J.R., Guffanti, M., and Muffler, L.J.P., (1979). Hydrothermal convection systems with reservoir temperatures ≥90◦C, In:Muffler, L.J.P. (Ed.), *Assessment of Geothermal Resources of the United States—1978*, 790. U.S Geological Survey Circular, 170p.

Capen, E.C. (1996). "A Consistent Probabilistic Definition of Reserves" *SPE Reservoir Engineering*, February 1996.

Capen, E.C. (2001). "Probabilistic Reserves! Here at Last?" *SPE Reservoir Evaluation &Engineering*, 387-394.

Carter, P.J. and Morales, E. (1998). "Probabilistic Addition of Gas Reserves Within a Major Gas Project," paper SPE 50113, *proceedings 1998 SPE Asia Pacific Oil & Gas Conference and Exhibition*, Perth, Australia.

Çengel Y. A., and Boles M. A. (2014). Thermodynamics: An Engineering Approach, 5th edition. Retrieved from https://entegila.files.wordpress.com/2012/06/thermodynamics-an engineering-approach-5th-edition-gengel-boles.pdf (Original work published 2014)

Coleman, H. W., and Steele, W. G. (1999). *Experimentation and Uncertainty Analysis forEngineers*, 2nd edition, Wiley & Sons, 275p.

Delfiner, P., and Barrier, R. (2008). "Partial Probabilistic Addition: A Practical Approach for Aggregating Gas Resources," SPE Reservoir Evaluation and Engineering, 379-385.

Demirmen, F. (2007). "Reserves Estimation: The Challenge for the Industry," *Journal of Petroleum and Technology*, 80-89.

DiPippo, R. (2008). *Geothermal Power Plants: Principles, Applications, Case Studies and Environmental Impact*, 2nd ed. Elsevier, Amsterdam, 493p.

DiPippo, R. (2012). *Geothermal Power Plants: Principles, Applications, Case Studies and Environmental Impact*, 3rd ed. Butterworth, Heinemann/Elsevier, Chapter 16.

Garg, S. K., and Combs, J. (2010). Appropriate use of USGS volumetric "Heat in Place" method and Monte Carlo Calculations. In: *Proceedings of 34th Workshop on Geothermal Reservoir Engineering*, Stanford University, Stanford, CA, 7p.

Garg, S. K., and Combs, J. (2011)**.** A reexamination of USGS volumetric "heat in place" method. In: *Proceedings 35th Workshop on Geothermal Reservoir Engineering*, Stanford University, Stanford, CA, 5p.

Garg, S. K., and Combs, J. (2015). A reformulation of USGS volumetric "heat-in-place" resource estimation method, *Geothermics*, Vol. 55, pp. 150-158.

Grant, M. (2015). Resource assessment, a review, with reference to the Australian code, In:*Proceedings of World Geothermal Congress* 2015, 19-25 April, Melbourne, Australia, 6 p.

Haklıdır, F. T. (2016). Providing sustainable geothermal reservoirs for power production in Turkey, *Izmir Geothermal Congress*, Turkey

IAPWS. (1996). Release on the IAPWS formulation 1995 for the thermodynamic properties of ordinary water substances for general and scientific use, International Association for the properties of water and steam; http://www.iapws.org.

Kagel, A. (2008). *The State of Geothermal Technology* (Report No: January 2008). US: Geothermal Energy Association.

Karacaer, C., and Onur, M. (2012). Analytical Probabilistic Reserve Estimation by Volumetric Method and Aggregation of Resources. *SPE, 162875*.

Kreyszing, E. (1972). *Advanced Engineering Mathematics*, 9th ed. John Wiley & Sons, Singapore, 1246p.

Lund, W. J., and Boyd, L. T. (2015). Direct utilization of geothermal energy 2015 worldwide review, *Proceeding World Geothermal Congress*, Melbourne, Australia, April 19-25.

Matek, B. (2016). *Annual U.S. & Global Geothermal Power Production Report* (Report No: March 2016). US: Geothermal Energy Association.

Matek, B. (2015). *Annual U.S. & Global Geothermal Power Production Report* (Report No: February 2015). US: Geothermal Energy Association.

MIT. (2006). *The future of geothermal energy – Impact of enhanced geothermal systems (EGS) on the United States in the* 21st*Century*, Massachusetts Institute of Technology; http://geothermal.inel.gov/publications/future_of_geothermal_energy pdf

Muffler, L. P. J. (1979). Assessment of geothermal resources of the United States-1978: U.S. Geological Survey Circular 790, 163p.

Muffler, L. P. J., and Cataldi, R. (1977). Methods for regional assessment of geothermal resources. U.S. Geological Survey Open-File Report 77-870, 78p.

Nathenson, M. (1975a). Physical factors determining the fraction of stored energy recoverable from hydrothermal convection systems and conduction-dominated areas. U.S. Geol. Survey Open.Hie Rept. ?5-525, 38 pp.

Nathenson, M. (1975b). Some reservoir engineering calculations for the vapor-dominated system at Larderello, Italy. U.S. Geol. Survey Open-File Rept. 75-142, 38 pp.

Nathenson, M., and Muffler, L.J.P. (1975). Geothermal resources in hydrothermal convection systems and conduction-dominated areas: In: White, D.E., Williaams, D.L. (Eds.), *Assessment of Geothermal Resources of the United States*—1975, 726. U.S Geological Survey Circular, 160p.

NIST. (2010). Thermophysical properties of fluid systems, The National Institute of Standards and Tech., http://webbook.nist.gov/chemistry/fluid/.

Onur M. (2015). Geothermal resource assessment for predicting power generation by volumetric methods, In: *Proceedings of Inerma – International Energy Raw Materials and Energy Summit 2015,* 1-3 October, Istanbul, Turkey, 14 p.

Onur M., Sarak, H., and Tureyen, O.İ. (2010). Probabilistic resource estimation of stored heat and recoverable thermal energy for geothermal systems by volumetric methods, In: *Proceedings of World Geothermal Congress 2010*, 25-29 April, Bali, Indonesia, 12 p.

Onur M., Sarak, H., and Tureyen, O.İ. (2009). Hacimsel yöntemlerle tahmin edilen depolanmış termal enerji ve üretilebilir güçteki belirsizliğin tayin edilmesi, *9.·Ulusal HVAC&R Kongresi* ***ve Sergisi*** *(TESKON 2009),* İzmir, Turkey, s. 213- 233.

Palisade@RISK Ver. 7. software. (2004). Palisade Corporation, NY, USA.

Parzen, E. (1962). *Modern Probability Theory and Its Applications*, John Wiley and Sons, 430 p.

Rice, J.A. (2007). *Mathematical Statistics and Data Analysis*, Third Edition, Thomson Corporation, USA, 685 p.

Saemundsson, K. (2009). Geothermal Systems in Global Perspective., *Short Course IV on Exploration for Geothermal Resources,* UNU-GTP, KenGen and GDC, Lake Naivasha, Kenya, 1-22 November.

Sanyal, S.K. (2005). Classification of geothermal systems – a possible scheme, Proceedings, Thirtieth Workshop on Geothermal Reservoir Engineering, Stanford University, Stanford, California, p. 85-88.

Sarak, H., Türeyen, Ö.İ., and Onur, M. (2009). Assessment of Uncertainty in Estimation of Stored and Recoverable Thermal Energy in Geothermal Reservoirs by Volumetric Methods., *proceedings 34th Workshop on Geothermal Reservoir Engineering*, Stanford University, USA, 9-11 February.

Satman, A. (2016). *Türkiye'de jeotermal enerjinin bugünü ve geleceği, Jeotermal Kaynaklar Sempozyumu* [PowerPoint slides]. Retrieved from http://docplayer.biz.tr/18789420-Turkiye-de-jeotermal-enerjinin bugunu-ve-gelecegi-paneli.html

Serpen, U., Aksoy, N., and Öngür, T. (2015). 2015 Reinjection Update of Salavatli Geothermal Field in Turkey, Proceedings World Geothermal Congress 2015, Stanford Melbourne, Australia, 19-25 April 2015.

Serpen, U., Aksoy, N., and Öngür, T. (2010). 2010 Present Status of Geothermal Energy in Turkey, Thirty-fifth Workshop on Geothermal Reservoir Engineering, Stanford University, Stanford, Feb. 1-3.

Tureyen, O. I., Sarak, H., Gulgor, A., Erkan, B., and Satman, A. (2014). A Study on the Production and Reservoir Performance of the Germencik Geothermal Field, Thirty-ninth Workshop on Geothermal Reservoir Engineering, Stanford University, Stanford, California, Feb. 24-26.

Unverdi, M., and Cerci, Y. (2013). Performance analysis of Germencik Geothermal Power Plant. *Energy*, Vol. 52, pp 192–200.

van Elk, J. F., Vijayan, K., and Gupta, R. (2000). "Probabilistic Addition of Reserves," paper SPE 64454 presented at the 2000 SPE Asia Pacific Oil & Gas Conference and Exhibition, Brisbane, Australia.

White, D. E., and Williams, D. L. (1975) Assessment of geothermal resources of the United States-1975. U.S. Geol. Survey Circular 726, 155 p.

Williams, C. (2014). Evaluating the volume method in the assessment of identified geothermal resources. *Geothermal Resources Council, Transactions*, Vol. 38, pp 967–974.

Williams, F. Colin., Reed, J. Marshall., and Arlene F. Anderson, and F. Arlene. (2011). Updating the Classification of Geothermal Resources. Thirty-Sixth Workshop on Geothermal Reservoir Engineering Stanford University, Stanford, California, SGP-TR-191.

Williams, F. Colin., Reed, J. Marshall., and Mariner H. Robert. (2008b). A Review of Methods Applied by the U.S. Geological Survey in the Assessment of Identified Geothermal Resources, USGS Report No. 1296, Virginia.

Zarrouk, J. S., and Moon, H. (2014). Efficiency of geothermal powerplants: A worldwide review. *Elsevier, 51,* 142-153.

Zeybek, A.D., Onur, M., Türeyen, Ö.İ., Ma, M.S., Al-Shahri, A.M., and Kuchuk, F.J. (2009). Assessment of Uncertainty in Saturation Estimated from Archie's Eq.," paper SPE 120517 to be presented at the 2009 SPE Middle East Oil Show and Conference, Bahrain, Kingdom of Bahrain, 15-18 March.

Url-1 <http:// https://en.wikipedia.org/wiki/Magma>, date retrieved 30.09.2016.

Url-2 <http://geografia.laguia2000.com/general/fosa-tectonica>, date retrieved 30.09.2016.

Url-3 <http://www.geogrify.net/GEO1/Lectures/PlateTectonics/#(10)>, date retrieved 30.08.2016.

Url-4 <http://cooklowery15.wikis.birmingham.k12.mi.us/Earth+Science>, date retrieved 30.08.2016.

Url-5 <*http://academic.evergreen.edu/g/grossmaz/heidtken.html*>, date retrieved 30.08.2016.

Url-6 <*http://slideplayer.com/slide/5708159/*>, date retrieved 30.08.2016.
Url-7 <*https://www.geothermal-energy.org/what_is_geothermal_energy.html*>, date retrieved 30.08.2016.
Url-8 <*https://en.wikipedia.org/wiki/Geothermal_power*>, <*http://en.openei.org/wiki/Binary_Cycle_Power_Plant*>, date retrieved 30.09.2016.
Url-9 <*http://www.MREI.gov.tr/v2.0/daire-askanliklari/ enerji/index.php? id= haritalar*>,date retrieved 03.09.2016.
Url-10 <*http://www.sepron.com.tr/dosyalar/sepron_jeotermal_enerji_saha_ozet _fizibilite_ raporu.pdf*>,date retrieved 01.10.2016.
Url-11 < https://www.researchgate.net/profile/Ipek_Barut/publication/280921788_*GECMISTEN_GUNUMUZE_DENIZLI_TERMAL_MINERALLI_SULARININ_HIDROKIMYASAL_OZELLIKLERI_ILE_KULLANIMININ_DEGERLENDIRILMESI_EVALUATION_FROM_PAST_TO_PRESENT_HYDROCHEMICAL_CHARACTERISTICS_WITH_USE_OF_THERMAL_MIN/links/55cb4bc308aebc967dfda136.pdf?origin=publication_list*>, date retrieved 01.10.2016.
Url-12 <*http://www.slideshare.net/SuatFurkanISIK/rifat-goksu*>, date retrieved 01.10.2016.
Url-13 <*http://www.MREI.gov.tr/v2.0/dairebaskanliklari/enerji/images/siteharitalar/10.jpg*>, date retrieved 30.08.2016.
Url-14 <*http://www1.eere.energy.gov/geothermal/pdfs/conversion.pdf*>, date retrieved 29.10.2016.
Url-15 < http://www.enggcyclopedia.com/2011/12/power-plant-efficiency/>, date retrieved 29.10.2016.
Url-16 <*http://mathworld.wolfram.com/UniformDistribution.html*>, date retrieved 16.10.2016.
Url-17 <*http://mathworld.wolfram.com/TriangularDistribution.html*>, date retrieved 16.10.2016.
Url-18 <*https://en.wikipedia.org/wiki/Relations_between_heat_capacities*>, date retrieved 30.10.2016.
Url-19 < *https://en.wikipedia.org/wiki/Triangular_distribution*>, date retrieved 25.01.2017.
Url-20 < http://www.guris.com.tr/EN,2121/2015---our-energy-investments-.html>, date retrieved 09.07.2017.

APPENDICES

APPENDIX A: Pentane Liquid and Vapor Phase Thermodynamic Properties on the Saturation Curve (NIST, 2010) - Ordered with 5 ^{o}C increment

APPENDIX B: Pentane Liquid and Vapor Phase Thermodynamic Properties on the Saturation Curve (NIST, 2010) - Ordered with 0.5 bar increment

APPENDIX C: Reservoir characteristics information used in volumetric probabilistic reserve estimations of 25 fields examined for electricity production potential

APPENDIX A

Table A.1: Pentane liquid phase thermodynamic properties on the saturation curve (NIST, 2010) - ordered with 5 ^{o}C increment.

Temperature (C)	Pressure (bar)	Density (kg/m3)	Volume (m3/kg)	Enthalpy (kJ/kg)	Entropy (J/g*K)	Cv (J/g*K)	Cp (J/g*K)
15	0.46447	630.56	0.0015859	-48.878	-0.16338	1.6993	2.2711
20	0.56558	625.7	0.0015982	-37.459	-0.12415	1.7161	2.2929
25	0.68345	620.78	0.0016109	-25.929	-0.085209	1.7333	2.3154
30	0.81993	615.82	0.0016239	-14.283	-0.046547	1.7508	2.3385
35	0.97699	610.79	0.0016372	-2.5183	0.0081391	1.7686	2.3624
40	1.1567	605.7	0.001651	9.3689	0.030032	1.7868	2.387
45	1.3611	600.54	0.0016652	21.382	0.067983	1.8052	2.4122
50	1.5925	595.3	0.0016798	33.525	0.10573	1.824	2.4382
55	1.8532	589.99	0.0016949	45.8	0.14329	1.8429	2.465
60	2.1454	584.59	0.0017106	58.213	0.18068	1.8622	2.4925
65	2.4717	579.1	0.0017268	70.766	0.21791	1.8816	2.5208
70	2.8346	573.51	0.0017436	83.464	0.25501	1.9012	2.5501
75	3.2365	567.82	0.0017611	96.31	0.29197	1.921	2.5802
80	3.6801	562.01	0.0017793	109.31	0.32882	1.941	2.6113
85	4.1682	556.08	0.0017983	122.47	0.36556	1.9612	2.6436
90	4.7034	550.01	0.0018181	135.79	0.40223	1.9815	2.677
95	5.2885	543.8	0.0018389	149.27	0.43882	2.002	2.7118
100	5.9265	537.42	0.0018607	162.93	0.47536	2.0227	2.7482
105	6.6203	530.88	0.0018837	176.78	0.51186	2.0435	2.7862
110	7.3729	524.14	0.0019079	190.8	0.54834	2.0644	2.8262
115	8.1874	517.18	0.0019335	205.03	0.58482	2.0855	2.8686
120	9.0671	510	0.0019608	219.46	0.62131	2.1068	2.9137
125	10.015	502.55	0.0019898	234.1	0.65785	2.1283	2.9619
130	11.035	494.82	0.002021	248.97	0.69446	2.15	3.0141
135	12.131	486.75	0.0020544	264.08	0.73116	2.1719	3.0711
140	13.305	478.31	0.0020907	279.46	0.768	2.1942	3.134
145	14.563	469.44	0.0021302	295.11	0.80502	2.2169	3.2045
150	15.908	460.08	0.0021735	311.07	0.84227	2.24	3.2849
155	17.345	450.14	0.0022216	327.36	0.87981	2.2638	3.3784
160	18.879	439.49	0.0022754	344.04	0.91773	2.2884	3.4903
165	20.515	428	0.0023365	361.15	0.95615	2.314	3.6288
170	22.259	415.44	0.0024071	378.79	0.99523	2.3412	3.8086
175	24.117	401.47	0.0024908	397.07	1.0352	2.3705	4.0579
180	26.099	385.55	0.0025937	416.19	1.0766	2.4032	4.4391
185	28.214	366.61	0.0027277	436.56	1.12	2.4413	5.1263
190	30.476	342.06	0.0029235	459.16	1.1677	2.4904	6.8485
195	32.91	299.26	0.0033415	488.8	1.2297	2.5746	21.225

Table A.2: Pentane vapor phase thermodynamic properties on the saturation curve (NIST, 2010) - ordered with 5 ^{o}C increment.

Temperature (^{o}C)	Pressure (bar)	Density (kg/m^3)	Volume (m^3/kg)	Enthalpy (kJ/kg)	Entropy (J/g*K)	Cv (J/g*K)	Cp (J/g*K)
15	0.46447	1.4354	0.69666	324.99	1.1341	1.5214	1.6528
20	0.56558	1.7249	0.57975	332.65	1.1384	1.5443	1.6782
25	0.68345	2.0583	0.48584	340.36	1.1433	1.5676	1.7043
30	0.81993	2.4402	0.4098	348.12	1.1489	1.5912	1.731
35	0.97699	2.8754	0.34777	355.92	1.155	1.6152	1.7584
40	1.1567	3.369	0.29682	363.75	1.1617	1.6395	1.7866
45	1.3611	3.9263	0.25469	371.63	1.1689	1.6641	1.8154
50	1.5925	4.5531	0.21963	379.54	1.1765	1.689	1.845
55	1.8532	5.2554	0.19028	387.47	1.1845	1.7142	1.8754
60	2.1454	6.0398	0.16557	395.43	1.1929	1.7396	1.9066
65	2.4717	6.9133	0.14465	403.41	1.2016	1.7653	1.9387
70	2.8346	7.8834	0.12685	411.41	1.2107	1.7912	1.9718
75	3.2365	8.9582	0.11163	419.41	1.22	1.8174	2.006
80	3.6801	10.147	0.098555	427.42	1.2296	1.8438	2.0413
85	4.1682	11.458	0.087272	435.42	1.2394	1.8705	2.0779
90	4.7034	12.904	0.077494	443.41	1.2493	1.8973	2.116
95	5.2885	14.496	0.068984	451.39	1.2595	1.9244	2.1557
100	5.9265	16.247	0.061548	459.33	1.2697	1.9517	2.1973
105	6.6203	18.173	0.055027	467.24	1.28	1.9793	2.2411
110	7.3729	20.29	0.049286	475.09	1.2903	2.0071	2.2876
115	8.1874	22.618	0.044213	482.88	1.3007	2.0351	2.3371
120	9.0671	25.179	0.039716	490.59	1.311	2.0635	2.3903
125	10.015	28.001	0.035713	498.2	1.3212	2.0922	2.448
130	11.035	31.114	0.03214	505.69	1.3312	2.1213	2.5114
135	12.131	34.556	0.028938	513.04	1.3411	2.1507	2.5817
140	13.305	38.374	0.026059	520.2	1.3507	2.1807	2.661
145	14.563	42.624	0.023461	527.15	1.36	2.2113	2.7521
150	15.908	47.377	0.021107	533.84	1.3687	2.2426	2.8587
155	17.345	52.726	0.018966	540.21	1.377	2.2747	2.9868
160	18.879	58.794	0.017009	546.18	1.3844	2.3079	3.1455
165	20.515	65.748	0.01521	551.65	1.3909	2.3425	3.3496
170	22.259	73.829	0.013545	556.48	1.3962	2.3789	3.6252
175	24.117	83.401	0.01199	560.44	1.3998	2.4176	4.0226
180	26.099	95.068	0.010519	563.18	1.4009	2.4598	4.6522
185	28.214	109.96	0.0090938	564.06	1.3983	2.5071	5.8151
190	30.476	130.82	0.0076439	561.56	1.3888	2.5632	8.7327
195	32.91	170.56	0.0058629	548.68	1.3576	2.6407	31.224

APPENDIX B

Table B.1: Pentane liquid phase thermodynamic properties on the saturation curve (NIST, 2010) - ordered with 0.5 bar pressure increment.

Temperature (ºC)	Pressure (bar)	Density (kg/m^3)	Volume (m^3/kg)	Enthalpy (kJ/kg)	Entropy (J/g*K)	Cv (J/g*K)	Cp (J/g*K)
16.848	0.5	628.77	0.0015904	-44.671	-0.14884	1.7055	2.2791
35.678	1	610.1	0.0016391	-0.91264	-0.0029463	1.7711	2.3657
48.073	1.5	597.33	0.0016741	28.83	0.091207	1.8167	2.4281
57.582	2	587.21	0.001703	52.193	0.16262	1.8528	2.4791
65.409	2.5	578.65	0.0017282	71.799	0.22095	1.8832	2.5232
72.119	3	571.11	0.001751	88.891	0.27069	1.9096	2.5627
78.028	3.5	564.32	0.0017721	104.16	0.31429	1.9331	2.5989
83.329	4	558.08	0.0017919	118.05	0.3533	1.9545	2.6327
88.153	4.5	552.27	0.0018107	130.85	0.38869	1.974	2.6645
92.589	5	546.81	0.0018288	142.75	0.42119	1.9921	2.6949
96.705	5.5	541.64	0.0018462	153.91	0.45129	2.0091	2.724
100.55	6	536.71	0.0018632	164.45	0.47937	2.025	2.7523
104.16	6.5	531.99	0.0018797	174.44	0.50574	2.04	2.7797
107.57	7	527.43	0.001896	183.97	0.53063	2.0542	2.8065
110.81	7.5	523.03	0.0019119	193.08	0.55422	2.0678	2.8329
113.88	8	518.76	0.0019277	201.83	0.57667	2.0808	2.8589
116.82	8.5	514.6	0.0019433	210.26	0.5981	2.0932	2.8847
119.63	9	510.54	0.0019587	218.39	0.61862	2.1052	2.9102
122.33	9.5	506.57	0.0019741	226.25	0.63832	2.1168	2.9357
124.92	10	502.67	0.0019894	233.87	0.65728	2.1279	2.9612

Table B.2: Pentane vapor phase thermodynamic properties on the saturation curve (NIST, 2010) - ordered with 0.5 bar pressure increment.

Temperature (C)	Pressure (bar)	Density (kg/m^3)	Volume (m^3/kg)	Enthalpy (kJ/kg)	Entropy (J/g*K)	Cv (J/g*K)	Cp (J/g*K)
16.848	0.5	1.5375	0.65039	327.81	1.1356	1.5298	1.6621
35.678	1	2.9389	0.34027	356.98	1.1559	1.6185	1.7622
48.073	1.5	4.3029	0.2324	376.48	1.1735	1.6794	1.8335
57.582	2	5.6499	0.177	391.58	1.1888	1.7273	1.8914
65.409	2.5	6.9889	0.14308	404.06	1.2024	1.7674	1.9414
72.119	3	8.3257	0.12011	414.8	1.2146	1.8023	1.9862
78.028	3.5	9.6637	0.10348	424.26	1.2258	1.8334	2.0272
83.329	4	11.006	0.090862	432.75	1.2361	1.8615	2.0655
88.153	4.5	12.354	0.080947	440.46	1.2456	1.8874	2.1017
92.589	5	13.71	0.072941	447.55	1.2546	1.9113	2.1363
96.705	5.5	15.075	0.066336	454.1	1.2629	1.9337	2.1696
100.55	6	16.45	0.06079	460.2	1.2708	1.9547	2.202
104.16	6.5	17.837	0.056062	465.92	1.2782	1.9746	2.2336
107.57	7	19.237	0.051983	471.29	1.2853	1.9935	2.2647
110.81	7.5	20.65	0.048425	476.35	1.292	2.0116	2.2953
113.88	8	22.078	0.045293	481.15	1.2984	2.0288	2.3257
116.82	8.5	23.522	0.042514	485.7	1.3044	2.0454	2.356
119.63	9	24.982	0.040029	490.03	1.3102	2.0614	2.3862
122.33	9.5	26.459	0.037794	494.15	1.3157	2.0768	2.4166
124.92	10	27.955	0.035772	498.09	1.321	2.0918	2.4471

APPENDIX C

Table C.1: Reservoir parameters used for Alasehir, Sarıkız-Manisa (Binary).

Parameter	Dist. Type	Min	Mode	Max
Reservoir Area (A, m^2)	Triangular	2.00E+06	4.00E+06	6.00E+06
Reservoir Thickness (H, m)	Uniform	250	-	500
Resource Temperature (T_R, °C)	Triangular	125	165	200
Porosity (ϕ , fraction)	Constant	0.01	0.06	0.13
Specific heat capacity of brine (c_p)$_f$, kJ/kg-°C)	Constant		4.18[1]	
Density of brine (ρ_f , kg/m^3)	Constant		904.07	
Specific heat capacity of rock (c_p)$_R$, kJ/kg-°C	Constant	0.85	0.9	0.95
Density of rock (ρ_R , kg/m^3)	Constant	2650	2750	2950
Volumetric specific heat capacity of rock $\left(\rho c_p\right)_R$ (kg/m^3-°C)	Triangular	2268	2553	2929
Recovery factor (R_g, fraction)	Triangular	0.07	0.18	0.24
Condenser temperature (T_c , °C)	Constant		40[1]	
Secondary fluid			Pentane[1]	
Turbine inlet pressure (p_{in}, bar)	Constant		4[1]	
Saturation temperature of secondary fluid (T_b, °C) @ p_{in}, bar	Constant		83.329[1]	
Assumed temperature differential (°C) between original and secondary fluid	Constant		5[1]	
Pinch point temperature (T_p, °C)	Constant		88.329[1]	
T_R-T_p (°C)	Triangular	36.671	76.671	111.671
Secondary fluid bubble point pressure (p_{sfb}, bar) @ T_c	Constant		1.1567[1]	
h_{sfl}(T_c=40 °C) (kJ/kg)	Constant		9.3689[1]	
h_{sfl}(T_b=83.329 °C) (kJ/kg)	Constant		118.05[1]	
s_{sfl} (T_c=40 °C) (kJ/kg-°C)	Constant		0.030032[1]	
h_{sfg}(T_b=83.329 °C) (kJ/kg)	Constant		432.75[1]	
s_{sfg} (T_b= 83.329 °C) (kJ/kg-°C)	Constant		1.2361[1]	
Heat of vaporization of secondary fluid h_{sfgl}(T_b=83.329 °C) (kJ/kg) (h_{sfg}-h_{sfl} @ T_b=83.329 °C)	Constant		314.7[1]	
V_{sf} (@ Tc= 40 °C and p_{sfb}= bar	Constant		0.001651[1]	
T_{cK}, K @ (T_c=40 °C)	Constant		313.15[1]	
Thermal conversion factor (fraction)	Constant		0.75[1]	
Project life (t_p, years)	Constant		25	
Load factor (L_F, fraction)	Constant		0.9	

[1] : These values are not repeated in the following Tables designed for binary power conversion systems because these values are accepted as constant and not changed.

Table C.2: Reservoir parameters used for Atça-Aydın (Binary).

Parameter	Dist. Type	Min	Mode	Max
Reservoir Volume (*V*, m³)	Triangular	5.70E+08	6.60E+08	9.70E+08
Resource Temperature (T_R, °C)	Uniform	125	-	150
Porosity (ϕ , fraction)	Constant	0.01	0.06	0.13
Density of brine (ρ_f , kg/m³)	Constant		928.18	
Specific heat capacity of rock (c_p)$_R$, kJ/kg-ºC	Constant	0.85	0.9	0.95
Density of rock (ρ_R , kg/m³)	Constant	2650	2750	2950
Volumetric specific heat capacity of rock $\left(\rho c_p\right)_R$ (kg/m³-ºC)	Triangular	2269	2559	2943
Recovery factor (R_g, fraction)	Triangular	0.07	0.18	0.24
T_R-T_p (ºC)	Uniform	36.671	-	61.671

Table C.3: Reservoir parameters used for Balçova (Binary).

Parameter	Dist. Type	Min	Mode	Max
Reservoir Area (*A*, m²)	Triangular	6.00E+05	1.00E+06	2.50E+06
Reservoir Thickness (*H*, m)	Triangular	250	350	1000
Resource Temperature (T_R, °C)	Triangular	110	135	145
Porosity (ϕ , fraction)	Constant	0.03	0.05	0.07
Density of brine (ρ_f , kg/m³)	Constant		934.75	
Specific heat capacity of rock (c_p)$_R$, kJ/kg-ºC	Constant		0.9	
Density of rock (ρ_R , kg/m³)	Constant	2600	2650	2700
Volumetric specific heat capacity of rock $\left(\rho c_p\right)_R$ (kg/m³-ºC)	Triangular	2387	2461	2533
Recovery factor (R_g, fraction)	Triangular	0.07	0.18	0.24
T_R-T_p (ºC)	Uniform	21.671	46.671	56.671

Table C.4: Reservoir parameters used for Caferbeyli-1 (Binary).

Parameter	Dist. Type	Min	Mode	Max
Reservoir Volume (*V*, m³)	Uniform	1.5E+09	-	2.2E+09
Resource Temperature (T_R, °C)	Uniform	130	-	150
Porosity (ϕ , fraction)	Constant	0.03	0.06	0.08
Density of brine (ρ_f , kg/m³)	Constant		925.94	
Specific heat capacity of rock (c_p)$_R$, kJ/kg-ºC	Constant	0.85	0.9	0.95
Density of rock (ρ_R , kg/m³)	Constant	2650	2750	2950
Volumetric specific heat capacity of rock $\left(\rho c_p\right)_R$ (kg/m³-ºC)	Triangular	2301	2559	2888
Recovery factor (R_g, fraction)	Triangular	0.07	0.18	0.24
T_R-T_p (ºC)	Uniform	41.671	-	61.671

Table C.5: Reservoir parameters used for Caferbeyli-2 (Flash).

Parameter	Dist. Type	Min	Mode	Max
Reservoir Volume (V, m^3)	Uniform	6E+09	-	1.32E+10
Resource Temperature (T_R, °C)	Uniform	180	-	200
Porosity (ϕ , fraction)	Constant	0.03	0.06	0.08
Resource Pressure(p_R, bar)	Constant		52[11]	
Specific heat capacity of brine ($c_p)_f$, kJ/kg-°C)	Constant		4.18[11]	
Density of brine (ρ_f , kg/m^3)	Constant		877.16	
Specific heat capacity of rock ($c_p)_R$, kJ/kg-°C	Constant	0.85	0.9	0.95
Density of rock (ρ_R , kg/m3)	Constant	2650	2750	2950
Volumetric specific heat capacity of rock $\left(\rho c_p\right)_R$, (kg/m^3-°C)	Triangular	2295	2546	2872
Recovery factor (R_g, fraction)	Triangular	0.07	0.18	0.24
Seperator pressure (p_{sep}, bar)	Constant		4[11]	
Plant seperator temperature (T_{sep}, °C)	Constant		143.608[11]	
T_R– T_{sep} (°C)	Triangular	36.392	-	56.392
Plant condenser temperature (T_c , °C)	Constant		40[11]	
Power conversion efficiency (η_c , fraction)	Constant		0.75[11]	
Project life (t_p, 25x31557600, **sec)**	Constant		788940000[11]	
Load factor (L_F, fraction)	Constant		0.9[11]	
h_{stm} (T_{sep}=143.608 °C) (kJ/kg)	Constant		2738.05[11]	
s_{stm}(T_{sep}= 143.608°C) (kJ/kg-°C)	Constant		6.89549[11]	
h_w (T_c=40 °C) (kJ/kg)	Constant		167.533[11]	
s_w(T_c=40 °C) (kJ/kg-°C)	Constant		0.572402[11]	
h_{gl} (T_{sep}= 143.608 °C) =(h_{stm}-h_w)	Constant		2133.397[11]	
T_{cK}, K @ (T_c=40 °C)	Constant		313.15[11]	

[11] : These values is not repeated in the following Tables designed for flash power conversion systems because these values are accepted as constant and not changed.

Table C.6: Reservoir parameters used for Dikili-İzmir (Binary).

Parameter	Dist. Type	Min	Mode	Max
Reservoir Volume (V, m^3)	Triangular	1.5E+09	4.5E+09	6E+09
Resource Temperature (T_R, °C)	Triangular	110	130	220
Porosity (ϕ , fraction)	Constant	0.01	0.06	0.13
Density of brine (ρ_f , kg/m^3)	Constant		913.66	
Specific heat capacity of rock (c_p)$_R$, kJ/kg-°C	Constant	0.85	0.9	0.95
Density of rock (ρ_R , kg/m^3)	Constant	2650	2750	2950
Volumetric specific heat capacity of rock $\left(\rho c_p\right)_R$ (kg/m^3-°C)	Triangular	2268	2556	2935
Recovery factor (R_g, fraction)	Triangular	0.07	0.18	0.24
T_R-T_p (°C)	Triangular	21.671	41.671	131.671

Table C.7: Reservoir parameters used for Germencik-Aydın (Flash).

Parameter	Dist. Type	Min	Mode	Max
Reservoir Area (A, m^2)	Triangular	3.00E+06	4.50E+06	7E+06
Reservoir Thickness (H, m)	Triangular	750	1500	2000
Resource Temperature (T_R, °C)	Triangular	205	220	235
Porosity (ϕ , fraction)	Constant	0.01	0.075	0.125
Density of brine (ρ_f , kg/m^3)	Constant		845.01	
Specific heat capacity of rock (c_p)$_R$, kJ/kg-°C	Constant	0.85	0.9	0.95
Density of rock (ρ_R , kg/m3)	Constant	2400	2700	2900
Volumetric specific heat capacity of rock $\left(\rho c_p\right)_R$, (kg/m^3-°C)	Triangular	2055	2513	2852
Recovery factor (R_g, fraction)	Triangular	0.07	0.18	0.24
T_R– T_{sep} (°C)	Triangular	61.392	76.392	91.392

Table C.8: Reservoir parameters used for Gümüşköy-Aydın (Binary).

Parameter	Dist. Type	Min	Mode	Max
Reservoir Volume (V, m^3)	Triangular	1E+010	1.7E+10	8.2E+10
Resource Temperature (T_R, °C)	Uniform	105	-	150
Porosity (ϕ , fraction)	Constant	0.01	0.06	0.125
Density of brine (ρ_f , kg/m^3)	Constant		936.8989	
Specific heat capacity of rock (c_p)$_R$, kJ/kg-°C	Constant	0.85	0.9	0.95
Density of rock (ρ_R , kg/m^3)	Constant	2650	2750	2950
Volumetric specific heat capacity of rock $\left(\rho c_p\right)_R$ (kg/m^3-°C)	Triangular	2269	2561	2942
Recovery factor (R_g, fraction)	Triangular	0.07	0.18	0.24
T_R-T_p (°C)	Uniform	16.671	-	61.671

Table C.9: Reservoir parameters used for Hıdırbeyli Kuzey-Aydın (Binary).

Parameter	Dist. Type	Min	Mode	Max
Reservoir Area (A, m^2)	Triangular	4.00E+06	6.00E+06	8.00E+06
Reservoir Thickness (H, m)	Triangular	750	1000	1500
Resource Temperature (T_R, °C)	Triangular	120	140	170
Porosity (ϕ , fraction)	Constant	0.01	0.08	0.13
Density of brine (ρ_f , kg/m^3)	Constant		922.93	
Specific heat capacity of rock (c_p)$_R$, kJ/kg-°C	Constant		0.9	
Density of rock (ρ_R , kg/m^3)	Constant	2400	2700	2900
Volumetric specific heat capacity of rock $\left(\rho c_p\right)_R$ (kg/m^3-°C)	Triangular	2058	2544	2898
Recovery factor (R_g, fraction)	Triangular	0.07	0.18	0.24
T_R-T_P (°C)	Triangular	31.671	51.671	81.671

Table C.10: Reservoir parameters used for Hıdırbeyli-Güney (Binary).

Parameter	Dist. Type	Min	Mode	Max
Reservoir Area (A, m^2)	Triangular	5.00E+06	7.00E+06	8.00E+06
Reservoir Thickness (H, m)	Triangular	750	1000	1250
Resource Temperature (T_R, °C)	Triangular	140	170	200
Porosity (ϕ , fraction)	Constant	0.01	0.08	0.13
Density of brine (ρ_f , kg/m^3)	Constant		897.52	
Specific heat capacity of rock (c_p)$_R$, kJ/kg-°C	Constant		0.9	
Density of rock (ρ_R , kg/m^3)	Constant	2400	2700	2900
Volumetric specific heat capacity of rock $\left(\rho c_p\right)_R$ (kg/m^3-°C)	Triangular	2057	2536	2885
Recovery factor (R_g, fraction)	Triangular	0.07	0.18	0.24
T_R-T_P (°C)	Triangular	51.671	81.671	111.671

Table C.11: Reservoir parameters used for İmamköy-Yılmazköy (Flash).

Parameter	Dist. Type	Min	Mode	Max
Reservoir Volume (V, m^3)	Triangular	1.2E+10	2.00E+10	3.20E+10
Resource Temperature (T_R, °C)	Triangular	145	180	220
Porosity (ϕ , fraction)	Constant	0.01	0.06	0.13
Density of brine (ρ_f , kg/m^3)	Constant		885.76	
Specific heat capacity of rock (c_p)$_R$, kJ/kg-°C	Constant	0.85	0.9	0.95
Density of rock (ρ_R , kg/m3)	Constant	2650	2750	2950
Volumetric specific heat capacity of rock $\left(\rho c_p\right)_R$, (kg/m^3-°C)	Triangular	2267	2549	2919
Recovery factor (R_g, fraction)	Triangular	0.07	0.18	0.24
T_R– T_{sep} (°C)	Triangular	1.392	36.392	76.392

Table C.12: Reservoir parameters used for Kavaklıdere (Flash).

Parameter	Dist. Type	Min	Mode	Max
Reservoir Volume (V, m^3)	Triangular	2.00E+10	4.00E+10	6.00E+10
Resource Temperature (T_R, °C)	Triangular	180	215	240
Porosity (ϕ , fraction)	Constant	0.03	0.06	0.08
Density of brine (ρ_f , kg/m^3)	Constant		854.10	
Specific heat capacity of rock $(c_p)_R$, kJ/kg-°C	Constant	0.85	0.9	0.95
Density of rock (ρ_R , kg/m3)	Constant	2650	2750	2950
Volumetric specific heat capacity of rock $\left(\rho c_p\right)_R$, (kg/m^3-°C)	Triangular	2292	2541	2864
Recovery factor (R_g, fraction)	Triangular	0.07	0.18	0.24
$T_R - T_{sep}$ (°C)	Triangular	36.392	71.392	96.392

Table C.13: Reservoir parameters used for Kızıldere-1 (Flash).

Parameter	Dist. Type	Min	Mode	Max
Reservoir Area (A, m^2)	Triangular	2.8E+06	3.1E+06	3.5E+06
Reservoir Thickness (H, m)	Triangular	900	1067	1200
Resource Temperature (T_R, °C)	Triangular	195	205	215
Porosity (ϕ , fraction)	Constant	0.01	0.08	0.13
Density of brine (ρ_f , kg/m^3)	Constant		861.29	
Specific heat capacity of rock $(c_p)_R$, kJ/kg-°C	Constant	0.85	0.9	0.95
Density of rock (ρ_R , kg/m3)	Constant	2400	2700	2900
Volumetric specific heat capacity of rock $\left(\rho c_p\right)_R$, (kg/m^3-°C)	Triangular	2056	2524	2865
Recovery factor (R_g, fraction)	Triangular	0.07	0.18	0.24
$T_R - T_{sep}$ (°C)	Triangular	51.392	61.392	71.392

Table C.14: Reservoir parameters used for Kızıldere-2 (Flash).

Parameter	Dist. Type	Min	Mode	Max
Reservoir Area (A, m^2)	Triangular	3.5E+06	3.6E+06	4.5E+06
Reservoir Thickness (H, m)	Triangular	1600	1700	1800
Resource Temperature (T_R, °C)	Triangular	230	240	245
Porosity (ϕ , fraction)	Constant	0.01	0.04	0.07
Density of brine (ρ_f , kg/m^3)	Constant		824.65	
Specific heat capacity of rock $(c_p)_R$, kJ/kg-°C	Constant	0.85	0.9	0.95
Density of rock (ρ_R , kg/m3)	Constant	2650	2800	2950
Volumetric specific heat capacity of rock $\left(\rho c_p\right)_R$, (kg/m^3-°C)	Triangular	2264	2557	2848
Recovery factor (R_g, fraction)	Triangular	0.07	0.18	0.24
$T_R - T_{sep}$ (°C)	Triangular	86.392	96.392	101.392

Table C.15: Reservoir parameters used for Nazilli-Aydın (Binary).

Parameter	Dist. Type	Min	Mode	Max
Reservoir Volume (V, m^3)	Uniform	2.00E+9	-	3.00E+9
Resource Temperature (T_R, °C)	Triangular	140	180	200
Porosity (ϕ , fraction)	Constant	0.01	0.06	0.13
Density of brine (ρ_f , kg/m^3)	Constant		894.19	
Specific heat capacity of rock (c_p)$_R$, kJ/kg-°C	Constant	0.85	0.9	0.95
Density of rock (ρ_R , kg/m3)	Constant	2400	2700	2900
Volumetric specific heat capacity of rock $\left(\rho c_p\right)_R$, (kg/m^3-°C)	Triangular	2057	2508	2883
Recovery factor (R_g, fraction)	Triangular	0.07	0.18	0.24
$T_R - T_{sep}$ (°C)	Triangular	51.671	91.671	111.671

Table C.16: Reservoir parameters used for Ortakçı-Aydın (Binary).

Parameter	Dist. Type	Min	Mode	Max
Reservoir Area (A, m^2)	Triangular	1.00E+06	2.00E+06	3.00E+06
Reservoir Thickness (H, m)	Uniform	500	-	1000
Resource Temperature (T_R, °C)	Uniform	135	-	165
Porosity (ϕ , fraction)	Constant	0.01	0.08	0.13
Density of brine (ρ_f , kg/m^3)	Constant		916.78	
Specific heat capacity of rock (c_p)$_R$, kJ/kg-°C	Constant	0.85	0.9	0.95
Density of rock (ρ_R , kg/m^3)	Constant	2400	2700	2900
Volumetric specific heat capacity of rock $\left(\rho c_p\right)_R$ (kg/m^3-°C)	Triangular	2058	2542	2895
Recovery factor (R_g, fraction)	Triangular	0.07	0.18	0.24
T_R-T_p (°C)	Uniform	46.671	-	76.671

Table C.17: Reservoir parameters used for Pamukören 1-Aydın (Binary).

Parameter	Dist. Type	Min	Mode	Max
Reservoir Volume (V, m^3)	Constant		1.50E+9	
Resource Temperature (T_R, °C)	Uniform	180	-	200
Porosity (ϕ , fraction)	Constant	0.01	0.06	0.13
Density of brine (ρ_f , kg/m^3)	Constant		877.16	
Specific heat capacity of rock (c_p)$_R$, kJ/kg-°C	Constant	0.85	0.9	0.95
Density of rock (ρ_R , kg/m3)	Constant	2400	2700	2900
Volumetric specific heat capacity of rock $\left(\rho c_p\right)_R$, (kg/m^3-°C)	Triangular	2056	2504	2873
Recovery factor (R_g, fraction)	Triangular	0.07	0.18	0.24
$T_R - T_{sep}$ (°C)	Uniform	91.671	-	111.671

Table C.18: Reservoir parameters used for Pamukören 2-Aydın (Flash).

Parameter	Dist. Type	Min	Mode	Max
Reservoir Volume (V, m^3)	Constant		2.00E+9	
Resource Temperature (T_R, °C)	Uniform	200	-	220
Porosity (ϕ , fraction)	Constant	0.01	0.06	0.13
Density of brine (ρ_f , kg/m^3)	Constant		855.9	
Specific heat capacity of rock (c_p)$_R$, kJ/kg-°C	Constant	0.85	0.9	0.95
Density of rock (ρ_R , kg/m3)	Constant	2400	2700	2900
Volumetric specific heat capacity of rock $\left(\rho c_p\right)_R$, (kg/m^3-°C)	Triangular	2055	2499	2862
Recovery factor (R_g, fraction)	Triangular	0.07	0.18	0.24
$T_R - T_{sep}$ (°C)	Uniform	56.392	-	76.392

Table C.19: Reservoir parameters used for Salihli Kuzey Doğu-Manisa (Binary).

Parameter	Dist. Type	Min	Mode	Max
Reservoir Area (A, m^2)	Triangular	2.00E+06	2.50E+06	3.50E+06
Reservoir Thickness (H, m)	Constant		500	
Resource Temperature (T_R, °C)	Constant		170	
Porosity (ϕ , fraction)	Constant	0.01	0.06	0.13
Density of brine (ρ_f , kg/m^3)	Constant		897.52	
Specific heat capacity of rock (c_p)$_R$, kJ/kg-°C	Constant	0.85	0.9	0.95
Density of rock (ρ_R , kg/m^3)	Constant	2400	2700	2900
Volumetric specific heat capacity of rock $\left(\rho c_p\right)_R$ (kg/m^3-°C)	Triangular	2057	2509	2885
Recovery factor (R_g, fraction)	Triangular	0.07	0.18	0.24
T_R-T_p (°C)	Uniform		81.671	

Table C.20: Reservoir parameters used for Salihli Doğu-Manisa (Binary).

Parameter	Dist. Type	Min	Mode	Max
Reservoir Volume (V, m^3)	Uniform	2.75E+09	-	8.50E+09
Resource Temperature (T_R, °C)	Uniform	150	-	170
Porosity (ϕ , fraction)	Constant	0.01	0.06	0.13
Density of brine (ρ_f , kg/m^3)	Constant		907.3	
Specific heat capacity of rock (c_p)$_R$, kJ/kg-°C	Constant	0.85	0.9	0.95
Density of rock (ρ_R , kg/m^3)	Constant	2400	2700	2900
Volumetric specific heat capacity of rock $\left(\rho c_p\right)_R$ (kg/m^3-°C)	Triangular	2058	2512	2890
Recovery factor (R_g, fraction)	Triangular	0.07	0.18	0.24
T_R-T_p (°C)	Uniform	61.671	-	81.671

Table C.21: Reservoir parameters used for Umurlu Güney-Aydın (Binary).

Parameter	Dist. Type	Min	Mode	Max
Reservoir Volume (V, m^3)	Uniform	1.05E+09	-	3.90E+09
Resource Temperature (T_R, °C)	Uniform	150	-	170
Porosity (ϕ , fraction)	Constant	0.01	0.06	0.13
Density of brine (ρ_f , kg/m^3)	Constant		907.3	
Specific heat capacity of rock (c_p)$_R$, kJ/kg-°C	Constant	0.85	0.9	0.95
Density of rock (ρ_R , kg/m^3)	Constant	2400	2700	2900
Volumetric specific heat capacity of rock $(\rho c_p)_R$ (kg/m^3-°C)	Triangular	2058	2512	2890
Recovery factor (R_g, fraction)	Triangular	0.07	0.18	0.24
T_R-T_p (°C)	Uniform	61.671	-	81.671

Table C.22: Reservoir parameters used for Salavatlı-Aydın (Binary).

Parameter	Dist. Type	Min	Mode	Max
Reservoir Volume (V, m^3)	Triangular	9.00E+09	1.60E+10	5.40E+10
Resource Temperature (T_R, °C)	Triangular	145	170	230
Porosity (ϕ , fraction)	Constant	0.01	0.06	0.13
Density of brine (ρ_f , kg/m^3)	Constant		885.76	
Specific heat capacity of rock (c_p)$_R$, kJ/kg-°C	Constant	0.85	0.9	0.95
Density of rock (ρ_R , kg/m^3)	Constant	2650	2750	2950
Volumetric specific heat capacity of rock $(\rho c_p)_R$ (kg/m^3-°C)	Triangular	2267	2549	2919
Recovery factor (R_g, fraction)	Triangular	0.07	0.18	0.24
T_R-T_p (°C)	Triangular	56.671	81.671	141.671

Table C.23: Reservoir parameters used for Seferihisar 1 (Binary).

Parameter	Dist. Type	Min	Mode	Max
Reservoir Volume (V, m^3)	Constant		2.50E+09	
Resource Temperature (T_R, °C)	Uniform	130	-	155
Porosity (ϕ , fraction)	Constant	0.03	0.06	0.08
Density of brine (ρ_f , kg/m^3)	Constant		923.68	
Specific heat capacity of rock (c_p)$_R$, kJ/kg-°C	Constant	0.85	0.9	0.95
Density of rock (ρ_R , kg/m^3)	Constant	2650	2750	2950
Volumetric specific heat capacity of rock $(\rho c_p)_R$ (kg/m^3-°C)	Triangular	2301	2558	2887
Recovery factor (R_g, fraction)	Triangular	0.07	0.18	0.24
T_R-T_p (°C)	Uniform	41.671	-	66.671

Table C.24: Reservoir parameters used for Seferihisar 2 (Binary).

Parameter	Dist. Type	Min	Mode	Max
Reservoir Volume (V, m^3)	Constant		1.250E+10	
Resource Temperature (T_R, °C)	Uniform	110	-	130
Porosity (ϕ , fraction)	Constant	0.03	0.06	0.08
Density of brine (ρ_f , kg/m^3)	Constant		943.19	
Specific heat capacity of rock $(c_p)_R$, kJ/kg-°C	Constant	0.85	0.9	0.95
Density of rock (ρ_R , kg/m^3)	Constant	2650	2750	2950
Volumetric specific heat capacity of rock $(\rho c_p)_R$ (kg/m^3-°C)	Triangular	2303	2563	2894
Recovery factor (R_g, fraction)	Triangular	0.07	0.18	0.24
T_R-T_p (°C)	Uniform	21.671	-	41.671

Table C.25: Reservoir parameters used for Simav-Kütahya (Flash).

Parameter	Dist. Type	Min	Mode	Max
Reservoir Volume (V, m^3)	Triangular	4.00E+09	6.00E+09	1.00E+10
Resource Temperature (T_R, °C)	Triangular	160	200	230
Porosity (ϕ , fraction)	Constant	0.03	0.06	0.08
Density of brine (ρ_f , kg/m^3)	Constant		870.16	
Specific heat capacity of rock $(c_p)_R$, kJ/kg-°C	Constant	0.85	0.9	0.95
Density of rock (ρ_R , kg/m3)	Constant	2650	2750	2950
Volumetric specific heat capacity of rock $(\rho c_p)_R$, (kg/m^3-°C)	Triangular	2294	2545	2869
Recovery factor (R_g, fraction)	Triangular	0.07	0.18	0.24
T_R– T_{sep} (°C)	Triangular	16.392	56.392	86.392

Table C.26: Reservoir parameters used for Tekkehamam 1-Denizli (Binary).

Parameter	Dist. Type	Min	Mode	Max
Reservoir Area (A, m^2)	Constant		8.00E+06	
Reservoir Thickness (H, m)	Constant		200	
Resource Temperature (T_R, °C)	Triangular	120	140	160
Porosity (ϕ , fraction)	Constant	0.01	0.06	0.13
Density of brine (ρ_f , kg/m^3)	Constant		925.94	
Specific heat capacity of rock $(c_p)_R$, kJ/kg-°C	Constant	0.85	0.9	0.95
Density of rock (ρ_R , kg/m^3)	Constant	2650	2750	2950
Volumetric specific heat capacity of rock $(\rho c_p)_R$ (kg/m^3-°C)	Triangular	2269	2559	2941
Recovery factor (R_g, fraction)	Triangular	0.07	0.18	0.24
T_R-T_p (°C)	Triangular	31.671	51.671	71.671

Table C.27: Reservoir parameters used for Tekkehamam 2-Denizli (Binary).

Parameter	Dist. Type	Min	Mode	Max
Reservoir Area (*A*, m²)	Constant		4.00E+06	
Reservoir Thickness (*H*, m)	Constant		200	
Resource Temperature (T_R, °C)	Triangular	140	180	200
Porosity (ϕ , fraction)	Constant	0.01	0.06	0.13
Density of brine (ρ_f , kg/m³)	Constant		894.19	
Specific heat capacity of rock (c_p)$_R$, kJ/kg-°C	Constant	0.85	0.9	0.95
Density of rock (ρ_R , kg/m³)	Constant	2650	2750	2950
Volumetric specific heat capacity of rock $\left(\rho c_p\right)_R$ (kg/m³-°C)	Triangular	2267	2551	2924
Recovery factor (R_g, fraction)	Triangular	0.07	0.18	0.24
T_R-T_p (°C)	Triangular	51.671	91.671	111.671

Table C.28: Reservoir parameters used for Tekkehamam 3-Denizli (Binary).

Parameter	Dist. Type	Min	Mode	Max
Reservoir Area (*A*, m²)	Constant		2.00E+06	
Reservoir Thickness (*H*, m)	Constant		1000	
Resource Temperature (T_R, °C)	Triangular	140	170	200
Porosity (ϕ , fraction)	Constant	0.01	0.06	0.13
Density of brine (ρ_f , kg/m³)	Constant		897.52	
Specific heat capacity of rock (c_p)$_R$, kJ/kg-°C	Constant	0.85	0.9	0.95
Density of rock (ρ_R , kg/m³)	Constant	2650	2750	2950
Volumetric specific heat capacity of rock $\left(\rho c_p\right)_R$ (kg/m³-°C)	Triangular	2267	2552	2926
Recovery factor (R_g, fraction)	Triangular	0.07	0.18	0.24
T_R-T_p (°C)	Triangular	51.671	81.671	111.671

Table C.29: Reservoir parameters used for Tuzla-Çanakkale (Flash).

Parameter	Dist. Type	Min	Mode	Max
Reservoir Area (*A*, m²)	Triangular	1.45E+06	2.20E+06	3.00E+06
Reservoir Thickness (*H*, m)	Triangular	200	500	1000
Resource Temperature (T_R, °C)	Triangular	170	200	230
Porosity (ϕ , fraction)	Constant	0.03	0.06	0.08
Density of brine (ρ_f , kg/m³)	Constant		866.63	
Specific heat capacity of rock (c_p)$_R$, kJ/kg-°C	Constant	0.85	0.9	0.95
Density of rock (ρ_R , kg/m3)	Constant	2650	2750	2950
Volumetric specific heat capacity of rock $\left(\rho c_p\right)_R$, (kg/m³-°C)	Triangular	2294	2544	2868
Recovery factor (R_g, fraction)	Triangular	0.07	0.18	0.24
T_R– T_{sep} (°C)	Triangular	26.392	56.392	86.392

Table C.30: Reservoir parameters used for Umurlu-Aydın (Binary).

Parameter	Dist. Type	Min	Mode	Max
Reservoir Volume (V, m^3)	Uniform	5.00E+09	-	1.50E+10
Resource Temperature (T_R, °C)	Uniform	150	-	170
Porosity (ϕ , fraction)	Constant	0.01	0.06	0.13
Density of brine (ρ_f , kg/m^3)	Constant		907.30	
Specific heat capacity of rock $(c_p)_R$, kJ/kg-°C	Constant	0.85	0.9	0.95
Density of rock (ρ_R , kg/m^3)	Constant	2400	2700	2900
Volumetric specific heat capacity of rock $(\rho c_p)_R$ (kg/m^3-°C)	Triangular	2058	2512	2890
Recovery factor (R_g, fraction)	Triangular	0.07	0.18	0.24
T_R-T_p (°C)	Uniform	61.671	-	81.671

Table C.31: Reservoir parameters used for Erciş- Zilan (Van) (Binary).

Parameter	Dist. Type	Min	Mode	Max
Reservoir Area (A, m^2)	Triangular	1.50E+06	2.50E+06	4.50E+06
Reservoir Thickness (H, m)	Constant	300	-	500
Resource Temperature (T_R, °C)	Triangular	120	140	168
Porosity (ϕ , fraction)	Constant	0.01	0.06	0.13
Density of brine (ρ_f , kg/m^3)	Constant		923.53	
Specific heat capacity of rock $(c_p)_R$, kJ/kg-°C	Constant	0.85	0.9	0.95
Density of rock (ρ_R , kg/m^3)	Constant	2650	2750	2950
Volumetric specific heat capacity of rock $(\rho c_p)_R$ (kg/m^3-°C)	Triangular	2269	2558	2940
Recovery factor (R_g, fraction)	Triangular	0.07	0.18	0.24
T_R-T_p (°C)	Triangular	31.671	51.671	79.671

CURRICULUM VITAE

Name Surname **:** Melek Altın

Place and Date of Birth **:** Istanbul 20.01.1979

E-Mail **:** melekaltin78@hotmail.com

EDUCATION **:**

- **B.Sc.** **:** 2000, Kocaeli University, Engineering Faculty, Geological Engineering

PROFESSIONAL EXPERIENCE AND REWARDS:

The Oil & Gas Year
Map Research Coordinator
(August 2016 - today), Istanbul, Turkey

- Working collaboratively to take information from the printed maps and turn it into accurate and useful GIS data for the resource platform and updating map database
- Researching oil and gas infrastructure to ensure that online maps are truly comprehensive

Transatlantic Petroleum Ltd
Senior Exploration & Development Geologist
2011 - 2013 (2 years), Istanbul, Turkey

- Deterministic static reservoir modelling of carbonate reservoirs by using Petrel with calculated total and secondary porosity data with seismically and geologically interpreted horizons and surfaces; and proposal new well location determination for the purpose of re-development of a producing field which is located on the SE of Turkey
- 3D seismic interpretation by using SMT Kingdom software to delineate the position of the discovery well drilled in a foreign license to evaluate the

hydrocarbon potential of the trap and structural closure; new prospect generation and evaluation; future plans and updates for the license
- Checked and supervised mud-loggers and wellsite geologists during drilling
- 2D seismic interpretation as a second opinion for two licenses on the southeastern part of Turkey, structural mapping, prospect generation
- Worked on the wireline and mud-log data of existing wells in Northern Thrace Basin area, determined new well tops and evaluated them with the seismic sections, made time to depth conversions by using seismic data and made synthetic seismograms for depth correlations by using SMT Kingdom software

Thrace Basin Natural Gas Co (TBNG)
Geologist
2006 – 2011 (5 years), Tekirdag, Turkey

- Deterministic static structural reservoir and log property modeling by Petrel by using wireline log and calculated effective porosity and facies data based on open hole wireline logs; determined new well locations based on the model, correlated with 2D seismic and prepared proposal well reports
- Data preparation for geological modelling
- Determined candidate perforation and frac zones
- Petrophysical interpretation on wireline log data, determined new and additional perforation zones; prepared behind pipe inventory for all the wells drilled in the southern part of Thrace Basin
- Worked on petrophysical Eq.s and parameters to be changed for each different reservoir zone, calibrated Eq.s and parameters according to recorded formation evaluation log data as CMR, core data and production well test results
- Done structural well and zone correlations, constructing database
- Organized weekly meetings for upcoming open and cased hole jobs with service companies
- Supervised and organized wellsite geologists
- Witnessed on perforation and frac jobs
- Witnessed on wireline open and cased hole log operations
- Prepared daily and weekly reports, done well correlations during drilling, prepared final and general well evaluation reports after the drilling has stopped
- Wellsite geologist; described drill cutting samples, was responsible for total mud-gas detection system to work properly, analyzed total mud-gas shows.

PUBLICATIONS, PRESENTATIONS AND PATENTS ON THE THESIS:

Altın M., Onur, M. (2017). "Jeotermal Kaynakların Elektrik Üretim (Güç) Potansiyelinin Hacimsel Yöntemlerle Belirlenmesinde Yeni Bir Uygulama Metodu" (A New Application Method for Estimating the Electricity (Power) Generation Potential of Geothermal Resources by Volumetric Approaches) presented at the 13. Ulusal Tesisat Mühendisliği Kongresi, İzmir, Türkiye, 19-21 April.